EXPERIMENTAL INVESTIGATION OF RESIDUAL STRESSES INTRODUCED VIA SHOT PEENING AND THEIR EFFECT ON FATIGUE LIFE OF BALL BEARINGS

A THESIS SUBMITTED TO
THE GRADUATE SCHOOL OF NATURAL AND APPLIED SCIENCES
OF
MIDDLE EAST TECHNICAL UNIVERSITY

BY

ALİ KÜÇÜKYILMAZ

IN PARTIAL FULFILLMENT OF THE REQUIREMENTS
FOR
THE DEGREE OF MASTER OF SCIENCE
IN
METALLURGICAL AND MATERIALS ENGINEERING

JANUARY 2010

Approval of the thesis:

EXPERIMENTAL INVESTIGATION OF RESIDUAL STRESSES
INTRODUCED VIA SHOT PEENING
AND THEIR EFFECT ON FATIGUE LIFE OF BALL BEARINGS

submitted by **ALİ KÜÇÜKYILMAZ** in partial fulfilment of the requirements for the degree of **Master of Science in Metallurgical and Materials Engineering Department, Middle East Technical University** by,

Prof. Dr. Canan Özgen
Dean, Graduate School of **Natural and Applied Sciences** _____

Prof. Dr. Tayfur Öztürk
Head of Department, **Metallurgical and Materials Engineering** _____

Prof. Dr. C. Hakan Gür
Supervisor, **Metallurgical and Materials Engineering Dept., METU** _____

Examining Committee Members:

Prof. Dr. Tayfur Öztürk
Metallurgical and Materials Engineering Dept., METU _____

Prof. Dr. C. Hakan Gür
Metallurgical and Materials Engineering Dept., METU _____

Prof. Dr. Cevdet Kaynak
Metallurgical and Materials Engineering Dept., METU _____

Prof. Dr. A. Bülent Doyum
Mechanical Engineering Dept., METU _____

Dr. İbrahim Çam
Central Laboratory, METU _____

Date: 01.02.2010

I hereby declare that all information in this document has been obtained and presented in accordance with academic rules and ethical conduct. I also declare that, as required by these rules and conduct, I have fully cited and referenced all material and results that are not original to this work.

Name, Last name : Ali KÜÇÜKYILMAZ

Signature :

ABSTRACT

EXPERIMENTAL INVESTIGATION OF RESIDUAL STRESSES INTRODUCED VIA SHOT PEENING
AND THEIR EFFECT ON FATIGUE LIFE OF BALL BEARINGS

KÜÇÜKYILMAZ, Ali

M. Sc., Metallurgical and Materials Engineering Department

Supervisor: Prof. Dr. C. Hakan GÜR

January 2010, 136 pages

In this study, residual stresses introduced via application of shot peening on the raceways of bearing rings and their effect on the fatigue life was investigated experimentally. For improvement of residual compressive stress state, shot peening operation with different parameters was utilized. Residual stress measurements were conducted via X-ray diffraction technique. Optimization of residual stress state during the production of ball bearings is the main target of this study. Process parameters for shot peening and super-finishing were studied for determination of the parameters that induce the most favorable residual stress state. The fatigue life of ball bearings were determined by life cycle tests and tabulated to show the results of the study. The results of the thesis are believed to help for optimization of residual stress distribution and improvement of service life of ball bearings.

Key words: Ball Bearing, Shot Peening, Residual Stress, Fatigue

ÖZ

BİLYALI SERTLEŞTİRME İLE OLUŞTURULAN KALINTI GERİLMELERİN VE BUNLARIN BİLYALI RULMANLARIN YORULMA ÖMRÜNE ETKİLERİNİN DENEYSEL İNCELENMESİ

KÜÇÜKYILMAZ, Ali

Yüksek Lisans, Metalurji ve Malzeme Mühendisliği Bölümü

Tez Yöneticisi: Prof. Dr. C. Hakan GÜR

Ocak 2010, 136 sayfa

Bu çalışmada, rulman bileziklerinin yuvarlanma yollarında bilyalı sertleştirme yoluyla oluşturulmuş kalıntı gerilmeler ve yorulma ömrüne etkisi deneysel olarak incelenmiştir. Kalıntı basma gerilmelerinin iyileştirilmesi amacıyla farklı parametrelerle bilyalı sertleştirme operasyonu uygulanmıştır. Kalıntı gerilmelerin ölçümü X-ışınları kırınımı tekniği ile yapılmıştır. Bilyalı rulman üretiminde kalıntı gerilmelerin optimize edilmesi, bu çalışmanın ana hedefidir. En uygun kalıntı gerilme durumunu oluşturan parametrelerin belirlenmesi için; bilyalı sertleştirme ve honlama proses parametreleri üzerinde çalışılmıştır. Bilyalı rulman yorulma ömrü, ömür testleri ile belirlenmiştir ve çalışmanın sonuçlarını göstermesi amacıyla çizelgelenmiştir. Elde edilen verilerin, bilyalı rulman bileziklerindeki kalıntı gerilme dağılımı ve kullanım ömrü optimizasyonu konularında fayda sağlayacağına inanılmaktadır.

Anahtar Kelimeler: Bilyalı Rulman, Bilyalı Sertleştirme, Kalıntı Gerilme, Yorulma

To My Parents,
My Wife and My Child

ACKNOWLEDGMENTS

The author would like to express his sincere gratitude to his supervisor Prof. Dr. C. Hakan GÜR for his excellent guidance, patience, advice, encouragements and insight through the research.

The author wishes also to thank Dr.-Ing. Feridun ÖZHAN, Mr. Turhan SAVAŞ, Mr. M. Faik KARAARSLAN and all other staff of Ortadoğu Rulman Sanayi ve Ticaret A.Ş. for creating a friendly and inspiring atmosphere, their suggestions, technical support and funding of the material and life cycle tests.

Among colleagues one especially would like to be acknowledged for his contribution to this work is Mr. Nazmi SAYDEMİR for residual stress measurements and performing the tests.

TABLE OF CONTENTS

LIST OF TABLES

TABLES

LIST OF FIGURES

FIGURES

CHAPTER 1

INTRODUCTION

Within this chapter, general information about ball bearings, related standards and tolerances, bearing steels, vibration, lubrication and service life issues are briefly given. Also, bearing ring production from three different routes is presented.

1.1 General Information about Ball Bearings

Ball bearing is one type of bearing coming from the rolling bearings family. Balls of different sizes and alignments, depending on bearing design based on the application for which the bearing is going to be used, are the rolling elements for this kind and that is why they are named as ball bearings. Rolling bearings consist of a set of rolling elements which the standard shapes are cylindrical rollers, needle rollers, tapered rollers, barrel rollers and balls. These rolling elements run in their raceways between two rings. Rolling bearings are classified generally according to their design parameters. As an example the main distinction between a thrust and a radial bearing is the loading direction, while as also stated above rolling element shape divides them into roller and ball bearings.

Ball bearings are the most commonly used machine elements in nearly all fields of industry. Main parts composing a radial ball bearing are the balls guided by a metal or polymer cage, which is preventing their mutual contact and make them uniformly separated and well aligned in their raceways, encircled by inner and outer rings. Depending on the application, metal shields or rubber seals are the elements used to

protect the balls and the precisely machined inner parts, especially raceways, from harmful particles. Not frequent but in some applications snap ring is also used. See *Figure 1.1* (ORS Bearings, 2005).

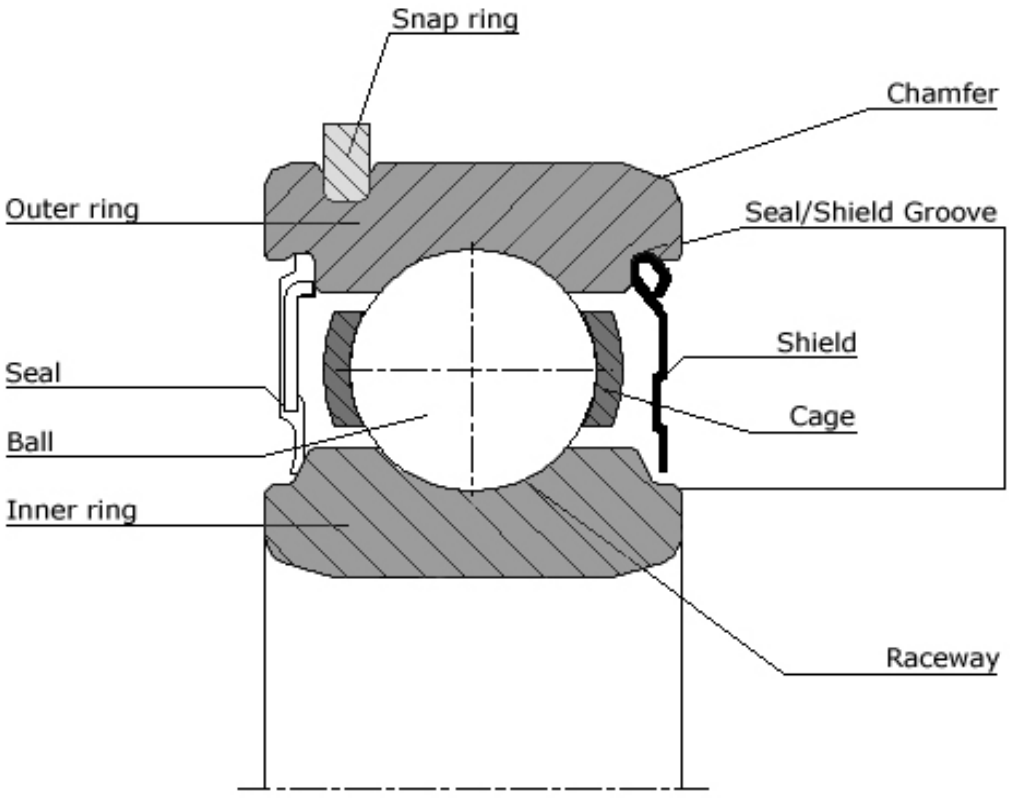

Figure 1.1 Components of a Radial Ball Bearing (ORS Bearings, 2005)

Classification of radial and thrust ball bearings are generally done according to their balls contact type with the raceways and row number etc… A helpful classification table of ball bearings is given in *Figure 1.2* (ORS Bearings, 2005).

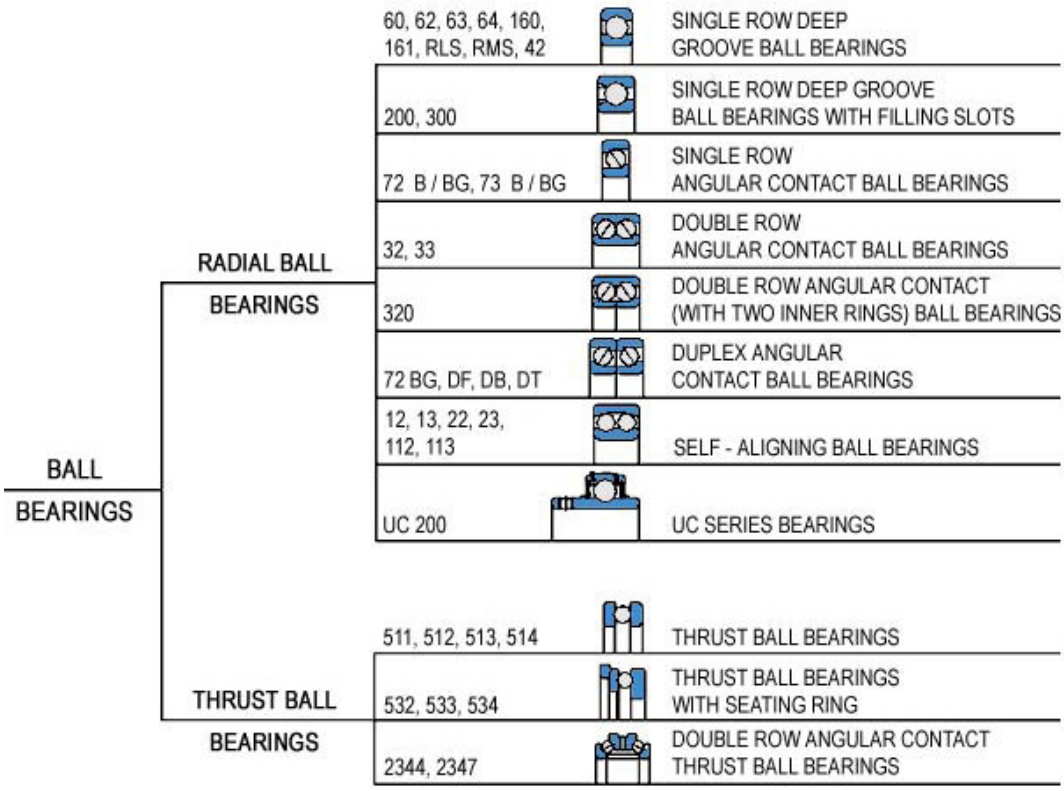

Figure 1.2 Classification of Ball Bearings (ORS Bearings, 2005)

1.2 Standards and Tolerances

Main dimensions and related tolerances (shape, clearance, eccentricity, run out etc…) of ball bearings are strictly stated via international standards. Consequently bearings in a standard series only can have dimensional alterations with exact steps. Tolerances tables with related standards can be found as tabulated by several standard associations like Japanese Standards (JIS), Turkish Standards, American National Standards Institute (ANSI), International Organization for Standardization (ISO), and Antifriction Bearing Manufacturers Association (AFBMA) etc... Tolerances are given as assigned to the nominal dimensions within a series. For

example, bore sizes between 20 and 100 mm change 5 mm for each step and external dimensions (outside diameter, width etc…) change with bore dimension steps. For each bore size numerous bearings are available with different outside diameter and width. Bearings can be classified as extra light, light, medium, heavy series according to proportion of width and outside diameter to bore. If the ratio is relatively high bearing can be said heavy duty series and light series in contrary. Series representation and this dimensional standardization makes customer to order easily and replace the malfunctioning bearing in his machine. So standards ensure bearings supplied by different manufacturers can be used instead of each other.

1.3 Bearing Steels

Material used in bearing applications has the most important role on performance and fatigue life. Bearing applications require resistance to heavy loads (static and cyclic), stresses in contact surfaces, different temperatures, wear, shock loading, vibrations etc… As a consequence material which is going to be used for bearing applications has to withstand these harsh working conditions.

Steel is the main raw material used to manufacture bearings. Depending on the application case hardening or through hardening steel qualities are used. Primary use of case hardening qualities is for roller bearings and through hardening qualities are predominantly used in ball bearing production. Standards related to bearing steels are well stating the requirements to be met. Among these the well known and currently applied are ASTM A295 and ISO 683-17. Concerning the items in these standards the most important is the inclusion content. Steel must be relatively free of impurities such as macro and micro inclusions coming from slag etc… Strictly controlled composition and manufacturing route makes these inclusions to be kept at minimum levels. Of the through hardening grades AISI E52100 (DIN 1.3505) is the most extensively employed.

Production route of a high micro and macro cleanness through hardening bearing steel is starting from high quality, clean scrap. Scrap is charged into electric arc furnace (EAF), after being molten; metal is transferred to the ladle furnace (LF) for ladle treatment (secondary metallurgy) for refining and alloying. Following this for final refining steel is degassed under vacuum (VD) and than bottom poured into ingots or continuously cast through application of shrouding. During casting carbide structure and segregations are controlled by well processed cooling and magnetic stirring so managed solidification kinetics. Finally steel is rolled into bar or tube shape and annealed in order for having spheroidized structure. Bars produced for hot forging are not spheroidize annealed, they are delivered as rolled.

AISI E52100 is a high carbon, chromium alloyed through hardening steel. This high carbon content with alloying elements, mainly chromium, makes this steel to achieve high hardness through the part cross section after heat treatment and resultant high resistance to wear and high load carrying capacity. Larger cross sections that need greater hardenability necessitate the use of molybdenum and/or manganese modifications of 52100 steel.

Low carbon carburizing steel grades for some applications are also utilized as bearing steels. Such qualities are AISI 8620, 9310, 5120, 4820, 4415, 3310, 1115 etc… Here the parts are carburized in an atmosphere that has a carbon potential around 0.9 – 1.0% in order to obtain a hard, wear resistant, strong surface while soft and ductile core is still present. By the use of these steels a tough, ductile core and a strong, wear resistant surface is the result.

All aforementioned steels are not suitable for high temperature applications; their use is restricted to temperatures up to 270 ^{O}C. For example, exposure of a bearing manufactured from AISI E52100 steel to 270 ^{O}C reduces its hardness from 62 ± 2 HRC to 53 ± 2 HRC. By the way load carrying capacity and wear resistance which are directly related with hardness are dropped also. As a result for temperatures over 250 ^{O}C high alloy steel such as high speed tool steels (M50, M2, T5 etc…) are

preferred which has better hardness retention up to 550 ^{O}C. Demand for bearings operating at still higher temperatures, especially in aerospace industry, makes cobalt and nickel base alloys rather than steel to be used. Stellite Star J (No 3, 19), AMS 5713 have been utilized successfully at temperatures as high as 800 ^{O}C.

Corrosion resistant bearings are manufactured from stainless martensitic grades; 440C is the most widely specified. This grade can be hardened up to 60 ± 2 HRC and withstand this hardness up to 450 ^{O}C. But upon exposure to such high temperatures corrosion resistance is dropped.

Cages are generally stamped from sheet steel St4 (DIN 1.0338). Some times brass sheets are also used. For some applications they are machined from tubes or cast or injection molded blanks, generally brass, sintered iron, steel or plastics (Polyimide 6.6). Like cages, shields are also manufactured from St4 steel sheet, while seals are made from FKM (Viton) and NBR (Nitrile Butadiene Rubber). Rivets that hold the cages together are made from USt 36-2 steel.

1.4 Vibrations in Ball Bearings

Today's industry is in a very merciless condition. Competition between same sector companies is now at the highest levels, especially this is more sensible for continuous production lines. Stoppage of a continuous production line, for example a hot rolling mill in a steel plant, is meaning directly loss of money because as a well known fact time is money for such kind of production lines. Unexpected stoppage can not be tolerated and as a result of this, preventive maintenance based on analyzing and continuous monitoring of critical signals that can warn maintenance people before failure became very popular and indefeasible within current industrial conjuncture.

Bearing vibration monitoring and analysis is a very well known and extensively employed preventive maintenance branch. By analyzing vibration data the life time remaining for a bearing can be foreseen and necessary precautions can be taken before unexpected failure of the machine element because of malfunctioning of this bearing. Replacing the bearing on time almost in all conditions costs very little when compared with the resultant disasters unless it is not renewed. Than from the maintenance point of view, it is very important to know how long a bearing will last after a certain level of vibration measured. In order for making this to be foreseen reference vibration values resembling the bearing deterioration level are used and by the way the condition of bearing is assessed.

Vibration, as being an indication of quality of a bearing is very important for ball bearings. Vibration means improper working of the machine that the bearing is mounted and it is the main reason of noise generation. There are two categories of outer ring vibrations: first is the vibration coming from the variations of compliance of the bearing to applied loads, second is the vibration due to rolling over geometrical imperfections on raceways of on the rolling element itself.

Concerning a ball bearing, variations of elastic deflections as a result of Hertzian stresses created by radial load with respect to the loading line cause vibrations which is named as variable contact compliance vibrations. Vibration in this type is both in load direction and in perpendicular direction to the application of load. Second type, variable flexural compliance vibrations are due to bearing deformation from the original circular shape. Waviness in one/or both of the rings as well as in the balls also cause vibrations that can be detected from the outer ring translational motion with reference to the inner ring.

Vibrations created by discontinuities on the raceways and/or on the balls ends up with continuous growth of the discontinuity present. Spalling, flaking, pitting caused by surface fatigue, smearing due to excessive acceleration, pitting due to electrical

current, cracks originating from the shape of bearing housing are some examples of these discontinuities causing vibrations.

1.5 Lubrication

Lubrication of ball bearings is somewhat less critical in comparison to sliding bearings. However, inadequate lubrication in contact areas where sliding is possible will result in early damage and shorter fatigue life. Main damage types that will originate due to improper lubrication are pitting, smearing (plastic flow), scuffing and oxide film generation. Lubrication is critical in between balls and the raceways where heavily loaded contact areas present. Existence of hydrodynamic film in between these highly stressed contacts has vital importance. Otherwise, if the hydrodynamic lubrication is not formed and the surfaces are not well separated by oil film the resulting friction can form tangential stresses which increases the stress intensity near and if it is relatively big on the surface. By the way the point of maximum shear stress becomes located at the surface. During normal fatigue under adequate lubrication conditions, maximum shear stress due to Hertzian stresses are several micrometers below the surface. In improper or insufficient lubrication case cracks that will nucleate very close to or just at the surface due to maximum shear stress location in this region makes fatigue to occur faster and so affects adversely the fatigue life. As a result, proper lubrication of ball bearings is essential to their performance and so the service life.

Depending on the application both grease and oils are used in bearing lubrication. The choice is dependent on the operating speed and temperature of the bearing. Oil is advantageous at higher speeds and operating temperatures thanks to the transfer of heat from heavily contacting surfaces as well as in terms of flushing the contaminants away. However grease is extensively used for ball bearings due to less maintenance need and simplified design in terms of housing and sealing.

1.6 Service Life

Ball bearing is a load carrying machine element and so selection of a bearing for a certain application is based on the load to be carried and the capacity of that bearing to cope with this loading condition. At a time of deciding of the appropriate bearing for an application, a certain degree of safety must also be considered for plastic deformation and premature bearing failure not to take place. Carrying an over load when stationery or during very slow motion will make the bearing unserviceable by plastic deformation of balls and the raceways which are under stress. Under excessive stress conditions metal fatigue will take place prematurely and raceways even the balls will start to flake and spall. Beside load carrying capacity, wear and environmental conditions have to be considered also during deciding the suitable bearing. Temperature, corrosiveness, lubrication conditions, dirt around will dictate the selection.

Bearings suffer two main kinds of stressing namely, static and dynamic stressing. In rolling bearing engineering the term static stressing refers to bearings carrying a load when stationary or when subjected to small oscillating motions; the load may be constant or variable (McCool, 1970). So by static operating condition of the bearing is referred, not the loading. Than, dynamic stressing can be described as; loading of a rotating bearing. Again the load may be constant or altering. Dynamic is related to bearing, not the load. When static loading is considered; experience shows that rolling bearings under static load can be stressed to such a degree that minor plastic deformations occur in the rolling surfaces. These indentations and flattened areas, however, should not be of such an extent that they impair the rotation of the bearing. Admissible static rolling element loading, therefore, means that the total deformation of rolling element and raceway does not exceed 0.01% of the rolling element diameter dw. For a ball of 10 mm diameter this corresponds to a plastic deformation of the two bodies of 1 μm (Brändlein et al., 1999).

Under dynamic stressing, depending on the loading and the magnitude of load applied, fatigue starts to emanate after a certain rotation cycles. Crack nucleation in bearing steels take place from weak points such as micro inclusions, segregated carbides and inhomogeneous distribution regions of alloying elements, local stress concentration sites or small hardness decay points, small indentations on surface etc… With further operation these cracks propagate and material flaking starts, finally small particles break away from the surfaces of balls or raceways, well known as spalling.

1.7 Production of Rings

Bearing ring production is performed via three different methods. Production from tube, production from bar and hot forging from bar material. For the first two methods steel is purchased as spheroidize annealed in order to be able to machine directly. For hot forging bars are delivered as rolled, not annealed so they are cheaper.

Production from tube method uses seamless steel tubes as raw material. Rings are cut from the tubes and machining is done. After heat treatment to achieve wear resistance and strength rings are transferred to grinding operation. Finally super-finishing application to raceways and than washing makes the rings ready for assembly. Flow chart for this production route is given in *Figure 1.3*.

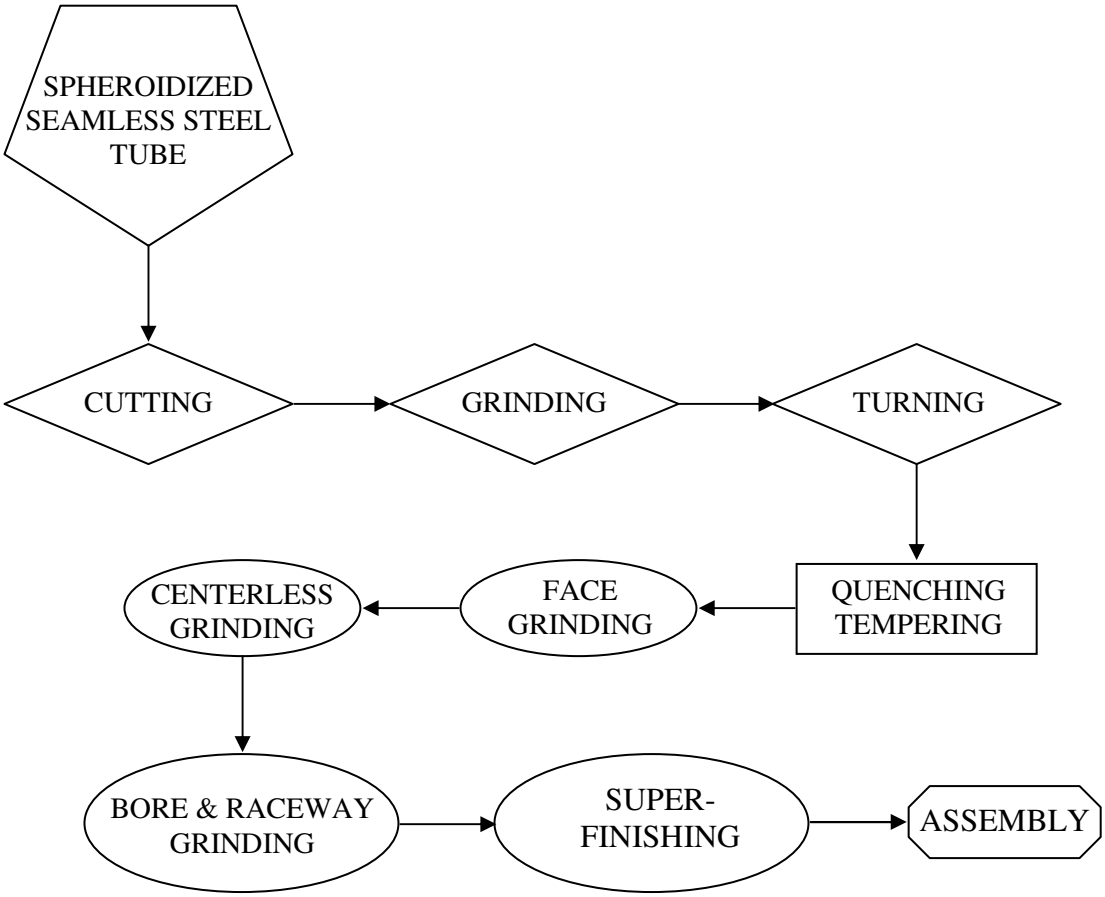

Figure 1.3 Ring Production from Tube

Row material for production from bar method is spheroidize annealed bars. First small pieces, blanks are cut and the center holes are drilled. The next step is face and centerless grinding and than turning. After being machined, trepanning and separation of inner and outer rings is done. Finally after finish turning the rings are following the same path as rings from tube. See *Figure 1.4* for flow chart.

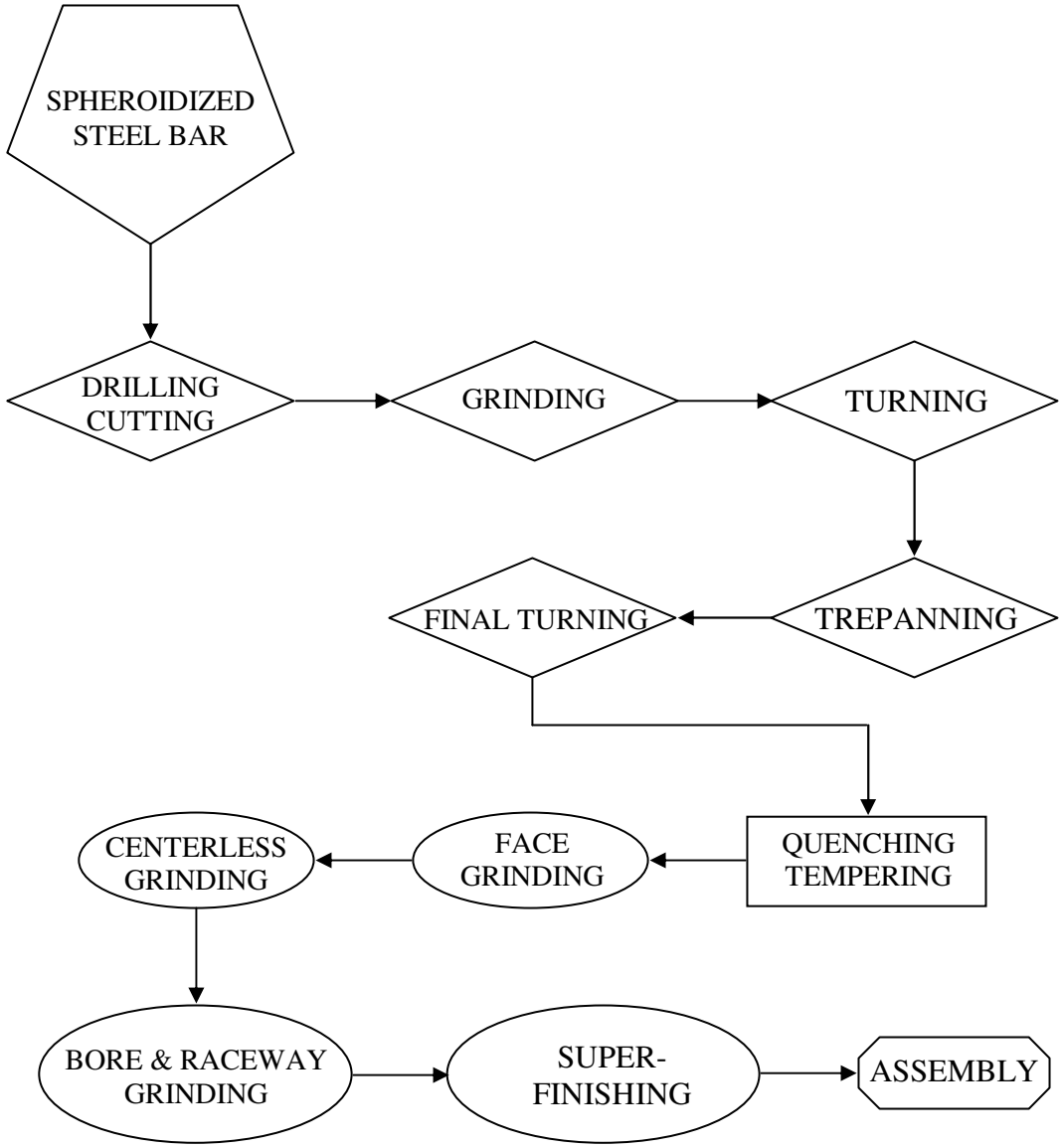

Figure 1.4 Ring Production from Bar

Production by hot forging utilizes again steel bars, but this time as rolled, not spheroidize annealed, are the raw material. Bars are induction heated first and than cut, forged to shape and finally inner and outer ring are separated by piercing, all covered as hot forging operation. Next step is spheroidize annealing for machinability and formability. After heat treatment sand blasting is applied for removing the thin scale from the surface. Finally rings are brought to diameter by

cold ring rolling process and the rest is same with production from tube. For mass production hot forging is the best in terms of speed and price. Flow chart can be seen in *Figure 1.5.*

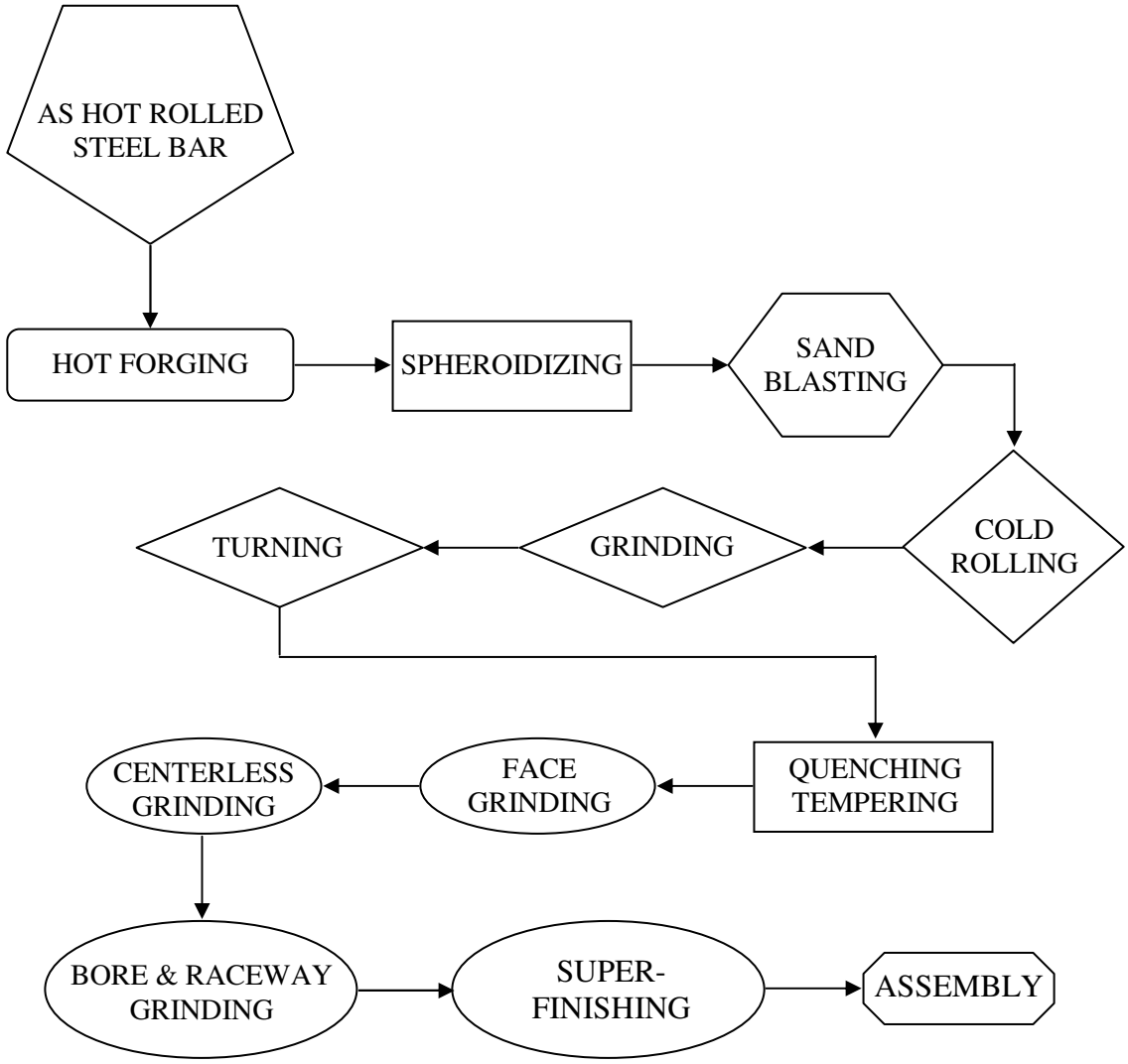

Figure 1.5 Ring Production by Hot Forging

1.8 Residual Stresses during Manufacturing Stages

Throughout this part, general information about residual stresses, their evaluation methods, residual stress development during bearing ring production at stage of the last two processes namely grinding and super-finishing is concerned. Focus is located on the last two processes due to the fact that residual stresses affecting life span of ball bearings are shaping during raceway grinding and super-finishing processes. Stresses developed before martempering heat treatment has no end effect on fatigue life of rings relying on the fact that they are relieved during austenitization. Heat treatment is known to be effective on residual stress development during final machining operations from the microstructure point of view. So in this section, heat treatment process is also described briefly.

Practically all machine part fractures occurring in normal service are fatigue fractures. Fully 90 percent of all fatigue failures occurring in normal service are traceable to design and fabrication errors. Fatigue fractures, as well as other brittle type fractures, occur only as a result of tensile stresses (Almen, Black, 1963). Residual stresses great effect on fatigue behavior of machine elements is a very well known fact. They can be detrimental or beneficial depending on the superposition with the applied load. As a simple definition of residual stress one can say that; they are the stresses which would present in an elastic body when all externally applied loads are removed. From this definition residual stresses exist under static equilibrium conditions, meaning that all resultant moments and forces acting on the body understood to be zero.

Residual stresses may be compressive or tensile and can promote or retard crack initiation, accelerate or decelerate crack propagation during fatigue. Compressive residual stresses are known to be beneficial in terms of prolongation of fatigue life. The later one is known to be destructive. Residual stresses can be subdivided as macro and micro scale stresses. Macro scale residual stresses act over numerous grains while micro scale stresses are valid only on a single grain or crystal lattice.

Macro scale residual stresses are added to the stresses exerted on the component during service. The resultant stress may be tensile or compressive. But if elastic limit is exceeded deformation so yielding takes place. Residual stresses are all confined to elastic limit of the material.

Mechanical, thermal, chemical effects may form residual stresses on components. Inhomogeneous plastic deformations during forming and machining, thermal gradients and phase transformations during heat treatment, corrosion and various surface treatments may lead to changes in residual stress distribution. Almost all manufacturing processes and treatments introduce residual stresses to the components (SAE International, 2003). Plastic deformation including rolling, drawing, forging, extruding, spinning, shot peening and laser peening etc…, machining, joining (welding, brazing), coating (CVD, PVD), cladding, grinding as manufacturing processes, quenching, carburizing, nitriding, induction hardening, ion plating as being thermal and thermo-chemical treatments are producing internal stresses.

As well as being important for fatigue life, residual stresses are also effective during manufacturing of components. For preventing unwanted deformations during machining, turning and grinding in ring production case, having a part free from residual stresses is ideal. In this study we do not care about the effect of stresses during manufacturing, what considered are the residual stresses on the ring raceways at the end of production which directly affects bearing service life.

Various destructive and nondestructive residual stress evaluation techniques are developed. Some of them are quantitative and some are qualitative. In destructive methods, logic is based on destruction of the equilibrium state of internal stresses. So, residual stress is measured by relaxing it. However measured is not the stress itself, it is only possible to measure the consequence of stress relaxation such as strain and displacement. Method of destructive measurement follows first creation of new stress state by layer removal or by machining and than detection of the local change in

strain or displacement by the way stress relaxed is calculated finally as a function of the strain measured from theory of elasticity. Most common methods include hole drilling, ring core technique, bending deflection and sectioning.

Nondestructive residual stress measurement is more useful for quality control purposes and feasible in terms of not scrapping lots of work and material spends for the component. In this method relationship between crystallographic or physical parameters and stress state is employed. Extensively used ones are X-ray diffraction, neutron diffraction, ultrasonic and magnetic methods. Neither destructive methods nor ultrasonic and magnetic methods are able to distinguish macro and micro scale stresses; the only evaluation possible is by diffraction techniques (X-ray, neutron). Peak shift is sensitive to macroscopic stresses where line broadening is sensing the microscopic ones (James, Lu, Roy, 1996).

Optimum choice for the method of measurement depends on:

- The type (macro or micro scale) and gradient of stress to be measured.
- Material (crystallographic, amorphous, magnetic or nonmagnetic).
- Measuring time and precision.
- Geometry of the component.
- Measurement place, on site or laboratory.
- Destruction of component is allowed or not.
- Cost of measurement and the measuring device.

Method used for residual stress measurement for the work described in this thesis is X-ray diffraction $\sin^2 \Psi$ technique.

1.8.1 Residual Stresses Induced by Heat Treatment

Bearing steels used to manufacture bearing rings and balls were mentioned in introduction part. Among these steels AISI E52100 is the grade used for production of sample batch of ball bearings for the life cycle tests in this thesis. Steel was

purchased in conformity with the related ORS Specification which is strictly describing all parameters for bearing quality steel. Incoming steel quality control results for the cast number used for thesis work are given in *Table 1.1*.

Table 1.1 Quality Control Results of Steel Cast

Steel Making Process													
Electric Arc Furnace, Ladle Refining, Vacuum Degassing, Continuous Casting, Hot Rolling from 560x400 mm to Ø 40 mm.													
Chemical Composition (H and O are in ppm, all other in weight percent)													
C	Si	Mn	P	S	Cr	Mo	Ni	Cu	Sn	Al	H	O	Ti
0.97	0.23	0.32	0.006	0.006	1.40	0.02	0.07	0.12	0.02	0.03	1.7	7	0.01
Micro Cleanliness Rating (ASTM E45-Method D)													
Thin Series				Heavy Series									
A	B	C	D	A	B	C	D						
1	0.5	0.0	0.0	0.5	0.0	0.0	0.0						
Grain Size (ASTM E112)													
6 - 8													
Carbide Banding (SEP 1520)													
CZ 6.2 – 7.1													

Inner and outer rings are both produced by hot forging from Ø 40 mm bar material. For production route see *Figure 1.5*. Spheroidize annealing is performed and metallurgical inspection in terms of carbide structure (carbide banding, carbide size and shape, carbide network, lamellar cementite content etc…) is performed on the samples taken from the batch according to SEP 1520. As expected, completely

globular cementite homogeneously distributed in ferrite matrix observed under microscope and all parameters checked were within the limits of a well solidified casting and spheroidized microstructure. Cold rolled and machined rings were brought to the workshop where they were heat treated for hardening.

Heat treatment related to metals, from a general perspective, is thermal cycling including subsequent heating and cooling of metal parts in a way to obtain desired microstructure and so the properties. There are several types of heat treatment for different purposes such as, stress relieving, normalizing, homogenization, hardening, carburizing, nitriding, ageing, sintering, tempering etc… All are performed to obtain desired strength, toughness, ductility, wear resistance and similar mechanical and also physical properties. AISI E52100 is a through hardening grade bearing steel as previously mentioned. So the rings are quenched and tempered in order to achieve tempered martensite microstructure through out the whole cross section.

In classical application, during hardening of parts, manufactured from AISI E52100 bearing steel, are heated up to austenitization temperature (800 – 900 ^{O}C) and soaked for a while (30 minutes up to 1 hour) in order to be sure about full austenite microstructure, then immediately dropped into cooling medium, namely quenched, in order for rapid cooling below M_{90} where minimum 90% transformation into martensite is completed. During quenching surface and core part of the component are not cooling with the same rate so a thermal gradient is developed. Due to this temperature difference thermal stresses are become exerted within the component. Beside these stresses, if stresses due to phase transformation are also added distortion of the part geometry, in the worst case even cracking may be encountered. Distortion of bearing rings during heat treatment is nightmare of the heat treater and must be kept at minimum. Several parameters like austenitization temperature, cooling rate during quenching, steel compositional homogeneity, geometry affected cooling rate differences on the ring, residual stress state before austenitization, charging style of the rings into the furnace and quenching medium, texture developed during preliminary manufacturing processes like forging and cold rolling etc… are effective

in development and control of distortion during hardening but this is out of the scope of this thesis. Aiming minimization of distortion of bearing rings a delayed quenching process which is called martempering is employed in ORS (CCT diagram is given in *Figure 1.6*). As can be seen form the figure, as quenching environment, one of single oil tank (Safed furnace cooling curve), double oil tank or salt bath is used. For the rings of this work double oil tank quenching is applied.

Martempering is rapid cooling from austenitization temperature to just above or below M_S (martensite start) temperature, holding in the quenching medium for the temperature gradient between core and surface to become zero, finally after uniform temperature through the cross section is get, cooling moderately to prevent temperature difference between inside and outside during transformation into martensite (ASM International, 1995).

Large stresses are developed during austenite to martensite transformation due to volume increase, so before transformation starts uniformity of temperature between center and surface is being obtained in martempering during bearing ring hardening. Subsequent cooling makes center and surface to be transformed into martensite so to have volume increase at nearly the same time. By the way distortion during heat treatment is minimized. Quenching temperature for martempering is chosen just below M_S in our case due to the risk of bainite structure formation and bainite in the microstructure is not allowed.

Martempering of bearing rings results in a microstructure mainly globular carbides distributed in martensite matrix plus a small restricted amount of retained austenite.
Because austenite at room temperature is an unstable phase, has a risk of transformation during temperature or stress application so resulting in unwanted dimensional alterations during service of the bearing. But also some amount of residual austenite is known to be beneficial in terms of crack arrest during fatigue so depending on the bearing type retained austenite percent is limited and specific.

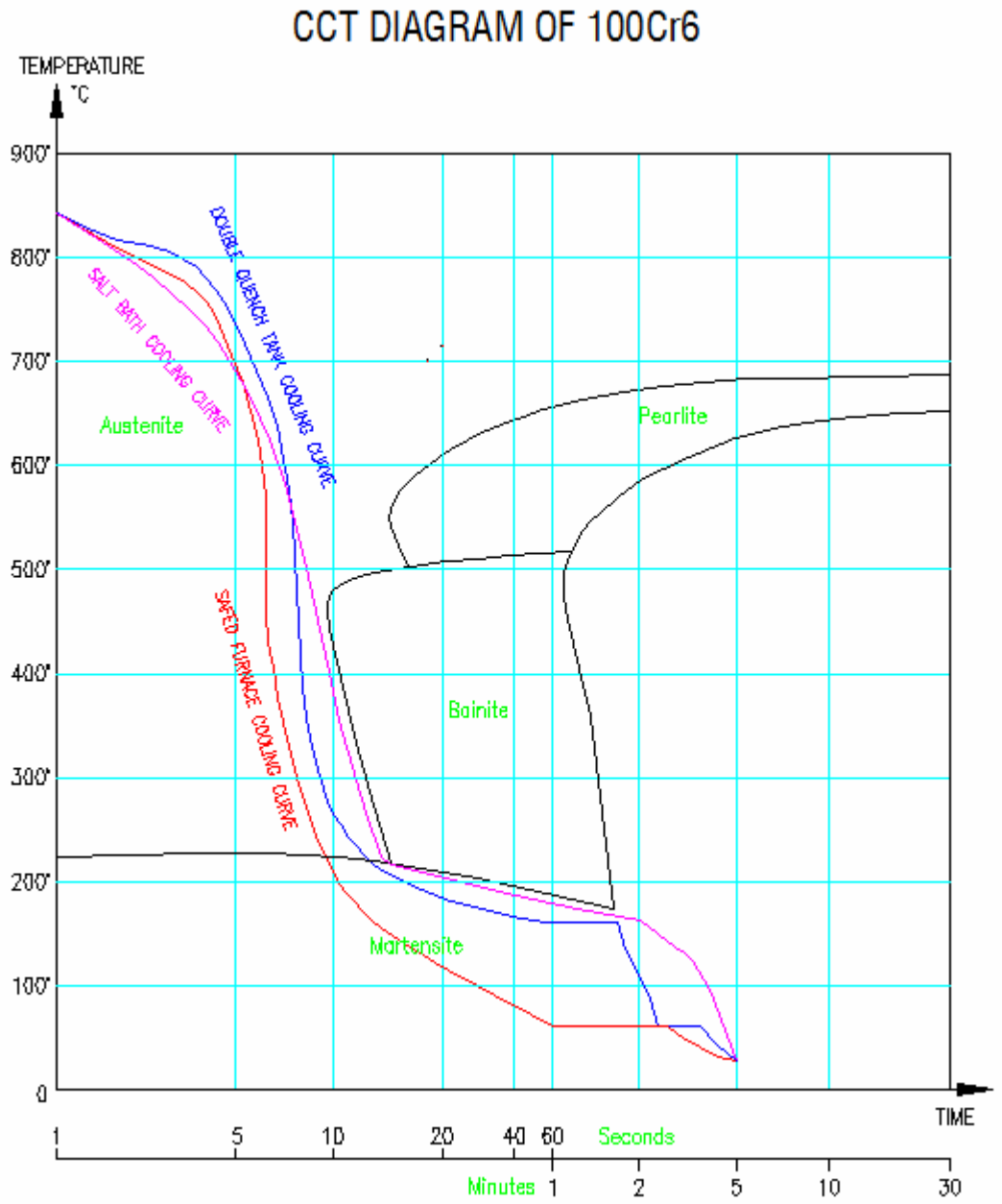

Figure 1.6 Continuous Cooling Transformation Diagram.

To achieve dimensional stability and some toughness by reduction of as quenched brittleness by allowing some diffusion to occur and transformation of austenite, tempering is applied between the temperatures 170 - 350 ^{O}C with duration of 90 – 120 minutes and some times double tempering depending on the application. Inner

ring, outer ring and balls have the same microstructure at the end of hardening and sample microstructure can be seen in *Figure 1.7*.

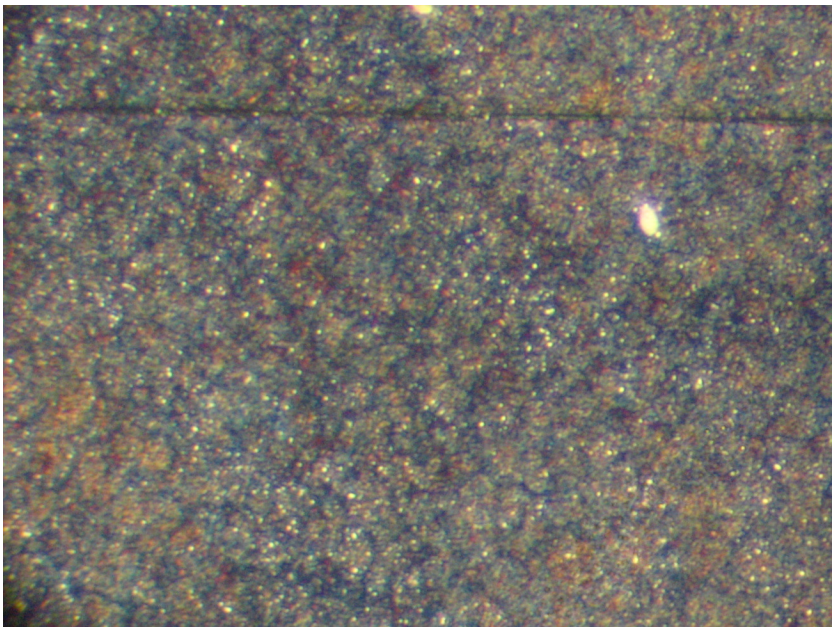

Figure 1.7 Optical Microscope Image of Quenched and Tempered AISI E52100 Steel (Magnification 500X)

Martensite in steels is a hard, strong and wear resistant phase. Hardness of martensite is due to internal strains present, very fine grain structure, large amount of dislocations formed during quenching and carbon atoms in the form of solid solution. So, all strengthening mechanisms are valid for martensitic structure of AISI E52100. However it is a very brittle structure due to low ductility and toughness. As quenched hardness is 65 ± 1 HRC and after tempering due to diffusion of carbon atoms and annihilation of some quenching dislocations also relief of internal strains some ductility and toughness is won by martensite. Tempered hardness is 53 – 63 HRC depending on tempering temperature and time. For the bearing type used in this thesis, allowed hardness after tempering was 61 ± 2 HRC.

Residual stresses during heat treatment of bearing rings are developed from the start of cooling after austenitization. Thermal stresses, due to contraction amount difference of core and surface when yield point is low due to high temperature put the surface under tension while core is under compression before the start of martensitic transformation and deform plastically the rings in an inhomogeneous manner. Thanks to the delayed quench during martempering, almost all transformation of center and surface takes place together. As a consequence of this plus the tempering makes surface stresses of rings to be nearly zero. So, among the effects of heat treatment, only residual stress developing reason can said to be thermal gradient throughout the cross section.

Distortion due to residual stresses before heat treatment, compositional inhomogeneity and geometrical factors etc… are not related with heat treatment. Thermal gradient is affected by austenitization temperature, quenching bath temperature and agitation, quenching medium cooling characteristics. Tempering time and temperature also has an effect on the final stress distribution. Güley (2004) worked on the effects of austenitization temperature, temperature of the bath, rinsing water temperature and tempering temperature on final residual stresses developed and observed the results tabulated in *Table 1.2*. Also an example stress distribution in circumferential and axial directions after heat treatment is given in *Figure 1.8* for more clear illustration of subject.

Table 1.2 Effects of Heat Treatment Parameters on Residual Stresses

Parameter	Austenitization Temperature	Oil Bath Temperature	Water Temperature	Tempering Temperature
Effect	Moderate	Important	Poor	Moderate

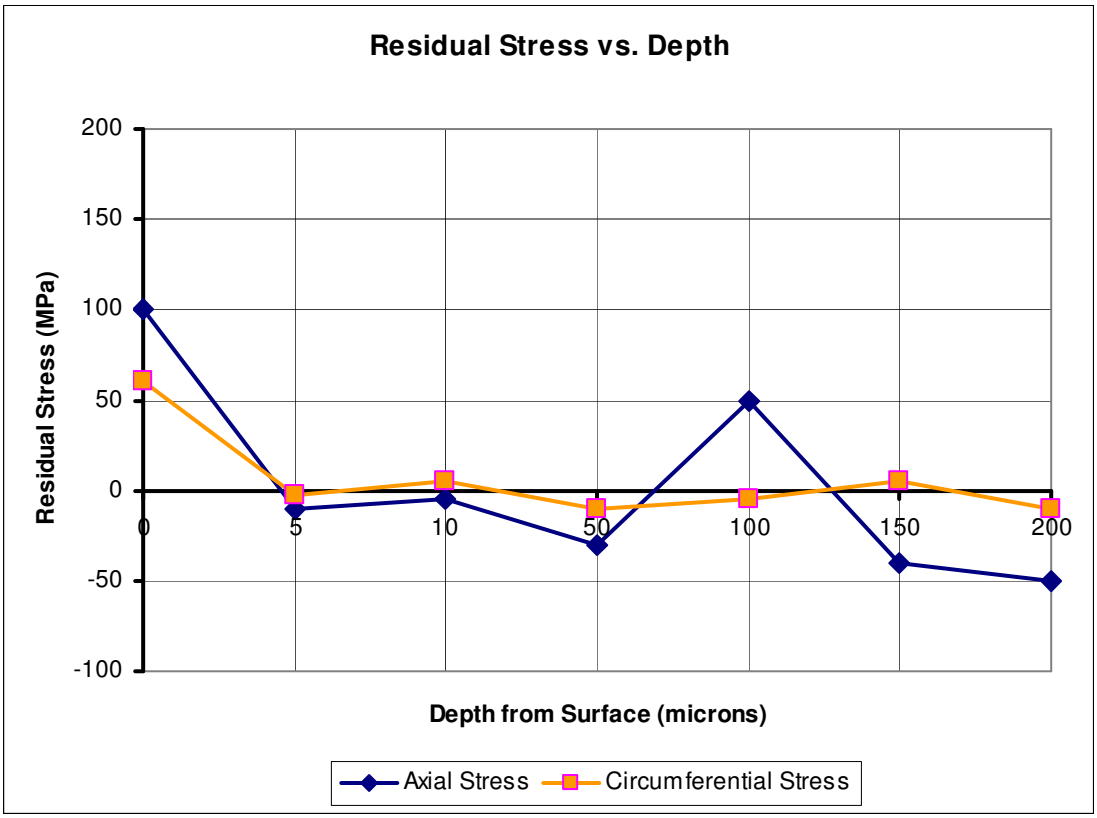

Figure 1.8 Residual Stress Distribution of a Bearing Ring After Being Quenched and Tempered

1.8.2 Residual Stresses Induced by Grinding

Grinding after heat treatment is the first process during which surface residual stresses are starting to be shaped. Grinding is basically a chip removal process in which the cutting tool is an individual abrasive grain (Kalpakjian, 1991). Abrasives commonly used in grinding are aluminum oxide (Al_2O_3) and silicon carbide (SiC) conventionally but for some applications super-abrasives namely cubic boron nitride (CBN) and diamond are used. Abrasives are very small compared to cutting tools and inserts and have sharper edges so they allow the removal very small quantities of material from the workpiece surface. As a consequence very fine surface finish and dimensional accuracy can be obtained.

Grit number is the number identifying the grain size of abrasive. The smaller is the grain size, the larger the grit number. Grinding wheels are bonded abrasives. Bonding types are mainly vitrified, resinoid, rubber and metal. Grade of a bonded abrasive, like in grinding wheels, is a measure of bond strength. Because strength and hardness are directly related grade is also said to be hardness of the wheel. Thus, a hard wheel has a stronger bond and larger amount of bonding material between the grains. In terms of structure of a wheel porosity is the main concern. Structure depending on the level of porosity ranges from open to dense.

Temperature effect is an important point of concern during grinding. Thermal gradients can distort the workpiece because of differential expansion and contraction. Excessive temperature rise can result in tempering effect of the hard surface and make it soften. Even sometimes metallurgical phase transformation of the workpiece surface by reaustenization followed by rapid cooling and martensite formation can take place. This is called metallurgical burn. This untempered, very brittle martensite surface layer is very dangerous in terms of service life. Thermal cracks may also sometimes form which is known as heat checking. Avoiding these defects is possible only by a strict control of grinding process parameters and by use of grinding fluids.

Residual stresses are formed due to temperature change and gradients within the part during grinding. Other factors contributing are the interaction of abrasives in material removal by chip formation and sliding of the wear flat along workpiece surface, causing plastic deformation. Because of the deleterious effect of tensile residual stresses on fatigue strength parameters like grinding wheel grade, wheel speed, workpiece speed, feed rate and spark out time must be well chosen and controlled.

Bearing rings are hard ground for dimensional precision before super-finishing. For outer rings; centerless grinding of face and outer diameter and finally raceway grinding is utilized, while for inner rings; centerless face grinding, raceway grinding and bore grinding are employed. In terms of fatigue raceways are critical surfaces because ball bearings fail due to fatigue on the raceways, so raceway grinding to be

focused on among grinding operations. In *Figure 1.9 raceway grinding is* schematically represented.

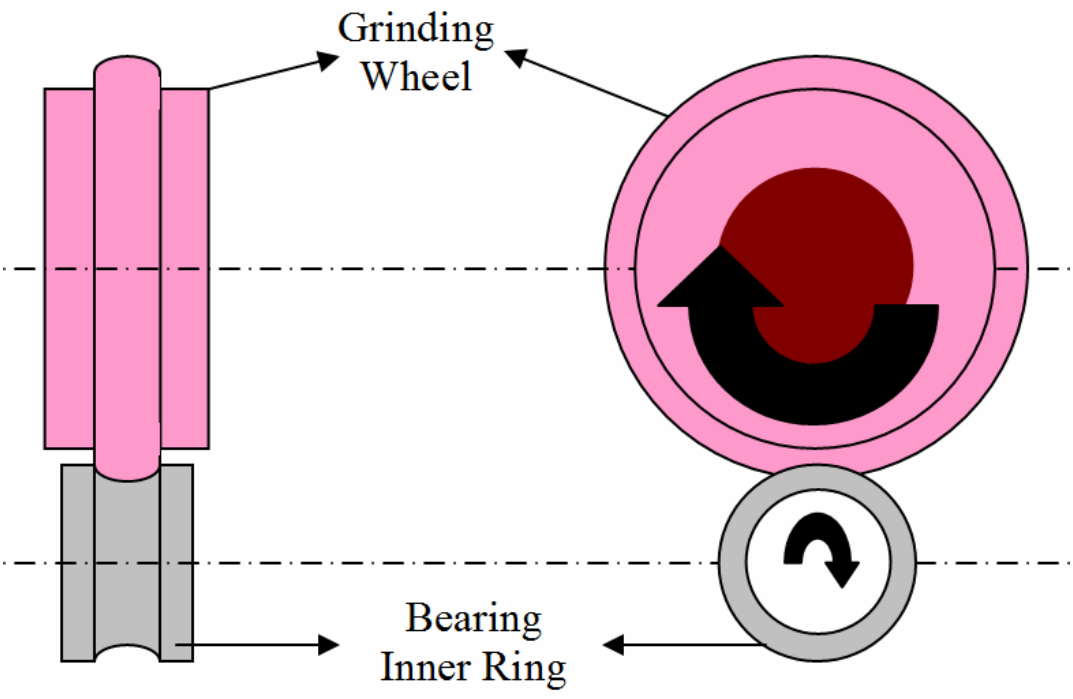

Figure 1.9 Illustration of Raceway Grinding of a
Single Row Ball Bearing Inner Ring

As can be seen from *Figure 1.9* bearing ring and grinding wheel are turning in the same direction but this cause counter movement at the point of contact so abrasion of steel chips from the raceway surface. As the wheel and workpiece revolve, the depth of cut gradually increases somewhere along the arc of contact of the wheel and the workpiece. Since the wheel usually rotates much faster than the work, the point of maximum cut depth is almost at the point where the wheel leaves the work. This maximum depth is known as the grain depth of cut (Society of Manufacturing Engineers, 1976). To the end of the production cycle grinding wheel just rotates without any feeding for a few seconds known as spark-out time.

Residual stresses developed on the raceway during grinding depend on grinding wheel selected (grade, structure etc…), cooling fluid, ring rotation speed, wheel rotation speed, feed rate, spark out time etc… Among these, Güley (2004) investigated the effects of spark out time, feed rate and workpiece speed in order to find optimum grinding sets while all other parameters are fixed according to ORS standard application and observed the results tabulated in *Table 1.3*.

Table 1.3 Ball Bearing Inner Ring Grinding Parameter Sets
For Favorable Residual Stress State (Güley, 2004)

Feed Rate (mm/sec)	**Ring Speed (m/sec)**	**Spark Out Time (sec)**
0.045	2.17	3

In this thesis work grinding parameters will not be investigated and kept out of scope, standard ORS grinding parameters are used during grinding of the test rings.
Residual stress distribution of a deep grove ball bearing inner ring raceway is exemplified in *Figure 1.10*.

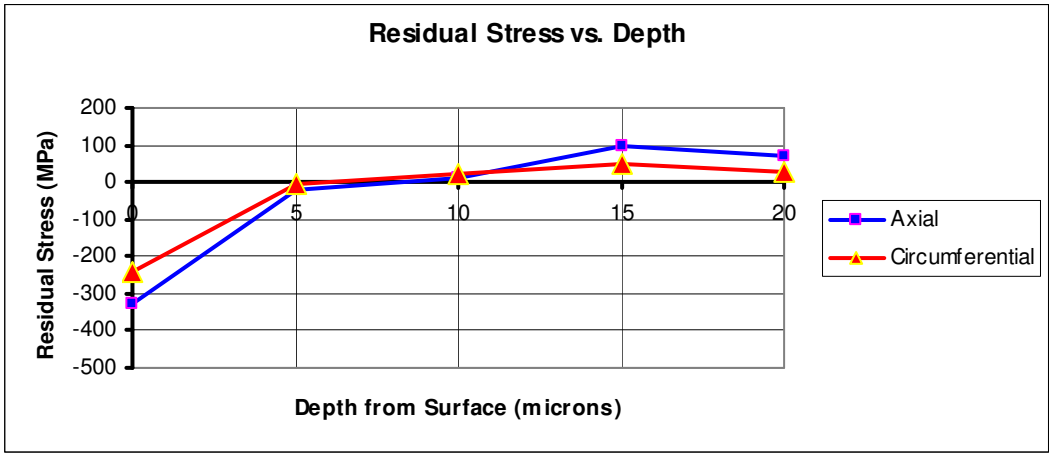

Figure 1.10 Residual Stress Profile on Raceway after Grinding.

1.8.3 Residual Stresses Induced by Super-finishing

Super-finishing is applied as final machining operation, namely finishing operation for bearing ring raceways in order to reach a fine surface finish having a surface roughness at nanometer levels. The tool used consists of a set of aluminum-oxide or silicon-carbide bonded abrasives and called as super-finishing stone. Stone is making an oscillation motion to radial left and right just like pinned to a center of a circle when the ring is rotating so producing a cross-hatched pattern on the raceway surface. Total stone motion is said to be sinusoidal. A schematic illustration of raceway super-finishing is given in *Figure 1.11*. The fineness of surface finish can be controlled by the type and size of abrasives, the speed of oscillation and ring rotation and the pressure applied. A fluid is again utilized to remove chips and keep temperatures low. The pressure applied is very light and stone motion has a short stroke. Process is controlled so that the grains do not travel along the same path along the raceway surface.

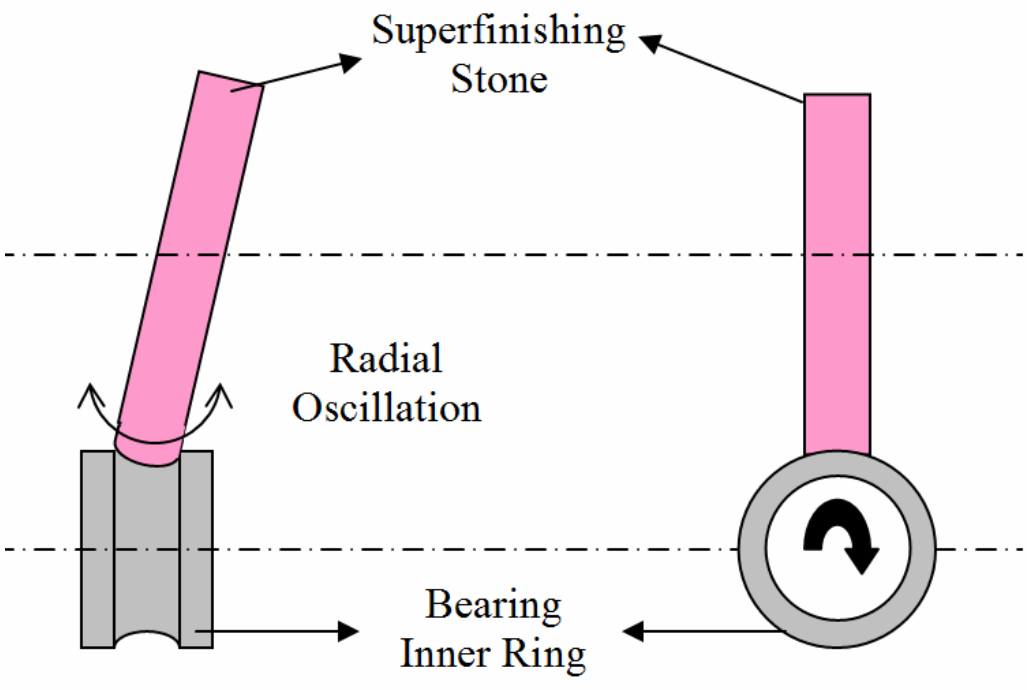

Figure 1.11 Schematic Illustration of Raceway Super-finishing of a Single Raw Ball Bearing.

The object of super-finishing is to remove surface fragmentation or smear metal, to correct inequalities in geometry such as grinding flats, and to restore surface integrity by eliminating surface stresses and burns (Society of Manufacturing Engineers, 1976). The metal removed from the surface is by shear cut and thanks to the sinusoidal stone movement in different directions. However, the aim of super-finishing is not material removal, in fact surface quality improvement by decreasing the average roughness (Ra) is aimed. Target Ra value is below 0.1 μm for bearing ring raceways.

Residual stress effect of super-finishing is related to super-finishing stone grade, cooling conditions, pressure, oscillation speed, ring rotation speed and application time. From these parameters Güley (2004) focused on the final three. The other parameters were kept constant as in ORS practical sets. His founding is given in *Table 1.4* for the best residual stress state for 6205 type inner ring.

Table 1.4 Super-finishing Parameter for Favorable Residual Stress State on 6205 type Bearing Inner Rings

Stone Oscillation Speed (cpm)	**Ring Rotation Speed (rpm)**	**Application Time (sec)**
158	2850	6

From the above given results, in terms of compressive residual stress profile development, the best super-finishing stone angle of movement can be achieved by 18 rotation of bearing ring when 1 oscillation of super-finishing stone completed. So for the work done in this thesis 18 rotation/cycle ratio is used during super-finishing of the test rings. The process parameter which the effect on residual stress is investigated in this study is the *pressure*.

In *Figure 1.12* a sample residual stress distribution on raceway after super-finishing can be see.

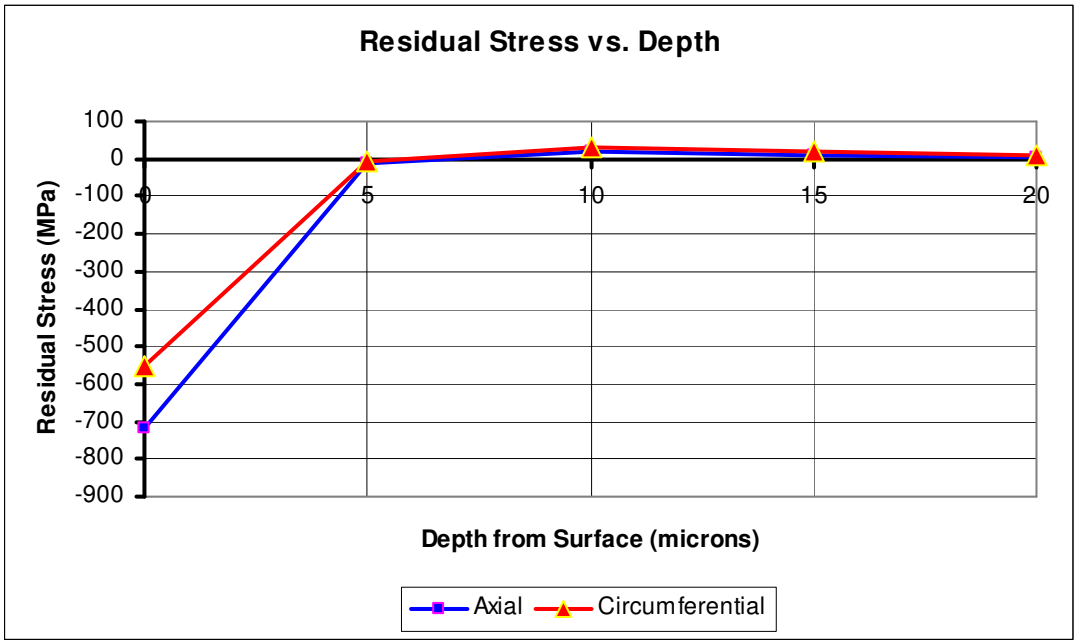

Figure 1.12 Residual Stress Profile on Raceway after Super-finishing.

1.8.4 Residual Stresses Induced by Shot Peening

Shot peening is a process of cold working the surface of structural or machine components by means of bombarding the surface by driven stream of hard shots (Almen, 1963). Shots used to hit repeatedly in order to form overlapping indentations on the surface to be strengthened are generally cast steel, chilled cast iron, conditioned cut wire, glass or ceramic small balls. By imparting compressive residual stresses on the applied surface due to causing nonuniform plastic deformation across part cross section shot peening improves fatigue life of components.

The discovery of the improvement in fatigue properties from shot peening originated from blasting of valve springs with grits by Buick Motor Division of General Motors. Blasting was conducted for the purpose of removing spots of scale but it was found that the fatigue properties of springs were remarkably improved. In the early stage it was thought that improvement was due to work hardening of the surface material, but soon learned the major part of benefits arise from the compressive stresses induced on surface (Almen, 1963).

Shot peening machines accelerate the shot on to the workpiece surface by either compressed air or by centrifugal means. With the impact taking place, kinetic energy of shots is transferred to the energy needed for deformation or phase transformation. Schematically the process of peening is given in *Figure 1.13*.

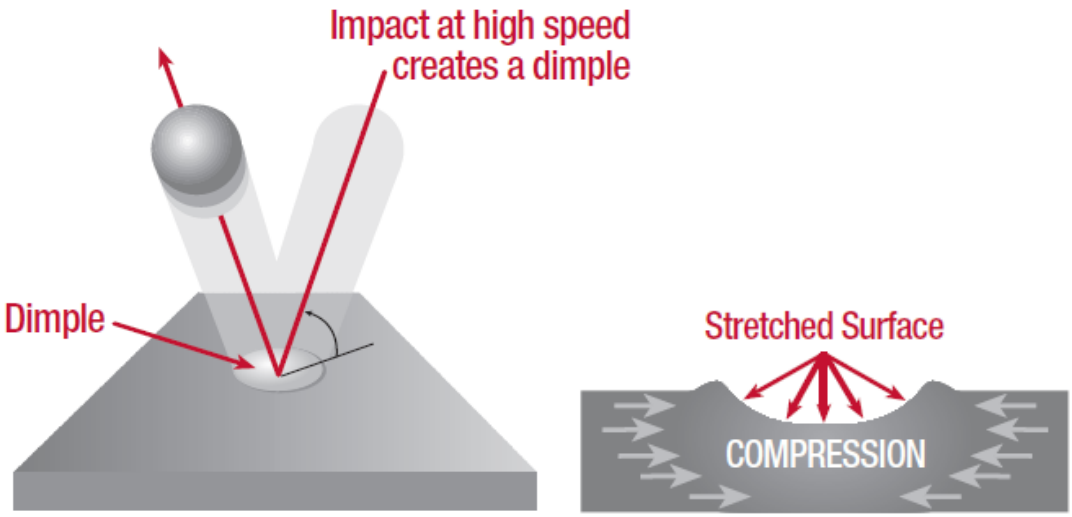

Figure 1.13 Schematic Illustration of Shot Peening Process
(Metal Improvement Company, 2005)

Quality of shot peening is determined by the magnitude, the depth of residual stress induced and coverage of the surface. For control of shot peening standard steel specimens or test strips known as Almen Strips are used (SAE International, 1997).

Standard Almen Strips are shown in *Figure 1.14*. Test strips are produced from cold rolled SAE 1070 grade spring steel, uniformly hardened and tempered to 44-50 HRC. They must be flat before shot peened in a ± 0.038 mm arc height range. For the purpose of intensity determination Almen Strip is attached to a holder of the form described by AMS-S-13165, mounted on a fixture and exposed to shot stream in a manner which simulates conditions used for the workpieces. After exposure, test strips are removed from the holder and the amount of deflection is measured by a micrometer. The arc height measured gives the intensity of shot peening which is the overall effect of induced stress.

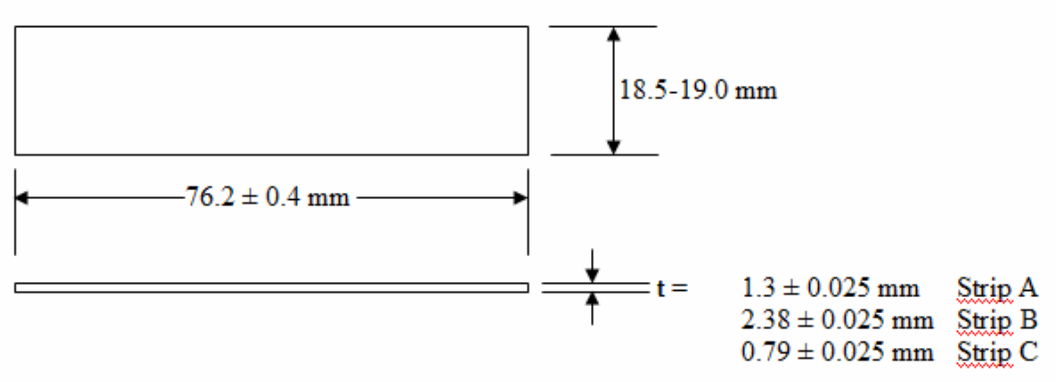

Figure 1.14 Almen Test Strips According to AMS-S-13165

Shot used generally for steel components that has a tensile strength greater than 1375 MPa are hard steel shot in the range of 55-65 HRC or ceramic shot with hardness in between 57-63 HRC. SAE International (1997) Standard describes the shot sizes and minimum dimensions for peening of certain intensity limits. Steel shots must be checked at least every 8 hours of operation to assure that not more than 10% of the batch by actual count is deformed or broken. Selection of shot size is done according to the workpiece shape, size of fillets (small shot for smaller fillets) and desired intensity and surface finish (larger shot for higher intensity and better surface finish at equal intensity).

Saturation curve for initial process development is utilized and very important for shot peening. The curve is plotted by exposing individual test strips for increasing time periods and plotting exposure time versus arc height. Saturation is said to be achieved when the exposure time of the test strip is doubled and the arc height does not increase by more than 10%. Peening over saturation time is generally not necessary or desirable.

Coverage of the shot peened surface must be 100% for a successful peening. For control of coverage; a control specimen of the actual workpiece is prepared by coating the related surface with a tracer fluorescent fluid. After checking the specimen under ultraviolet light in order to be sure that it is completely covered by the tracer fluid after drying, shot peening is applied with specified parameters for 100% coverage and is reexamined under ultraviolet light. If the tracer residue is completely removed coverage is said to be okay, otherwise further work is necessary to achieve 100% coverage.

Intensity developed as a result of shot peening, meaning the residual stress, depends on the shot flow rate, air pressure or centrifugal wheel speed, impact angle, distance of nozzle to the workpiece surface, relative motion of workpiece and nozzle (vertical nozzle velocity, workpiece rotation per minute), shot size, shot shape and hardness and coverage (Metal Improvement Company, 2005). Residual stress profile for a ball bearing inner ring which is developed after the application of shot peening is given in *Figure 1.15* for clear illustration of application reason to the bearing inner rings as scope of this study. In this thesis work focus is located on the following parameters:

- Compressed air pressure
- Shot flow rate
- Coverage

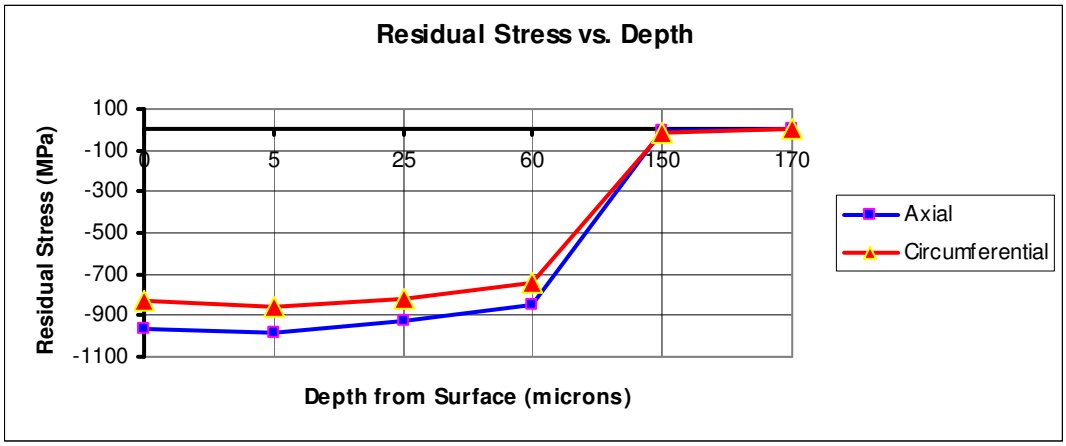

Figure 1.15 Residual Stress Profile on Raceway after Shot Peening.

1.9 Aim of the Study

Surfaces subjected to repeated rolling and sliding contacts under high loading are exposed to contact fatigue. It is a major failure cause in mechanical applications, such as ball bearings. Failure of almost all ball bearings, under normal service conditions which are described in specifications are obeyed, reaches to end by fatigue phenomena on their raceways. So, the endurance of bearing steel to metal fatigue has been a major concern for ball bearing producers.

The surface damage created by rolling contact fatigue has been given various names in the literature. The damage starting with a subsurface crack formation and as this crack propagates due to cyclic loading ends up with metal particles breaking away from the raceway of the ring forming millimeter sized crater, namely spall is called spalling (Tallian, 1992). For improvement of the fatigue life, so the life time of rolling bearing, spalling has to be prevented or delayed. In this respect, residual stress state on bearing rings is very important. Residual compressive stresses are known to be very beneficial in terms of rolling contact fatigue life of bearings because of the fact that cracks can not form and propagate easily as in the case where residual compressive stresses are absent. By knowing these, the main aim of this

study is stated as the optimization of residual compressive stresses on the raceways to prolong the fatigue life of ball bearings.

Within this thesis work, shot peening of bearing inner rings in order for improvement of compressive residual stress state, both the magnitude and especially the depth, is employed. Application is done on the inner rings because as an experience of failure analysis performed in ORS by the author, most of deep grove ball bearing service life terminations under normal working conditions occur from inner ring fatigue. Reason for this is known to be the load carrying surface, namely contact surface with the balls for inner rings is smaller in comparison to the outer rings due to geometry, so contact stresses are higher on the inner rings, and in most applications outer ring is stationery and inner ring is rotating so prone to cyclic loading with a higher frequency.

Residual stress development during the processes after martempering is shaping the final residual stress state on the raceways, so focus in this work is on the final process, super-finishing and mainly the shot peening that is applied before super-finishing. Information about quenching and tempering, grinding, shot peening and super-finishing are summarized in Chapter 1.

In Chapter 2, recent literature and the work done on shot peening is presented, and the effect of residual stresses on fatigue life is discussed briefly. Chapter 3 gives the required theoretical background about shot peening and residual compression development, X-ray diffraction residual stress and retained austenite measurement.

In Chapter 4, introduction of shot peening facility and X-ray diffraction measuring facility, fatigue life test equipment and procedure are given. The effect of process parameters in shot peening and stone pressure in super-finishing are investigated in Chapter number 5.

Fatigue life tests, evaluation of test results and correlation of residual stress and life duration of tested bearings are investigated in Chapter 6. The discussion of the results obtained and conclusion takes place in Chapter 7. Recommendations and suggestions regarding further work on this topic are presented in Chapter 8.

CHAPTER 2

LITERATURE SURVEY

Throughout this chapter, work related to the current study as literature is reviewed and discussed. Residual stress and fatigue relationship during rolling contact, shot peening and super-finishing process parameters and residual stresses are summarized.

2.1 Fatigue and Residual Stress

All dynamically loaded machine elements, also as in rolling bearings, in modern high-duty machines suffer or benefit from residual stresses. The purpose of this section is to review studies conducted on how residual stresses affect the functioning of compressively loaded rolling bodies.

Every rolling bearing rotating under load above the endurance strength limit has a definite fatigue life depending on the number of cycles and the load. A crack is created and it often originates from a predamaged spot on the raceway surface, perhaps a particle indentation (Brändlein et al., 1999). Although the damage process is not fully understood some events are confirmed (Tallian, 1992). Failure process can be divided into three phases. During the first phase, bulk changes in the material structure occur in the highly stressed volume under the contact path. Changes may occur in hardness, residual stresses, austenite and martensite structure. The surface roughness is decreased through reduction of both asperity heights and asperity sharpness through wear and local plastic deformation (Voskamp, 1985). In the second phase, deformation bands, described as white etching areas, are created by the

micro-plastic flow. When created around a defect such as an inclusion or an asperity they may be designated as butterflies. Sometime during this stable phase micro-cracks are initiated at defect locations within the plastically deformed material. The micro-cracks usually occur at the contact surface or between that and the depth of maximum Hertzian shear stress. Even if the stresses induced by cyclic loading between rolling elements and raceways are generally below the fatigue limit, additional stresses can be caused locally by material inhomogenities and defects acting as stress concentrators. These stresses are superimposed on those arising due to normal bearing operation (Voskamp, 1997). When numerous micro-cracks initiate at the surface the phase is named surface distress. As one of these micro-cracks grows, a macro-crack is formed and the last phase of the spalling failure process starts. The macro-crack, driven by high Hertzian stresses, propagates down into the material to a level corresponding to the maximum Hertzian shear stress where it turns to a surface parallel direction. In bearing applications the macro-crack branches upward to the free surface to create a spall, bounded by fracture surfaces. Spalling fatigue and surface distress are the most frequently occurring types of metal fatigue damage in bearings (Voskamp, 1997). A spalled deep grove ball bearing inner ring can be seen in *Figure 2.1*.

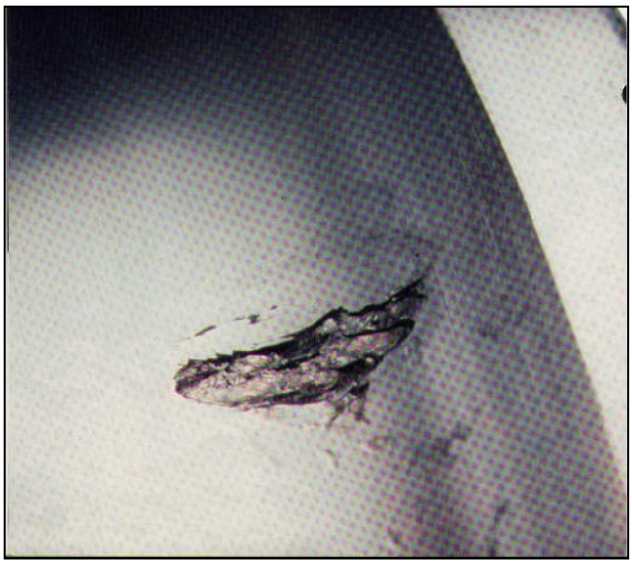

Figure 2.1 Spalling on Raceway of a Deep Grove Ball Bearing Inner Ring.

In terms of fracture mechanical approach, combined mode I (tearing under tension) and II (sliding under shear) fatigue loading, as exist during the spalling macro-crack propagation phase, has been reviewed by Qian et al. (1996). These reviews indicate that the possibility to propagate a crack in another direction than mode I is dependent on material, load magnitude and loading sequence. Thus, in hard bearing steel subjected to mode I and mode II load, other directions of crack propagation other than mode I is unlikely. Gao et al. (1985) performed mixed mode (mode I and II) fatigue propagation experiments on steel and stated that; the effect of a mode II field is twofold: Firstly, the crack will turn towards the pure mode I direction and secondly, the mode II field reduces the mode I fracture toughness threshold, and therefore promote crack propagation.

Experiments by Lorösch (1982) on smooth surfaces and clean lubricants, without asperity contact, show a significant increase in life and a different, sub-surface initiated spalling damage. This crack is produced by tensile residual stresses. However, tensile stresses normal to the crack face are responsible for both surface and sub-surface initiated contact fatigue.

Voskamp (1997) tested 6209 type ball bearings produced from AISI E52100 steel in order to evaluate the effect of residual stress on their fatigue life and concluded that; in the case of a rolling contact fatigue as experienced by the inner ring of a ball bearing, fatigue life is shortened if tensile residual stresses occur in the axial and circumferential directions parallel to the inner ring surface. However, such kind of tensile residual stresses are impossible with normal bearing ring manufacturing route and only possible due to grinding abuse (grinding burns).

Widmark et al. (1999) performed contact fatigue resistance tests in a roller to roller rig. Two carburizing grade steels were used and the parts are tested in a lubricant with impurities. From the tested samples, the shot peened samples gave the least amount of contact fatigue damage.

Agha et al. (2000) investigated specimens that were hard turned using different cutting parameters produced form AISI 52100 with hardness of 62-63 HRC. Surface roughness, residual stress, and micro-hardness were measured. The workpieces were then tested for the rolling contact fatigue life under several maximum Hertzian contact stresses. Results indicate that the choice of the cutting parameters greatly affects the surface integrity aspects of the hard turned parts and consequently, the fatigue life. Finally it is concluded experimentally; the effect of cutting conditions is very significant on the fatigue life of the hard turned workpieces. The differences in fatigue life can be 40 times for the range of the cutting conditions used.

The study on contact fatigue mechanisms performed by Alfredsson (2000), adds to the understanding of how and why contact fatigue develop. The research work focuses on a new test procedure named Standing Contact Fatigue (SCF). Work done includes test analysis and implications for the understanding of rolling contact fatigue, supported by the experimental findings. Recommendations of this work are as given below:

- Surface irregularities such as asperities serve as local stress raisers in the surface. A smooth surface in combination with good lubrication conditions will prevent surface initiation of spalls.
- Wear particles and other contaminations can destroy an initially smooth surface. An indentation leading to an asperity or adhered contamination will be more detrimental than a small crater. Note that once contaminations have been present and created surface irregularities the surface resistance to spalling is decreased.
- Compressive residual surface stresses counteract the local tensile stresses from asperities and will therefore give extra protection against surface initiated spalling.
- Plastic deformation below the surface from the maximum Hertzian shear stress leads to tensile residual stresses perpendicular to the surface. These stresses will eventually be responsible for sub-surface initiated spalling.

Hardened surfaces with high compressive residual surface stresses can better withstand plastic deformation below the surface.

- Sub-surface material inclusions serve as local stress raisers and crack initiation sites. If plastic deformation from the maximum Hertzian shear stress is present below the surface, then the residual tensile stresses from this macro-scale plastic deformation will continue to propagate the micro-cracks initiated at the inclusions.

Webster et al. (2001) evaluated the influence of residual stress distribution on fatigue lifetimes of structural engineering components. Residual stress profiles are obtained by neutron diffraction method. Examples of beneficial stresses produced by such processes as autofrettage, cold hole expansion and shot peening are presented. It is demonstrated that, provided an accurate knowledge of the residual stress profiles generated is available and allowance is made for stress redistribution and the multiaxial nature of residual stresses, reliable predictions of fatigue performance can be made. Relation of maximum residual stress and fatigue strength obtained is given in *Figure 2.2*.

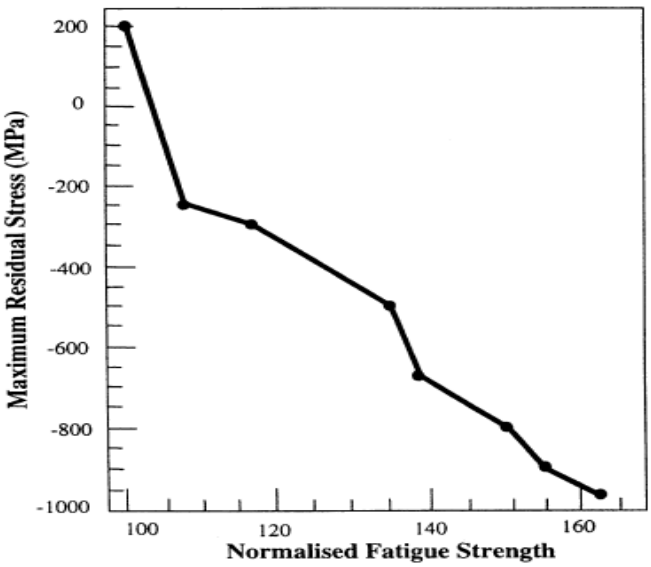

Figure 2.2 Improvement in Fatigue Strength due to Near Surface Compression Induced by Shot Peening (Webster, 2001).

From all the above reference studies, compressive residual stresses on rolling contact surfaces are understood to have a positive contribution on fatigue life. However, residual stress relaxation reduces this benefit. Zhuang et al. (2001) worked on the residual stress relaxation under cyclic load and investigated the mechanism behind this relaxation. An analytical model is proposed in this work but also stated the need for an experimental study on cycle-dependent residual stress relaxation is required to benchmark the analytical and numerical models.

Torres et al. (2002) investigated the gain in fatigue life of AISI 4340 steel, used in landing gear, under four shot peening conditions. Rotating bending fatigue tests were conducted and the compressive residual stress field (CRSF) was measured by an X-ray diffraction prior and during fatigue tests. It was observed that relaxation of the CRSF occurred due to the fatigue process. It is observed that the shot peening treatment pushes the crack sources beneath the surface in most of medium and high cycle cases due to the CRSF induced.

Güley (2004) conducted several life cycle tests with different residual stress levels on raceways of ball bearing rings. For obtaining different residual stress distributions, grinding and super-finishing parameters are changed. Residual stresses are measured by X-ray diffractometer. Experimentally found that compressive residual stresses in the loading zone leads to longer fatigue lives.

2.2 Shot Peening and Residual Stress

Knowing the benefits of residual compression on rolling contact surfaces in improvement of fatigue behavior the process of bombarding the raceways with hard steel balls, called shot peening, for mainly developing compressive residual stresses to higher depths from surface is applied. Through out this section studies about shot peening and residual stress results obtained on hard steel components are reviewed.

Gain in fatigue life of AISI 4340 steel, used in landing gear, is evaluated under four shot peening conditions by Torres et al. (2002). Rotating bending fatigue tests were conducted and the residual stress profile was measured by an X-ray tensometry prior and during fatigue tests. An increase in shot peening intensity resulted in an increase in the maximum compressive residual stress and of the residual stress depth. However, the surface residual stress was nearly independent of the peening conditions. Measured residual stresses after fatigue tests and peening intensities are tabulated in *Table 2.1*. It was concluded that; it is very complex to determine the best shot peening condition to increase the fatigue strength, because it depends on many variables.

Table 2.1 Residual Stress Values after 10^5 Cycles (Torres et al., 2002)

Almen A Intensity	Depth (mm)			
	0	0.05	0.10	0.15
0.0063	-660 MPa	-600 MPa	-420 MPa	-40 MPa
0.0083	-480 MPa	-570 MPa	-120 MPa	-60 MPa
0.0141	-870 MPa	-460 MPa	-430 MPa	-250 MPa

A fatigue crack initiates at an early stage even if the applied stress range is lower than the fatigue limit. To increase the fatigue limit, it is important to arrest the fatigue crack at the beginning of its propagation. The improvement of fatigue properties by increasing the compressive residual stress is due to decreasing the effective tensile stress at the crack tip. The mechanism by which compressive residual stress improves the fatigue strength was studied by Naito et al. (Nippon Steel Corporation). Analyzed the process of fatigue fracture and the way for increasing the compressive residual stress in carburized steels by shot peening was investigated. The results obtained are as follows:

- It is important for increasing fatigue limit to arrest the fatigue crack at the beginning of its propagation.
- The improvement of fatigue properties by increasing the compressive residual stress is due to decreasing effective tensile stress at the crack tip.
- The compressive residual stress of gear surface is effectively increased by increasing the peening intensity.

Hashimoto et al. (Sumitomo Heavy Industries), in order to clarify precisely the effects of shot peening on the fatigue strength of carburized gear steels, investigated residual stress, retained austenite and hardness in the surface layers before and after shot peening and conducted fatigue tests also using fillet type specimens as a model of gear with two kinds of steels of carburized and shot peened. They observed that the maximum values of the compressive residual stresses as well as hardness near the surface layer increase by increasing duration of shot peening. And also they saw volume fraction of retained austenite gets to degregate gradually, according as the duration of shot peening become longer. And it was also found that the fatigue life strength is improved remarkably by shot peening because of the increases of the compressive residual stresses and hardness near the surface layer.

A series of rolling contact fatigue tests have been done by Hongbin et al. (Luoyang Institute of Technology) using carburized steel with and without shot peening. The distribution and change of the residual stress in the course of rolling were measured. The changes of microstructure were observed with TEM. Distributions of retained austenite before and after shot peening were determined by X-ray. They observed after having been carburized and shot peened, the specimens micro-hardness is raised, the defects are decreased, part of the retained austenite is transformed into the strain induced martensite, the dislocation density is increased, the substructures are refined in the surface layer and finally concluded that the contact fatigue limit can be raised by %6 or the contact fatigue life can be elongated about %30 at the lower contact stress by shot peening in the carburized steel 20CrMnTi.

Kobayashi et al. (1998) studied the mechanism of creation of compressive residual stress by shot peening via application of a static compression test and a dynamic impact test using a single steel ball against a flat steel plate. They observed and concluded, in the dynamic impact test, tensile residual stress was created near the center of the ball indentation mark and compressive residual stress was created outside the indentation and the tensile residual stress in the center of the first ball indentation mark changed to compressive stress as the density of the ball indentations surrounding the first indentation mark increased. So, the compressive stress formed by shot peening is considered to be the result of the superposition of residual stress produced by surrounding shots.

Effects of peening parameters on compressive stress development in carburized steels were examined by Seno et al. (Tokyo Heat Treating Co.). Various peening parameters consist of shot flow rate (15, 20, 27 kg/min.), exposure time (1, 5, 10 sec.), the distance between the tip of a nozzle and the work surface (100, 130, 180 mm), shot diameter (0.6, 0.8 mm) and shot hardness (HRC 53, 58) were investigated. Finally they concluded for the conditions of the study conducted, contribution of various peening parameters on compressive residual stress is in the following order: Shot hardness>exposure time>distance between the tip of a nozzle and work surface, shot flow rate, shot size.

Transmission electron microscopy (TEM) analysis of shot peened martensitic steel performed by Wang et al. (Xi'an Institute of Technology) showed that; shot peening can not change the dislocation array in martensitic steels because of the high original dislocation density in martensitic crystal. Additional dislocations caused by shot peening cannot be resolved by TEM, so that TEM analysis will not distinguish the difference between the microstructures before and after shot peening.

About the determination of residual stresses developed by shot peening, Prevéy (1990) worked on the theory and practice of x-ray diffraction residual stress measurement as applied to shot peened materials. The need to obtain a complete

description of the subsurface residual stress distribution, in order to accurately characterize the residual stress distribution produced by shot peening is emphasized. As conclusion stated that; a given level of surface residual compressive stress is necessary, but not sufficient, condition to indicate that shot peening was performed properly. Many surface treatments other than shot peening produce similar levels of surface compressive stress, as will shot peening to different Almen intensities. So, subsurface residual stress measurement, with correction for penetration of x-ray beam and stress relaxation caused by electropolishing, is necessary to accurately and reliably characterize residual stress distributions produced by shot peening. Finally it is claimed that; X-ray diffraction (XRD) residual stress measurement is the best developed and most accurate method available for the characterization of the residual stress distributions produced by shot peening.

Barzoukas et al. (92096 Paris La Defense) studied ceramic shot versus steel shot difference in shot peening of 300M (modified AISI 4340) steel fatigue test samples with a coverage of 200% hardened to 53 – 55 HRC and tabulated the obtained results as can be seen in *Table 2.2*. There were 6 samples in a group.

Table 2.2 Shot Peening Parameters and Results
(Barzoukas et al, 92096 Paris La Defense)

Group	Shot Hardness	Shot Size	Peening Intensity	Fatigue Cycles	%Cycles Incresae
Control	Without Shot Peening			16 465	0
Steel Shot					
1	46 HRC	S 170	6 A	18 513	12
2	46 HRC	S 170	10 A	17 974	9
3	46 HRC	S 230	6 A	24 731	50
4	46 HRC	S 230	10 A	23 073	40

Table 2.2 (continued)

Group	Shot Hardness	Shot Size	Peening Intensity	Fatigue Cycles	%Cycles Incresae
5	46 HRC	S 230	16 A	18 823	14
6	65 HRC	S 170	6 A	29 204	77
7	65 HRC	S 170	10 A	25 086	52
8	65 HRC	S 230	6 A	27 735	56
9	65 HRC	S 230	10 A	23 672	44
10	65 HRC	S 230	16 A	19 353	18
Ceramic Shot					
11		S 170	6 A	26 689	62
12		S 170	10 A	20 189	23
13		S 230	6 A	26 212	59
14		S 230	10 A	20 631	25
15		S 230	16 A	18 119	10

Intensity conversion: 6 A = 0.15 mm Almen A
10 A = 0.25 mm Almen A
16 A = 0.40 mm Almen A

From the above tabulated results, they concluded that hard steel and ceramic shots with low intensity peening (6 A) resulted in the best fatigue life.

As a reference also the ninth edition of Shot Peening Applications book written by Metal Improvement Company (2005) is reviewed. There are several applications and case studies about shot peening improvement of residual stresses and by the way fatigue life of components used in different industries.

2.3 Super-finishing and Residual Stress

In super-finishing process, material removal from the surface is very small, so compared to other machining processes like grinding and hard turning lower degree of plastic deformation is occurring on the material surface. Güley (2004) worked about the effects of super-finishing parameters on residual stress development on ball bearing inner rings and concluded that; oscillation speed of super-finishing stone and bearing rotation speed can be considered together which defines how the super-finishing stone moves on the surface of the specimen and determined the ratio of bearing ring rotation over super-finishing stone oscillation cycle as 18. As process time he observed 12 seconds is better in terms of higher compression than 6 seconds.

CHAPTER 3

THEORY

In this chapter, related with the residual stress development via application of shot peening, an introduction to basic concepts in austenite to martensite transformation in high carbon steels, theory of strain induced martensitic transformation and fundamentals of increase in dislocation density during plastic deformation are reviewed. Following, X-rays and residual stress and retained austenite measurement by X-ray diffraction are detailed.

3.1 Shot Peening and Residual Stress Development

In order to understand clearly the mechanisms of residual stress development during shot peening of high carbon hardened steels, plastic deformation, mainly cold working and strain induced transformation of austenite into martensite phenomena would better to be known.

High carbon steels are quenched from austenite phase into a hard and very strong, so wear resistant phase known as martensite. Martensite, as possessing high strength is also very brittle due to high internal stresses and strain energy as a result of carbon interstitial atoms distorting the lattice and high dislocation density. For elimination of these high lattice strains, by diffusion of carbon atoms and annihilation of some dislocations, up to a certain extent and so achieving some ductility and toughness martensitic structures are always tempered.

Martensitic transformations in steels, unlike other solid state phase transformations that referred to nucleation and growth transformations, do not follow the Avrami type kinetic equation. Consequently, martensitic transformation is not classed as nucleation and growth type. However, there exists a nucleation and growth stage during transformation but the growth rate is so high that the rate of volume transformation is controlled almost entirely by nucleation stage (Verhoeven, 1975). When steels having carbon contents greater than 0.6% weight percent are heated into face centered cubic (fcc) austenite (γ) region and quenched at a sufficient rate a martensitic transformation occurs and transform into metastable body centered tetragonal (bct) martensite (α^{I}). Martensite grows as platelets in the austenite at a rate of less than 0.0001 seconds for all growth to finish after nucleation. Since martensite is a metastable phase it only forms on very rapid cooling.

In austenite phase (fcc), the interstitial carbon atoms as they are in solid solution state, are positioned in octahedral hole and one is surrounded by six iron atoms arranged on the corners of an octahedron. Such voids are at the center of cube edges and at the cube centers and their size is changing between 0.052 nm largest to 0.028 nm smallest in radius. Carbon atoms have a radius of 0.080 nm. So, carbons reside in octahedral sites with an expansion of austenite lattice (Leslie, 1991). The bcc (body centered cubic) packing is not as close packed as fcc, atomic packing factors are 0.68 and 0.74 respectively. This can also be seen from the densities at Ac_3 temperature where density of ferrite (α) is 7.5706 g/ml and density of austenite (γ) is 7.6327 g/ml. Interstitial carbon atoms in ferrite (bcc) are expected to be in tetrahedral hole which has a radius on the order of 0.036 nm. In fact measurements show that octahedral sites in bcc iron are preferred by carbon atoms that are 0.019 nm in radius. Therefore, during quenching from fcc austenite into bcc martensite, carbon atoms located in octahedral sites of fcc lattice can not diffuse to form $Fe_3C + \alpha$ (pearlite) structure, and remain in octahedral voids of bcc causing high amount of distortion, thus a highly supersaturated solution of carbon in bcc iron forms and the structure is no more cubic it is tetragonal due to carbon atoms that could not diffuse during transformation with c/a ratio nearly 1.045 – 1.050 for AISI E52100 grade steel

(Kumar, Physical Metallurgy of Iron and Steel). As a consequence, during this transformation volume increase is inevitable and dilatation experiments show 4% of volume expansion.

In a classical paper published in 1924, E. C. Bain proposed a scheme by which an fcc unit cell would be transformed into a bct unit cell. This is shown schematically in *Figure 3.1*. The tetragonal unit cell in between two fcc unit cells form bct martensite when contracted 20% along (x3) direction and expanded 12% in (x1) and (x2) directions. This lattice expansion and contraction is called Bain distortion (Porter, Easterling, 1992). The positions occupied by carbon atoms in bct (α^I) do not exactly correspond to equivalent octahedral positions in parent fcc (γ) structure, and it is assumed that small shuffles of C atoms take place during transformation.

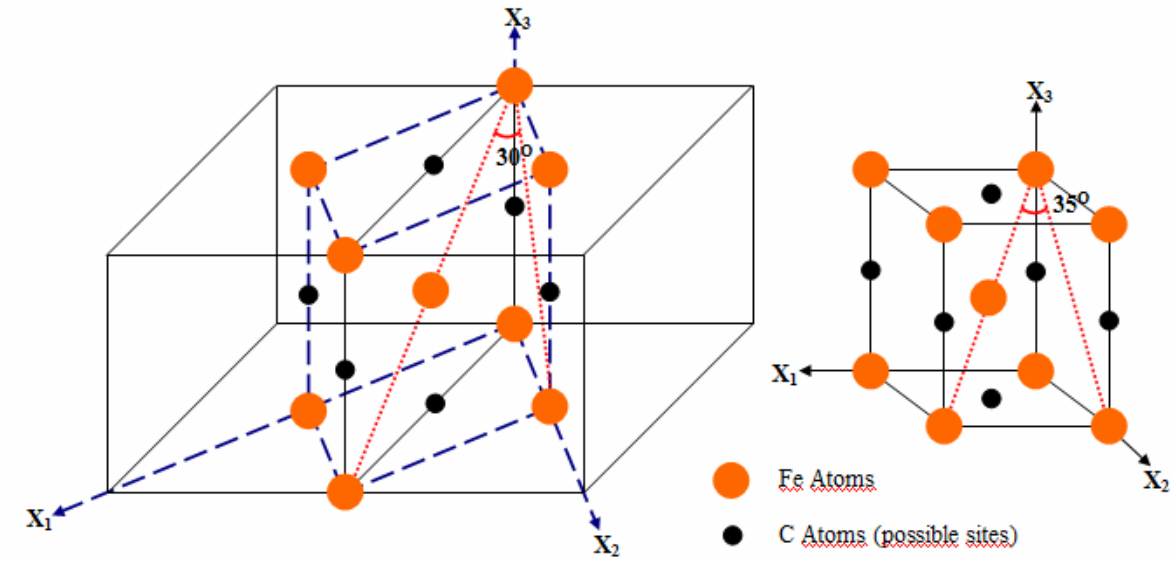

Figure 3.1 Bain Correspondence for $\gamma \rightarrow \alpha^I$ transformation. Left γ unit cell is contracted about 20% in (x3) axis and expanded 12% in (x2) and (x1) axis to obtain right α^I unit cell, namely possessed Bain Distortions.

Observations have shown that, at least macroscopically, the transformed regions, martensite areas, during martensitic transformation appear coherent with the surrounding austenite matrix. Interface between austenite and martensite during transformation allows growth after nucleation within 10^{-7} seconds (Porter, Easterling, 1992). Such formation of a coherent martensite in austenite is only possible in certain crystallographic orientations dependent on alloy content, and on a macroscopically undistorted, zero rotation plane which is called the habit plane. Since martensitic transformation is a shear transformation, deformation due to shear takes place by a homogeneous shear parallel to the habit plane, namely the invariant plane. But atomic displacements during transformation are known to take place at a slight angle to the invariant plane (Verhoeven, 1975). Hence, the martensitic transformation involves simple shear parallel and uniaxial tension or compression normal to the habit plane. Habit plane is {225} and shear strain component and normal strain component are 0.19, 0.09 respectively for Fe – (0.5-1.4 C%) like in AISI E52100 (Porter, Easterling, 1992).

During austenite to martensite transformation high amount of stresses are formed by the action of rapid cooling, so thermal stresses are exerted on the lattices. In fcc structures due to high number of slip systems atomic motion takes place by slip but in bcc systems twinning becomes significant at low temperatures, for bct crystal structures twinning is the mechanism of deformation in which atomic movement is much less than an interatomic distance, so lattice strains needed to produce a twin are small and twin boundaries as a result required deformation energy is smaller when compared to slip. At low temperatures and high rates of deformation, like in martensitic transformation, in certain crystallographic directions on crystallographic planes, energy needed to distort the lattice and break the bonds between atoms becomes very high, so stress necessary to start slip (critically resolved shear stress) sometimes becomes higher than stress necessary for twinning. Under these conditions twinning is the main mechanism of deformation. During martensitic transformation in order to keep habit plane not rotated, so keep coherency between austenite matrix and martensite, some shear deformations preventing the crystal

structure from changing take place which are slip along parallel planes and twinning stacks (Verhoeven, 1975). This is known as lattice invariant shear and shown schematically in *Figure 3.2*. As a result of these twinning and slip martensitic structure has a high dislocation density and twins.

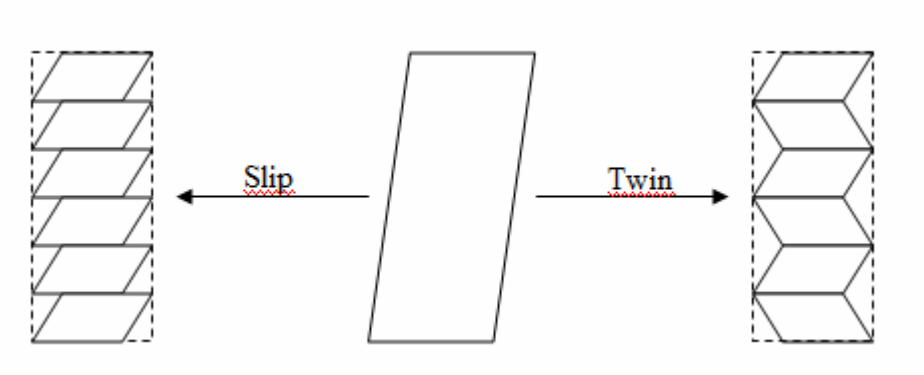

Figure 3.2 Lattice Invariant Shears

Applying lattice invariant shears analogy to the Bain model, an internally slipped or twinned martensite plate can form in austenite by undergoing Bain distortions along different axes, by the way net distortion of material is compensated. So habit plane undergoes no net distortion in macro scale meaning that when averaged over many twins it is zero.

In high carbon steels like AISI E52100 martensite morphology is plate martensite twinned with a midrib. The first formed plates grow across the entire austenite grains. Additional plates then nucleate in the remaining austenite and grow between the first formed ones and grain boundaries. As austenite is more partitioned by plates, regions of austenite become smaller and plates formed in become smaller. So in high carbon steels we have non parallel plates with size variations (Verhoeven, 1975). Finally, the structure becomes large number of martensite plates and in between retained austenite. Retention of austenite is due to high elastic stresses arising from lattice strains suppress the further growth of last nucleated martensite plates. As C%

increases, because Bain distortions so strain energy necessary to transform increase, Ms and M_F decrease and amount of retained austenite increases.

In terms of free energy change, nucleation of martensite in austenite can be formulized as given below:

$$\Delta G = A\gamma + V\Delta G_S - V\Delta G_V - \Delta G_D \quad (3.1)$$

ΔG : Total increase in Gibbs free energy due to martensite nucleation.
A : Total surface area.
γ : Interfacial surface free energy.
V : Volume of nucleus.
ΔG_S : Strain energy per unit volume.
ΔG_V : Volume free energy per unit volume for fcc to bct transformation at temperature of transformation, $\Delta G_{\gamma\text{-M.}}$
ΔG_D : Dislocation interaction energy.

First term ($A\gamma$) because of generation of a new interface increases the free energy so has a positive contribution for free energy increase. Second term ($V\Delta G_S$) due to formation of lattice strains during martensitic transformation increases the free energy so contribute positively. There exists large strain energies associated with the transformation due to Bain distortions so the most important term increasing the free energy is strain free energy. Third term ($V\Delta G_V$) is the free energy difference between martensite and austenite phases at temperature of transformation and has a negative effect on increasing free energy so favors transformation. This free energy difference is shown in *Figure 3.3*. Last term (ΔG_D) is the dislocation strain field interaction energy. Because of the fact that around dislocations there exist a strain field and this is contributing the Bain strains so decreasing strain energy due to nucleation, this term has a negative effect in free energy increase so favors transformation (Porter, Easterling, 1992).

Martensite forms from austenite at Ms temperature because it has a lower free energy. At a temperature T_E martensite and austenite are at equilibrium, below martensite has lower free energy above austenite has lower energy. Ms is far below this T_E because there is a strong nucleation energy barrier due to large lattice strains (Bain distortions) forming during transformation so a certain amount of supercooling is necessary for driving the process (Verhoeven, 1975).

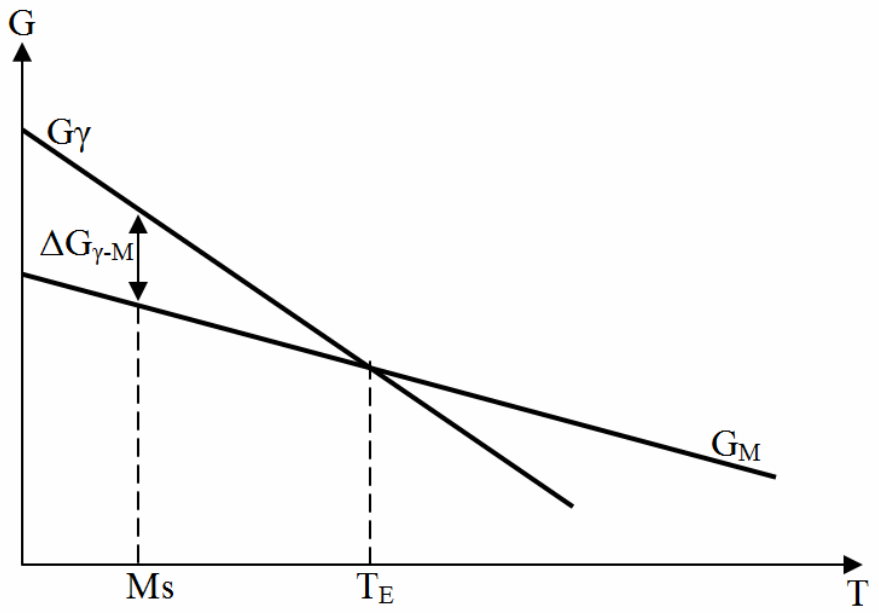

Figure 3.3 Free Energy versus Temperature Curves of Austenite and Martensite.

Quenched steel contains relatively high levels of residual stress. This stress is due to cooling rate differences and so temperature gradient between core and surface and volume increase during transformation of austenite into martensite. Also microstresses arise due to supersaturated carbon interstitials and so Bain distortions. In this condition martensite is very brittle and has a high tendency for crack development. By tempering residual stresses are substantially relieved by localized plastic flow and carbon redistribution by diffusion. By the way tendency for

spontaneous cracking is removed and some ductility and toughness is achieved. Tempering of high carbon steels like AISI E52100, means tempering of plate martensite. At temperature up to 200 ^{O}C ε carbide ($Fe_{2.5}C$) precipitation as Widmanstatten arrays occur, as the temperature increases precipitates grow in size. Between 200 – 300 ^{O}C a second type precipitate in the from of Fe_5C_2 forms in between twins. Above 300 ^{O}C equilibrium Fe_3C begins to form in plate shape and twins starts to disappear. Above 450 ^{O}C Fe_3C starts to spheroidize, martensite transform into ferrite and recovery starts. Recrystallization becomes important at around 600 ^{O}C and no more dislocations exist in the structure (Verhoeven, 1975). Tempering transforms metastable retained austenite into lower bainite with ε carbide precipitates in between 200 – 300 ^{O}C. Carbide precipitation as $Fe_{2.5}C$ is up to 200 ^{O}C and below this temperature for high carbon steels austenite does not transform into any phase.

Tempered martensite structure is a hard and strong structure due to the following mechanisms:

- Precipitation hardening due to hindered dislocation motion by carbide precipitates.
- Grain boundary strengthening as a result of very fine martensite grains grain boundary area is too large.
- Dislocation hardening, due to high dislocation density and high lattice strains prevent dislocation motion.
- Solid solution strengthening due to carbon interstitials act as barriers for dislocation motion.

In view of martensite growth dependence on dislocation nucleation or twinning to occur, an externally applied stress will aid the generation of dislocations and twins hence aids growth of martensite. Beside growth, external stress can also aid martensite nucleation if external strain components contribute to Bain distortions and so reducing the energy barrier for nucleation (Porter, Easterling, 1992). Also, plastic deformation of austenite by the increase in dislocation density aids nucleation of

martensite via increasing possible nucleation sites. Increase in nucleation density increases the last term in equation (3.1). Driving force for transformation to take place, for overcoming the energy threshold, is the free energy difference of supercooled unstable austenite and martensite and if exists the external stress in terms of contribution in Bain distortions. This equation can be modified as below by consideration of external stress effect as (ΔG_σ):

$$\Delta G = A\gamma + V\Delta G_S - V\Delta G_V - \Delta G_D - \Delta G_\sigma \quad (3.2)$$

Strain, stress, induced martensitic transformation in AISI E52100 steel is observed by Rivero et al. (2004) during his study about deviation of residual stress patterns on bearing balls surface after rolling contact due to inherent microstructural alterations. Results from his measurements of retained austenite before and after rolling contact tests showed that approximately 2.08% of retained austenite transformed to martensite. As a result it is concluded that the main changes in residual stresses during rolling contact prior to spalling are due to microstructural transformations and, in particular, to retained austenite's transformation to martensite. In a study conducted by Dommarco et al. (2004) rolling contact fatigue lives of different variants of SAE 52100 bearing steel were evaluated in a 5-ball-rod rolling contact fatigue machine under testing conditions leading to surface nucleated failure. Observations were same as the study by Rivero et al. (2004); the rolling contact deformation induced the transformation of retained austenite and resulted in the redistribution of stresses in the sub-surface regions. After 10^8 rolling cycles 70-80% retained austenite at surface, 45-50% at 100 microns below the surface, 20-30% at 40 microns below the surface transformed into martensite by the action of rolling contact stresses. Finally in another study, Huo et al. (2005) experimented strain induced martensitic transformation near crack tip of thin foil specimens manufactured from carburizing grade steel and carburized and tempered. TEM is used for microstructural analysis of crack tips and result observed is retained austenite inside the plastic zone at the fatigue crack tip has been transformed into martensite due to plastic deformation.

The above given studies exemplify and experimentally prove again the well known fact; the internally and/or externally stress assisted transformation of martensite.

Shot peening is a cold working process in which the surface of a part is bombarded with small spherical media called shot. Each piece of shot striking the metal acts as a tiny peening hammer imparting a small indentation or dimple on the surface. In order for the dimple to be created, the surface layer of the metal must yield in tension (Metal Improvement Company, 2005). When individual particles of a shot in a high velocity stream contact a metal surface, they produce the rounded small depressions in the surface via stretching it radially and causing plastic flow of surface metal at the instant of contact. The effect usually extends to about 0.13-0.25 mm below the surface (ASM Handbook, Volume 5). Schematic illustration of formation of an indentation at time of impact is given in *Figure 3.4*.

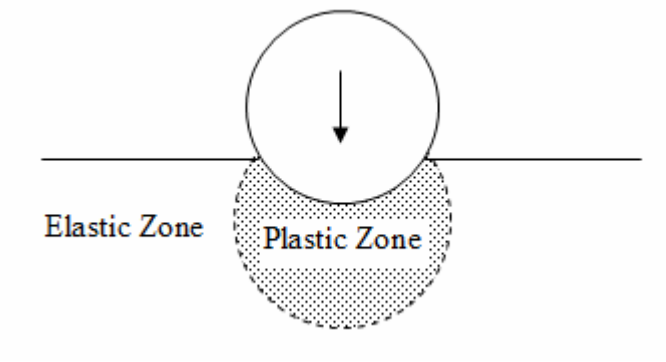

Figure 3.4 Plastic and Elastic Zone Under a Shot at Time of Impact

Plastic zone under the indentation is surrounded with elastic part which acts to hinder plastic flow in a manner similar to the die constraint forces in a closed die forging. Due to this constraint the mean compressive stress required to cause plastic flow of surface near region exceeds that in simple compression. By application of slip line field theory constraint factor is found as 2.57. However, shot peening indentation is an elastic-plastic phenomena and Hertz's theory of contact application is more

suitable. Elastic-plastic analysis results in a constraint factor of 3. In order for plastic yielding minimum applied stress must be 3 times the nominal pure compressive strength (Dieter, 1988).

In shot peening a shot hitting the surface has a blow energy which is equal to the kinetic energy of the shot generated by acceleration of the shot towards peening surface via compressed air or centrifugal force and given by the formula:

$$E = 0.5mV^2 \qquad (3.3)$$

E is the kinetic energy, m is the mass of shot, V is the velocity at time of impact at start of deformation. This kinetic energy during elastic-plastic collision is partitioned as absorbed energy by peened material and kinetic energy after collision of the shot. Focus is located on the energy absorbed by the peened material. The important portion of this energy is the energy plastically deforming the near surface region and energy causing retained austenite to transform into martensite.

Shot peening of a steel part, that has high carbon content hardened and tempered surface, results in micro-hardness increase, transformation of part of the retained austenite into the strain induced martensite and dislocation density is increase as stated after experimental observations by Hongbin et al.

The unstable retained austenite phase in the microstructure of high carbon martensitic steel structures, up to an extent, when shot peened is transforming into martensite, which is the lower free energy phase at that temperature by the following reasons:

- Applied external load aids dislocation nucleation and twinning which are the growth mechanisms for already existing martensite plates into retained austenite. So aids increase in martensite percentage.
- By contribution of strain caused by shot to Bain distortions, new martensite plates are nucleated (ΔG_σ in equation 3.2).

- Plastic deformation of austenite by increase in dislocation density favors nucleation of martensite. By increase in dislocation density possible nucleation sites become increased so ΔG_D in equation 3.2 increases.

When austenite (fcc) transformed into martensite (bct) a net volume increase arises and so the near surface transformation poses a volume expansion. Also because of plastic yielding, surface becomes elongated. Due to these two, the compressed grains below the surface try to restore the surface to its original shape producing a hemisphere of cold-worked metal highly stressed in compression. Consequently the residual compressive stress after shot peening depends on the amount of retained austenite to martensite transformation and deformation.

Parameters that affect impact energy will directly affect the amount of phase transformation and surface deformation hence residual stress. Shot peening parameters that affect residual stress are:

- Shot flow rate, compressed air pressure and centrifugal force for accelerating shots changes V (velocity) in equation 3.3. So directly proportional with square.
- Shot weight is the m (mass) in equation 3.3 so directly proportional.
- Shot size changes the contact surface so changes exerted stress. When compared in same load basis, smaller shot size exerts higher stress than bigger shot.
- Shot hardness changes the energy portion that is absorbed by shot itself due to deformation. Harder the shot smaller the collision energy absorbed by shot so wasted.
- Nozzle angle affects the impact angle so force component parallel and perpendicular to the peening surface thus, very big nozzle angles will result in a weaker peening effect due to small perpendicular component.
- Nozzle to part distance, changes the amount of kinetic energy loss from nozzle to the part surface. As distance increases due to gravity if horizontal peening is the case and air drag effect lost kinetic energy will

be higher. All items up to now are directly affecting the intensity of peening because they are energy related items.

- Coverage as a sign of how completely an area has been hit by shot particles affects the part fatigue behavior. Peening less than 100% coverage is ineffective because of the amount of unpeened surface.

3.2 XRD Measurement of Retained Austenite

Residual stress measurement by X-ray diffraction basically measures the angles at which the maximum diffracted intensity occurs. Measuring these angles, by using Bragg's Law one can find the spacing of diffracting lattice planes, by the way strain in the crystal lattice is measured. Then utilizing linear elasticity theory, the stress producing this strain at the point of measurement can be obtained. In measurement of retained austenite in high carbon steels, because intensity of the diffraction pattern of a particular phase depends on its concentration in the mixture, intensity of austenite peaks are measured and from this measurement amount of retained austenite is determined. In this section, the theory of X-ray diffraction measurements of residual stresses and retained austenite in high carbon bearing steel is discussed.

Quantitative analysis by diffraction is based on the fact that the intensity of the diffraction pattern of a particular phase in a mixture of phases depends on the concentration of that phase in the mixture (Cullity, 1967). Diffractometers are used instead on Debye-Scherrer cameras and microphotometers because intensity measurement times are shorter and the absorption factor is independent of the angle Θ (half diffraction angle).

Direct comparison method has been the widely used method for the amount of retained austenite in hard steel. Since, measurement of the concentration or percentage of a particular phase depends on the measurement of the ratio of the intensity of a diffraction line from that phase to the intensity of a reference line,

which is a line from the other phase in direct comparison method, direct comparison method determination of retained austenite is based on measurement of the ratio of intensity of an austenite line to a martensite line.

Austenite (γ) and martensite (α) have same composition but different crystal structure, namely face centered cubic and body centered tetragonal respectively. The main equation of intensity for retained austenite determination is:

$$I\gamma = (KR\gamma C\gamma) / (2\mu) \quad (3.4)$$

Iγ : Integrated intensity of austenite per unit diffraction line.
K : Constant, depends on diffractometer and radiation used.
μ : Linear absorption coefficient of steel (austenite-martensite mixture).
Cγ : Volume fraction of austenite.

$$R\gamma = (1/v^2) [F^2\rho((1+\cos^2 2\Theta) / (\sin^2\Theta\cos\Theta))]e^{-2M} \quad (3.5)$$

v : Unit cell volume.
F : Structure factor.
ρ : Multiplicity factor.
Θ : Bragg angle.
e^{-2M} : Temperature factor.

Mass absorption coefficient (μ/ϱ), where ϱ is density, is a constant material property and does not change with physical state (gas, liquid, solid). So, by knowing the density at measurement temperature, linear absorption coefficient (μ) is known.

Integrated intensity (I) is the area under intensity versus 2Θ curve for the diffraction line. Unit cell volume (v) is calculated from the measured lattice parameters by simple volume calculation for cubic (austenite) and tetragonal (martensite) geometries. Measurement of interplanar spacing between (hkl) planes (d_{hkl}) with high

accuracy is important and, by knowing wavelength of the beam (λ) and diffraction angle (2Θ), done according to the formula:

$$\lambda = 2d_{hkl}\sin\Theta \text{ (Bragg's Law)} \quad (3.6)$$

By knowing d_{hkl} lattice parameter of austenite (fcc) is calculated by:

$$a = d_{hkl}\sqrt{(h^2+k^2+l^2)} \quad (3.7)$$

a : Cube edge so unit cell volume is a^3.

During determination of lattice parameter the diffraction angle (2Θ) determination is very critical because it directly alters the precision. Due to the fact that Θ is contributing the formula as sinΘ, and sin function close to 90^O is less sensitive to changes peaks at large diffraction angles (near to 180^O) are preferred for small errors. For example; 1% error in diffraction angle determination at $2\Theta = 170^O$ results in 0.1% error for sin85. Lattice parameters of martensite (bct) are calculated by using two highest diffraction angles for at first calculation of approximate values of a_1 and c_1 by the formulas:

$$a = (\lambda/2\sin\Theta)\,[(h^2+k^2)+(l^2/(c/a)^2)]^{1/2} \quad (3.8)$$

$$c = (\lambda/2\sin\Theta)\,[l^2+(h^2+k^2)(c/a)^2]^{1/2} \quad (3.9)$$

from a_1 and c_1 approximate c/a ratio is calculated and used for a_2 and c_2 calculation and so finally third extrapolation will be sufficient for the precisely determined lattice parameters (a and c). By knowing these, volume of martensite unit cell is a^2c.

Atomic scattering factor (f) is the efficiency of an atom to scatter an X-ray in a given direction and depends on the wavelength and Bragg angle. Tabulated data for atomic scattering factor for different λ/sinΘ values are available. Structure factor (F) is the

efficiency of a unit cell in terms of scattering the X-ray beams in a given direction so dependent on the (hkl). F for austenite (fcc) structure and martensite (bct) structure are as given below:

- F = 2f when h+k+l = even and F = 0 when h+k+l = odd for martensite (bct).
- F = 4f when h,k,l are all even or odd and F = 0 when h,k,l are mixed (some are even some are odd) for austenite (fcc).

So, from the above given F values all diffracting planes (hkl) for austenite have to posses h,k,l all even or all odd, if some odd some even such planes will not have a line on diffractogram. For martensite diffracting planes (hkl) have to fulfill the requirement h+k+l = even otherwise no peak will appear in the diffractogram.

When λ (wavelength of X-ray beam) is very near to the absorption edge (K) of the scattering element which is λ_K a correction for atomic scattering factor (f) will be applied and this Δf is tabulated and plotted also as f vs. $\lambda/\sin\Theta$ in the literature (Cullity, 1967). The new f will be $f + \Delta f$. For ($\lambda << \lambda_K$) f is directly used no correction is necessary.

Multiplicity factor (ρ) is the number of different planes in a form having the same interplanar spacing and it depends on the crystal system. Values of this factor as a function of crystal system (hkl) and are also tabulated in the literature (Cullity, 1967).

Temperature factor (e^{-2M}) is inserted inside the equation due to the vibrating motion of atoms forming the crystal. Because of the thermal vibrations lattice planes are more like plate like regions of not well defined thickness so reinforcement of diffracted beams are not as perfect as it is assumed to be for a crystal of well defined planes with fixed atoms. Temperature factor (e^{-2M}) versus $\sin\Theta/\lambda$ plots can be found and used from the literature (Cullity, 1967).

After all of these explanations coming back to equation 3.4, same intensity equation is valid for martensite which is:

$$I\alpha = (KR\alpha C\alpha) / (2\mu) \qquad (3.10)$$

Dividing of 3.4 by 3.10 results:

$$I\gamma / I\alpha = (R\gamma C\gamma) / (R\alpha C\alpha) \qquad (3.11)$$

So, using the integrated intensities for martensite and austenite that are calculated from the area under the intensity versus diffraction angle curve and calculating the $R\gamma$ and $R\alpha$ parameters from equation 3.5; $C\gamma / C\alpha$ can be found. Knowing that: $C\gamma + C\alpha = 1$ the amount of retained austenite in volume percent becomes determined. In fact phase mixture of a hardened high carbon steel like AISI E52100 is not completely martensite and retained austenite, we have some amount of globular Fe_3C (cementite) distributed in the matrix. If this is wanted to be measured $I\gamma / I_{Fe3C}$ or $I\alpha / I_{Fe3C}$ must be determined in the same manner as $I\gamma / I\alpha$, and by calculating R_{Fe3C}, $C\gamma / C_{Fe3C}$ or $C\alpha / C_{Fe3C}$ can be determined and from $C\gamma + C_{Fe3C} + C\alpha = 1$ percentage of each phase is evaluated.

Cementite (Fe_3C) has an orthorhombic lattice structure with constant lattice parameters which are as follows:

a = 0.509 nm b = 0.674 nm c = 0.452 nm (Leslie, 1991)

So the unit cell volume is from v = abc is 0.1551 nm^3. Also for austenite and martensite lattice parameters, following formulas can be found in the literature (Cullity, 1967):

$$a = 0.3555 + 0.0044(\text{wt \%C}) \text{ nm} \quad \text{for austenite.} \qquad (3.12)$$

For martensite,

$a = 0.2867 - 0.0013(\text{wt \%C})$ nm and $c = 0.2867 + 0.0116(\text{wt \%C})$ (3.13)

From these equations calculated lattice parameters and cell volumes of retained austenite and martensite for AISI E52100 by taking wt %C as %1 are as given below:

$a = 0.3599$ nm and $v = 0.0466$ nm^3 for austenite.

$a = 0.2854$ nm and $c = 0.2983$ nm so $v = 0.0243$ nm^3 and $c/a = 1.0452$ for martensite, well matching with the calculated value taken from Kumar, (Physical Metallurgy of Iron and Steel).

Specimens for retained austenite measurement have to be prepared by wet grinding to remove surface layer which may be decarburized followed by metallographic polishing and etching, or electropolishing. Care must be taken during grinding and polishing not to produce excessive heat which would cause phase redistribution.

In measurement of diffraction line intensity integrating the area under the curve is better than using maximum intensity, because due to variations in microstrain and fine grain size of this phase mixture large variations in line shape can occur. This line shape variations has no effect on integrated intensity but large effect on maximum intensity.

Microabsorption which is a phenomena for phase mixtures having much different linear absorption coefficients and extinction valid for crystals having perfectly parallel planes due to lower reflecting power resulting in a decrease of intensity, are negligible for austenite-martensite phase mixture. This is because; due to having same composition and nearly the same volume also roughly the same particle size, linear absorption coefficients are practically identical. Extinction is also absent because of having highly imperfect nature and so high reflecting power.

3.3 XRD Measurement of Residual Stress

XRD residual stress measurement is based on the fact; the spacing d_{hkl} of the atomic planes (hkl) in a crystalline material is changed via the residual stress and that the d_{hkl} can be determined by measuring the angular position of a diffracted X-ray beam from the Braggs Law. The fractional change in d_{hkl} is a strain from which the stress can be calculated by use of elastic theory.

Under the surface of a specimen, each element will be subjected to the three principal stresses: σ_{11}, σ_{22} and σ_{33}. At the surface, which the X-ray diffraction measurements are done, plane stress conditions are assumed to exist so σ_{33} that is the parallel stress with surface normal is considered to be zero. Hence, due to Poisson's ratio ε_{33} (lateral contraction) in the surface normal direction exists. Schematic illustration of diffraction from a plane stress condition and principal axes are shown in *Figure 3.5*.

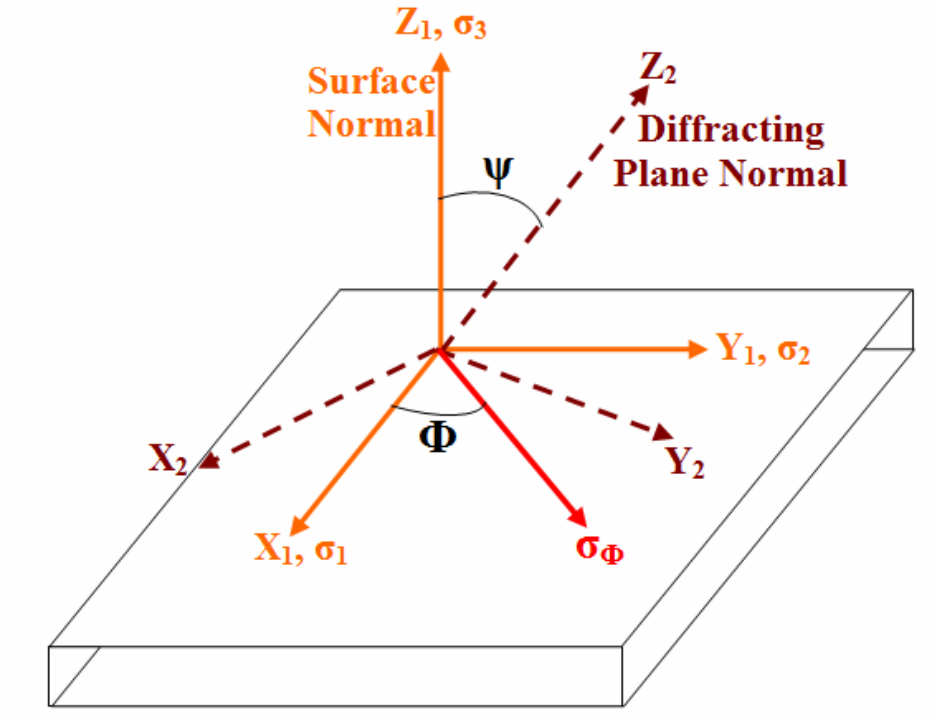

Figure 3.5 Illustration of Coordinate Systems in Plane Stress Condition.

Elastic theory gives the relation given below:

$$\varepsilon_\psi - \varepsilon_3 = \sigma_\Phi(1+\nu)\sin^2\psi / E \qquad (3.14)$$

ε_ψ, ε_3 : Strains in Z_2 and Z_1 directions.

σ_Φ : Stress in Φ direction.

ν : Poisson's ratio.

E : Modulus of elasticity.

$$(d_\psi - d_0) / d_0 - (d_3 - d_0) / d_0 = (d_\psi - d_3) / d_0 = \sigma_\Phi(1+\nu)\sin^2\psi / E \qquad (3.15)$$

d_ψ, d_3, d_0 : Interplanar spacing in Z_2, Z_1 directions and stress free condition.

Replacing d_0 in the denominator with d_3 will cause a very little error so;

$$\sigma_\Phi = [E / (1+ \nu)\sin^2\psi] [(d_\psi - d_3)/d_3] \qquad (3.16)$$

thus for determination of the stress it is not necessary to know principal stress directions and stress free lattice spacing. By differentiating the Braggs law;

$$\Delta d/d = - (\cot\Theta \, \Delta 2\Theta)/2 \qquad (3.17)$$

and combining with equation 4.16 gives the following equation:

$$\sigma_\Phi = [E \cot\Theta/(2(1+ \nu)\sin^2\psi)] \, \Delta 2\Theta \qquad (3.18)$$

where, $\Delta 2\Theta = (2\Theta_{\psi = 0}) - (2\Theta_{\psi = \psi})$.

So during stress measurement, essentially the quantity measured is $\Delta 2\Theta$, which means the shift in the diffraction peak position due to stress as the angle ψ is changed.

The choice of a diffraction peak has a significant impact on precision, higher the angle greater the precision due to the cotΘ term. Practical methods generally necessitate the use of 2Θ angles bigger than 120^{O}. *Table 3.1* lists the recommended diffraction data for AISI E52100 (ASM Handbook, Volume 10).

Table 3.1 Recommended X-ray Data for AISI E52100.

Radiation	Plane (hkl)	Angle (2Θ)	E/(1+ν) GPa	μ cm^{-1}	K_{45} MPa
Cr Kα	(211)	156^{O}	173.7±2.1	714	645

Elastic constants are determined by four point bending test and K_{45} is the magnitude of stress needed for 1^{O} shift in 2Θ when $\psi = 45^{O}$. Because the diffraction angles have to be determined with an accuracy of 0.01^{O}, the sample must be positioned at the center of rotation of the 2Θ and ψ axes. Therefore extremely precise positioning of the sample with 0.025 mm is necessary. Instrument alignment requires coincidence of the Θ and ψ axes of rotation and positioning of the sample such that the diffracting volume is centered on these coincident axes. All these features of alignment can be checked readily using a stress-free powder sample. If the diffraction apparatus is properly aligned for residual stress measurement, a loosely compacted powder sample producing diffraction at approximately the Bragg angle to be used for residual stress measurement should indicate not more than ±14 MPa (±2 ksi) apparent stress (ASTM E915, 1984).

Determination of diffraction peak position is also a very important factor for precision. Several position determination techniques exist but the SAE literature recommends calculating the vertex of the parabola defined by three points confined to the top 15% of the peak. A significant improvement in precision can be achieved, approaching the 0.01° resolution of most diffractometers, by collecting 5 to 15 data

points in the top 15% and fitting a parabola by least squares regression before calculation of the peak vertex.

Subsurface measurements for stress profile beneath the surface are necessary for applications like shot peening. Because X-rays penetrate only around 5 microns under the surface for subsurface measurements the only stress free methods appear to be electrolytic and chemical polishing. Electrolytes generally used for AISI E52100 are perchloric or sulphuric acid solutions.

CHAPTER 4

EXPERIMENTAL PROCEDURE

Throughout this chapter, shot peening machine, X-ray diffractometer facilities and stress, retained austenite measurement methodology, fatigue life test device and test procedure are discussed.

4.1 X-ray Diffractometer and Measurement Methodology

Seifert XRD 3003 PTS system is the X-ray diffraction (XRD) system used in this thesis to measure retained austenite and residual stress. System basically consists of four parts as can be seen on *Figure 4.1*. X-ray tube is the generator of X-rays and produced X-rays are directed to specimen surface via a collimator. All the necessary movements, rotations are provided by the Goniometer, TSA and X-Y Stage. X-rays diffracted from the measurement point on the surface of specimen are detected by a Position Sensitive Detector (PSD).

X-rays are produced by hitting of the high voltage accelerated electrons, generated by heated filament, to the target anode metal. When decelerating electrons emit energy in the form of x-rays and this is called white or fluorescent radiation. Characteristic radiation, used as X-rays of known wavelength, are emitted by the electrons coming back to their unexcited energy level from an upper energy level which they were excited by the action of electron impact. Because, energy magnitude for each electron shell is constant and characteristic of the target metal (anode), the emitted energy by electrons turning back to the lower energy level is equal to the

difference between two energy levels. As a consequence these x-rays have constant, characteristic energy so constant wavelength. All these characteristic radiations (sharp intensity maxima) and white radiation up to a certain extent filtered in order to have monochromatic radiation (known, constant wavelength radiation). In XRD system used in this work the target (anode) is chromium (Cr) and the filter is vanadium (V) with atomic numbers 24 and 23 respectively.

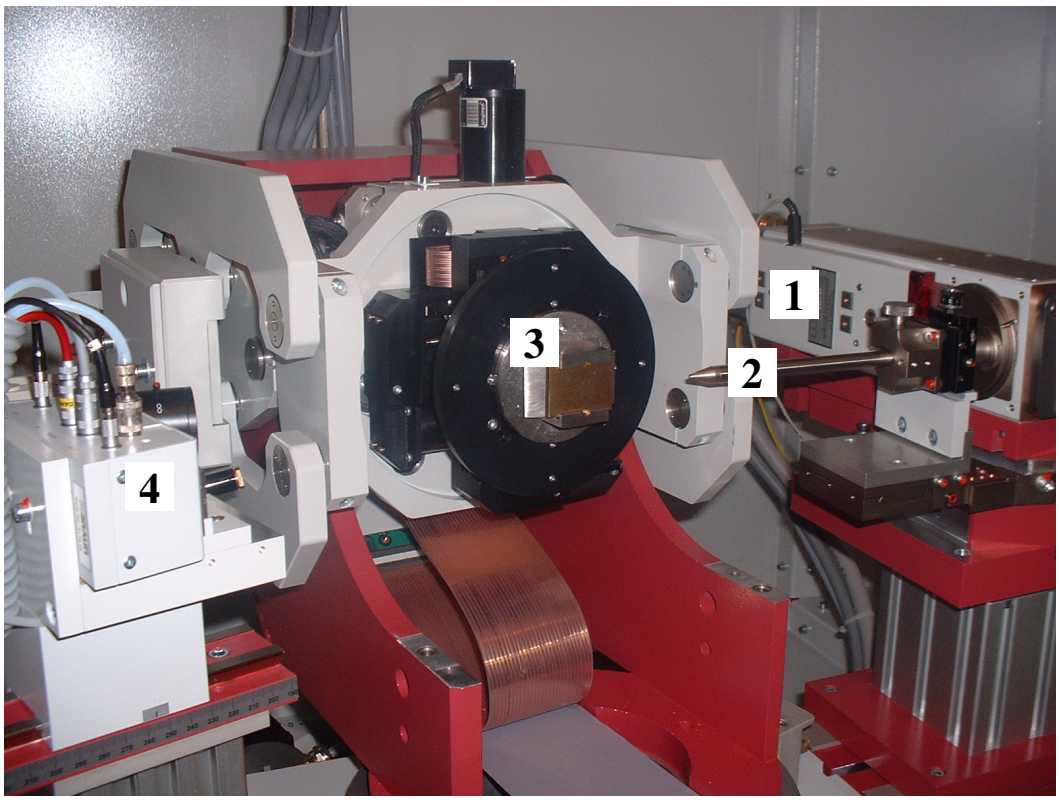

Figure 4.1 XRD System Components 1. X-ray tube, 2. Collimator, 3. Goniometer, TSA, X-Y stage, 4. Detector (Güley, 2004).

In this sealed X-ray tube; electrons from heated tungsten filament are accelerated towards Cr anode by applied 40 kV and 40 mA potential difference and current. They travel in a vacuum environment inside the tube and from the X-rays, produced

by hitting to target, Cr Kα characteristic radiation is filtered by vanadium filter which has a wavelength 2.28962 A^o (Cullity, 1967). Through the collimator these high energy rays are then guided to the specimen surface measuring point.

Goniometer and X-Y stage provides all the necessary movements for the measurements. All movements with limits are given in *Table 4.1* and equipment is shown in *Figure 4.2*.

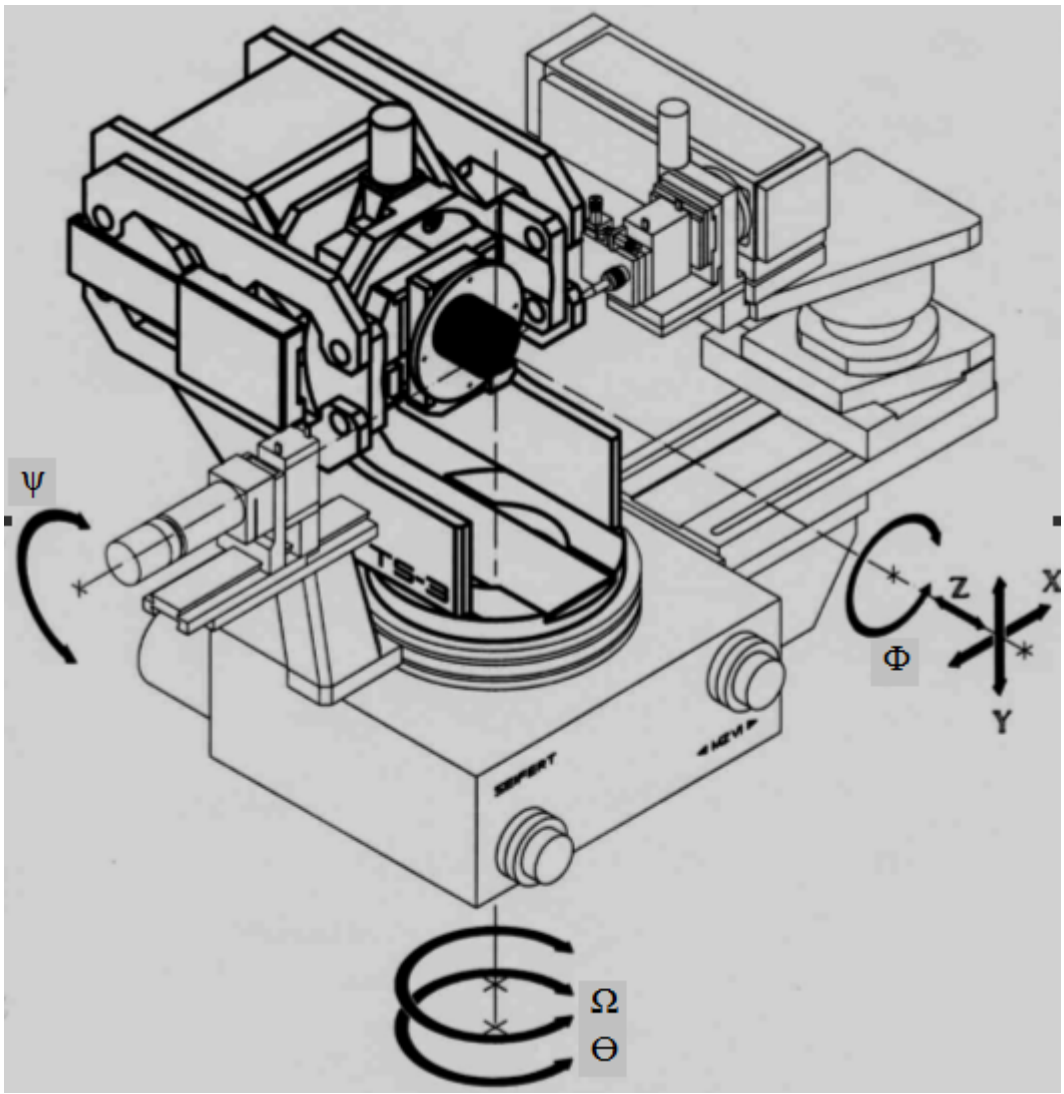

Figure 4.2 Goniometer, TSA and X-Y Stage (Güley, 2004).

Residual stress and retained austenite measurements are based on Θ - 2Θ movements. Θ axis holding the detector moves two times the Ω axis holding the Goniometer. Φ axis enables measurements at different directions (axial, circumferential). X, Y, Z stage is for moving the specimen to center.

Table 4.1 Goniometer, TSA, X-Y Stage Movements

Axis	**Name**	**Limits**
ψ	Chi	$\pm 90^{O}$
Ω	Omega	$-3^{O} - 182^{O}$
Θ	Theta	$-5^{O} - 163^{O}$
Φ	Phi	Infinite
X, Y	Axes	0-50 mm
Z	Axis	0-25 mm

Position Sensitive Detector (PSD) is capable of counting 50000 pulses per second. It is a gas detector, 10% CH_4 + 90% Ar mixture (P10 gas) used, with a flow rate of approximately 1 dm^3/h. It is detecting the rays so the angle by analyzing the X-rays entering the cylinder. When X-rays enter inside, the gas inside the cylinder is ionized, producing electrons, which move under the influence of electric field toward the wire anode, and positive gas ions, which move toward the cathode shell. If the voltage is high enough, the electrons acquire enough energy to knock electrons out of other gas atoms, and these in turn cause further ionization. As a result of this amplification a veritable avalanche of electrons hits the wire and causes an easily detectable pulse of current in the external circuit.

4.1.1 Residual Stress Measurement

Residual stress measurements on raceways of bearing rings are conducted by placing the ring to specimen holder on goniometer, then X-ray from the tube are focused on the point of measurement and the diffracted beams are detected with PSD. Finally, intensity versus 2Θ profiles obtained are evaluated for stress determination. First surface stress is determined but generally subsurface stresses are also points of concern so in order for achieving subsurface regions electropolishing is the method utilized.

After locating the ring into the specimen holder by centering to the measurement circle using X, Y, Z axes, next step is setting the angles of measurement which are ψ, Θ and Φ. As can be seen from *Table 4.1*, ψ can be adjusted in between ± 90^O but due to loss of intensity angles over 45^O are not used. Cr Kα, as tabulated in *Table 3.1* gives diffraction at (211) plane with 2Θ = 156^O, so the range of 2Θ used is 148^O – 164^O. For full stress tensor determination, at least three angles must be used; Φ is set to 0^O, 45^O and 90^O.

For one Φ angle, five intensity versus 2Θ curves are evaluated at ψ = ± 45^O, ± 30^O, 0^O. By using 0^O, 45^O and 90^O as Φ angles totally 15 diffraction curves are evaluated during one measurement. For one diffraction curve to be analyzed it takes 3 – 4 minutes, so with these sets, measurement of one ring takes 45 – 60 minutes.

Following diffraction curves determination some corrections are applied before using them. Necessity for these corrections is due to nonideal conditions in reality. Braggs law is for ideal diffraction conditions and only one line should exist at a certain diffraction angle but this is not the case in real and a broadened peak is the result obtained during XRD applications. Reasons for this broadening are as explained below:

1) Braggs law assumes only diffracted beams differing in path length by exactly an integral number (beams in phase) reinforce each other and all other are destructively interfere and become disappeared. For a beam that is not in phase in order to be eliminated the counter beam should appear to be diffracted from somewhere in the specimen and this is only possible when specimen has an infinite thickness. Thus, specimens are not infinite thickness some parasites not annihilated will always exist around exact 2Θ angle.

2) It is assumed for Bragg law all the incident X-ray beams are perfectly parallel to each other, but this is also impossible. Never perfectly parallel beams have produced in laboratory so some diffraction is taking place at angles around exact 2Θ.

3) Wavelength of X-rays even they are characteristic are not perfectly monochromatic. Kα line itself has a width of about 0.001 A^o (Cullity, 1967). Due to the fact that for each value of λ there exists a value for 2Θ, broadening around exact 2Θ occurs.

4) Atoms in a crystal are not arranged in a perfectly regular lattice. Lattice is broken into a number of tiny blocks slightly disoriented one from another. This angle of misalignment also makes diffraction possible around the exact 2Θ.

As a result of the above mentioned facts; intensity of reflection is greatest at exact Bragg angle but at angles slightly deviating also we have appreciable intensity so the peak is broadened. Since the integrated intensity is the area under intensity versus 2Θ curve, it is proportional to maximum intensity at exact Bragg angle (I_{max}) multiplied with amount of peak width (B) at half intensity ($1/2I_{max}$). BI_{max} is in turn proportional to 1/sin2Θ.

When an X-ray beam, due to its oscillating electric field, encounters with an electron in ring surface set the electron into oscillatory motion so the accelerating and decelerating electron will emit X-rays also. So under the action of incident beam

coming from X-ray tube, electrons in bearing ring also emit X-rays due to put into oscillatory motion by incident X-rays and these X-rays from bearing ring electrons are called scattered beams. Thus the intensity counted by PSD is including also scattered beams so needs a correction proportional to ½(1+cos^{2}2Θ) (Cullity, 1967).

Combining Lorentz factor and Polarization factor, during measurements the intensity is corrected according to the following formula by Seifert 3003 PTS System:

$I = I_m \sin^2\Theta/(1+\cos^2 2\Theta)$ (User Manual, Seifert 3003 PTS) (4.1)

I_m : Measured intensity, not corrected.

Background correction is applied by drawing a line from the minimum point of data cloud to the left and to the right of peak. Using Savitzky-Golay algorithm with 5 points smoothing is performed following the formula from User Manual (Seifert 3003 PTS):

$$I_{2\Theta i} = [-3(I_{m2\Theta i-2}+I_{m2\Theta i+2})+12(I_{m2\Theta i-1}+I_{m2\Theta i+1})+17I_{m2\Theta i}]/35 \quad (4.2)$$

Following the finalization of intensity corrections peak position determination is the next step. Peak position determination method in this thesis work is parabola fit above 40% threshold value. A parabola is fitted through all data points that have intensities above 40% of intensity maxima. The automatically determined number of data points above this threshold value is forced to be odd for each peak. Because there should be equal number of points on the left and on the right of determined 2Θ.

Having in hand the determined 2Θ, $\sin^2\psi$ versus $\Delta 2\Theta$ becomes obtained for 0^O, $\pm 30^O$, $\pm 45^O$ for a certain Φ angle (0^O, 45^O, 90^O). From equation 3.18 stress in the direction of Φ is calculated.

$$\sigma_\Phi = [E \cot\Theta/(2(1+\nu)\sin^2\psi)]\ \Delta 2\Theta \quad (3.18)$$

where, $\Delta 2\Theta = (2\Theta_{\psi = 0}) - (2\Theta_{\psi = \psi})$.

For subsurface residual stress measurements, done by material removal from the surface by electropolishing, correction needed was analyzed in thesis study performed by Güley (2004). His observation was proving that in material removal on the order of micrometers up to 200 microns no improvement obtained by depth correction applied. Thus in this thesis work also there is no need for depth correction.

Residual stress measurements were performed on (211) martensite plane as recommended in ASM Handbook Volume 10 and also as done for most of the studies in the literature for high carbon martensitic microstructures. Some amount of retained austenite exists on the order of 15 – 20 % for the rings produced in this study. As performed in the study by Rangaswamy et al. (2000) on carburized 5120 steel residual stress measurements, stresses in retained austenite phase from (220) reflection, as well as from martensite phase is better to be measured. Due to the fact that; data in hand as archive measurements and measurements performed in previous studies (Güley, 2004) also during commercial use of XRD device for production quality control samples are performed only in martensite phase, in order for measurements performed in this thesis to be comparable with these data, measurements were done only in martensite.

In the case of Cr Kα radiation incident on AISI E52100 steel and one hour measurement time, error in residual stress values in the stress tensor is maximum ± 20 *MPa* independent of its value (Güley, 2004).

4.1.2 Retained Austenite Measurement

Bearing rings for retained austenite measurement after heat treatment before grinding are surface prepared by wet grinding to remove surface layer which may be decarburized followed metallographic polishing or electropolishing. For

measurements from ground or super-finished raceway surfaces, surface preparation is not necessary.

Following surface preparation, specimen is located to the center of specimen holder in the same manner as done for residual stress measurement. X-ray beams via collimator are focused on the point of measurement and the diffracted beams are detected with PSD. By the way, intensity versus 2Θ profiles obtained.

Angles set for measurement are as follows: Due to the fact that Θ is contributing the Bragg formula as sinΘ and sin function close to 90^O is less sensitive to changes, peaks at large diffraction angles (near to 180^O) are preferred for small errors. So the range of 2Θ used is 90^O – 167^O. ψ and Φ angles are not necessary to be changed. Retained austenite measurement accuracy depends on the intensity counts per 2Θ angle so depends on time. General application, also performed for this work is 30 – 45 minutes per measurement. This means, the 2Θ angle range 90^O – 166^O is scanned in 30 – 40 minutes meaning the goniometer angular speed is 1.7^O – 2.5^O per minute.

Next step after diffraction curve determination, same corrections with residual stress measurement are applied before using them. Since the integrated intensity is the area under intensity versus 2Θ curve, it is proportional to maximum intensity at exact Bragg angle (I_{max}) multiplied with amount of peak width (B) at half intensity ($1/2I_{max}$). BI_{max} is in turn proportional to 1/sin2Θ. Combining Lorentz factor and Polarization factor, during measurements the intensity is corrected according to the equation 4.1 and smoothing with equation 4.2. Background correction is applied and after all corrections being applied peak position is again determined by parabola fit above 40% threshold. One example measurement is given in *Figure 4.3*.

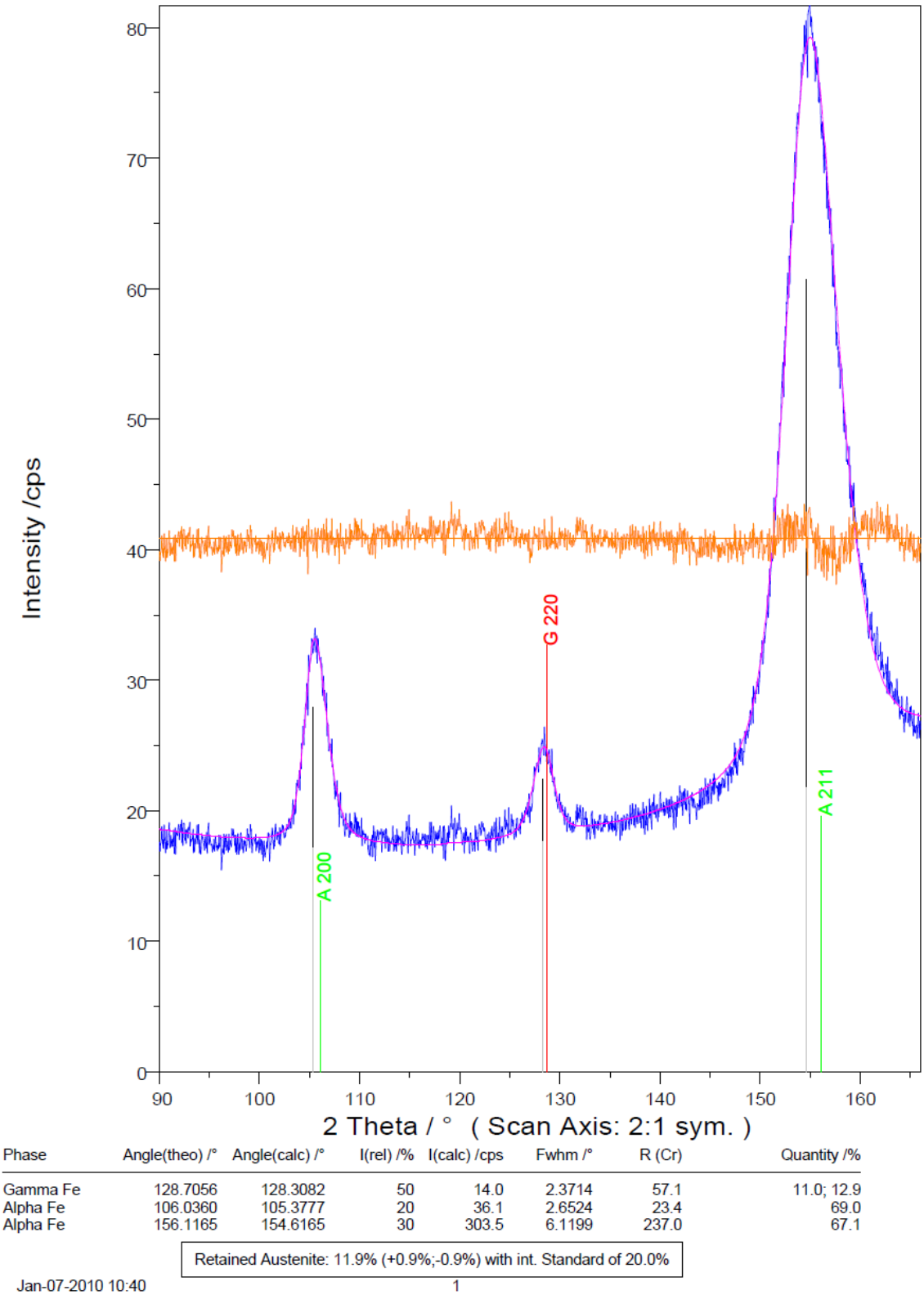

Figure 4.3 Example Retained Austenite Measurement Diffractogram.

Orange line is for background correction and also shows the 40% threshold for (211) plane diffraction of α-iron applied during parabola fit. Peak maxima is at 73.07 cps and curve starts from 23.42 cps so 23.42 + (73.07 – 23.42)0.4 = 43.28 cps, which is nearly the orange line cps value. As the result of parabola fit determined angles are represented with "Angle(calc)" in diffractogram.

Lorentz-polarization correction factors used during intensity calculations are:

$\sin^2 64.1541/ (1+\cos^2 128.3082) = 0.585$ for (220) plane γ -iron.
$\sin^2 52.6889/ (1+\cos^2 105.3777) = 0.591$ for (200) plane α-iron.
$\sin^2 77.3083/ (1+\cos^2 154.6165) = 0.524$ for (211) plane α-iron.

Lattice parameters calculated from the determined angles are:

By using equations 3.6 and 3.7 for fcc (γ -iron):
$a = (\lambda/2\sin\Theta)\sqrt{(h^2+k^2+l^2)} = (2.28962/2\sin 64.1541)\sqrt{(4+4+0)} = 0.35979$ nm,

By using equation 3.12 for fcc (γ -iron):
$a = 0.3555 + 0.0044(\text{wt \%C}) = 0.3555 + 0.0044(0.97) = 0.35977$ nm.

By using equations 3.8 and 3.9 for bct (α-iron) and extrapolation:
a = 0.2856 nm and c = 0.2981 nm,

By using equation 3.13 for bct (α-iron):
$a = 0.2867 – 0.0013(0.97) = 0.28544$ nm, $c = 0.2867 + 0.0116(0.97) = 0.29795$ nm.

Structure factor (F) calculated by using the following relations are:

For martensite (bct);
F = 2f = 28.9 for (200) plane α-iron, by taking f = 14.45 (Cullity, 1967)
F = 2f = 25.3 for (211) plane α-iron, by taking f = 12.65 (Cullity, 1967)

For austenite (fcc);

F = 4f = 41.2 for (220) plane λ-iron, by taking f = 10.3 (Cullity, 1967)

R calculations according to equation 3.5 are performed by using v = 24.315 A^{o3} for martensite (bct) and for austenite (fcc) v = 46.574 A^{o3}, and structure factors calculated above.

Integrated intensities are calculated by multiplication of half maxima peak width with Imax at exact 2xBragg angle:

$I(calc) = BI_{2\Theta} = F_{whm}I_{2\Theta}$ = 2.3714x(23.11-17.21) = 14.00 for (220) plane γ-iron.

= 2.6524x(31.69-18.08) = 36.1 for (200) plane α-iron.

= 6.1199x(73.01-23.42) = 303.5 for (211) plane α-iron.

From equation 3.11 and knowing Cγ + Cα = 0.8, 0.2 was analyzed to be carbides by Seifert for AISI E52100 for standard heat treated samples;

$C\alpha_{(200)}$ / Cγ = (36.1/14)x(57.1/23.4) = 6.292 so, Cγ = 0.11, Cα = 0.69

$C\alpha_{(211)}$ / Cγ = (303.5/14)x(57.1/237) = 5.223 so, Cγ = 0.129, Cα = 0.671

By averaging the two obtained values from two different angles of α-iron:

$$C\gamma = (11+12.9)/2 = 11.9 \pm 0.9\ \%.$$

4.2 Shot Peening Machine and Methodology

Principal components of a shot peening machine are shot propelling device, shot cycling arrangements and a work handling conveyor. All parts of the equipment that are exposed to shot stream are enclosed and protected by rubber for confine the shot and permit it to be recycled.

Two methods of propelling the shot are used extensively for the process: One uses an electric motor driven bladed wheel, rotating at high speed. The other uses a continuous stream of compressed air which is like in this thesis work. In wheel method, shot is propelled by a combination of radial and tangential forces to impart necessary velocity to the shot. The air blast method introduces the shot by direct pressure into a stream of compressed air directed through a nozzle onto the work piece. Air blast method is able to produce higher intensities with small shot sizes, permits peening of deep holes and cavities by the help of nozzle and consumes less shot.

Equipment for shot recycling consists of devices for separation and removal of dust and undersized shot from the used shot mixture. An air curtain or air wash adjusted to the size of shot being used passes through the separator. Air blows the dust and undersized shot from the mixture, allowing the useful shot fall into a container for storage until reuse. A shot adding device automatically controls the level of shot in storage container and adds shot from a supply container as required.

Work handling equipments are differing from each other according to the application and work piece dimensions. For this work, rotating satellite type equipment is used with a shaft at center. Rings were mantled over the vertical shaft and rotation of work around the vertical axis is established by electric motor driven satellite.

Nozzle guiding the shot to the work piece surface is adjustable in terms of angle with vertical axis. This adjustment results in changing the angle of impingement of shot to the ring surface. As angle of impingement increases portion of the kinetic energy of shot applied to work piece surface by impact increases. As the angle decreases peening effectiveness decreases. In this thesis work angle of impingement was 80^{O}.

All peening work and controls are performed in conformance with AMS-S-13165 standard (SAE International, 1997).

4.3 Fatigue Life Tests

Test set-up is designed and manufactured by ORS Bearings for testing ball bearings under radial load. Test equipment main shaft, which the test bearings are mounted on, is supported by two self aligning type roller bearings. This shaft is made turn by electric motor with a 1540 rpm rotation speed, via a belt and because motor hub diameter is 2.6 times the diameter of main shaft, tested bearings are rotating with 4000 rpm. Radial load is applied through a lever mechanism and measured by load cell which is shown in *Figure 4.4*. Load measured by the load cell is half the applied load. Lubrication is supplied by a pump fed oil. The oil is filtered by a 5 µm filter and cooled by an air blower.

During life test period, temperature is continuously monitored by use of resistance temperature measurement transducers (PT-100) and load is recorded coming from the load cell. Vibration measurements are also done in periodic intervals generally 1 or 2 times a day.

Test batches with 16 different predetermined parameter sets were manufactured as mentioned through out the previous chapters. 5 bearings for each making totally 80 bearings were prepared for the tests plus the standard production 85 bearings were aimed to be tested. Standard production is without shot peening application and with super-finishing stone pressure 1.8 bars. Depending on the manufacturing process and applied parameter sets final residual stress distribution on bearing raceways were observed to be different from each other. For determination of the effect of these residual stress patterns on ball bearing fatigue life these life cycle tests were utilized.

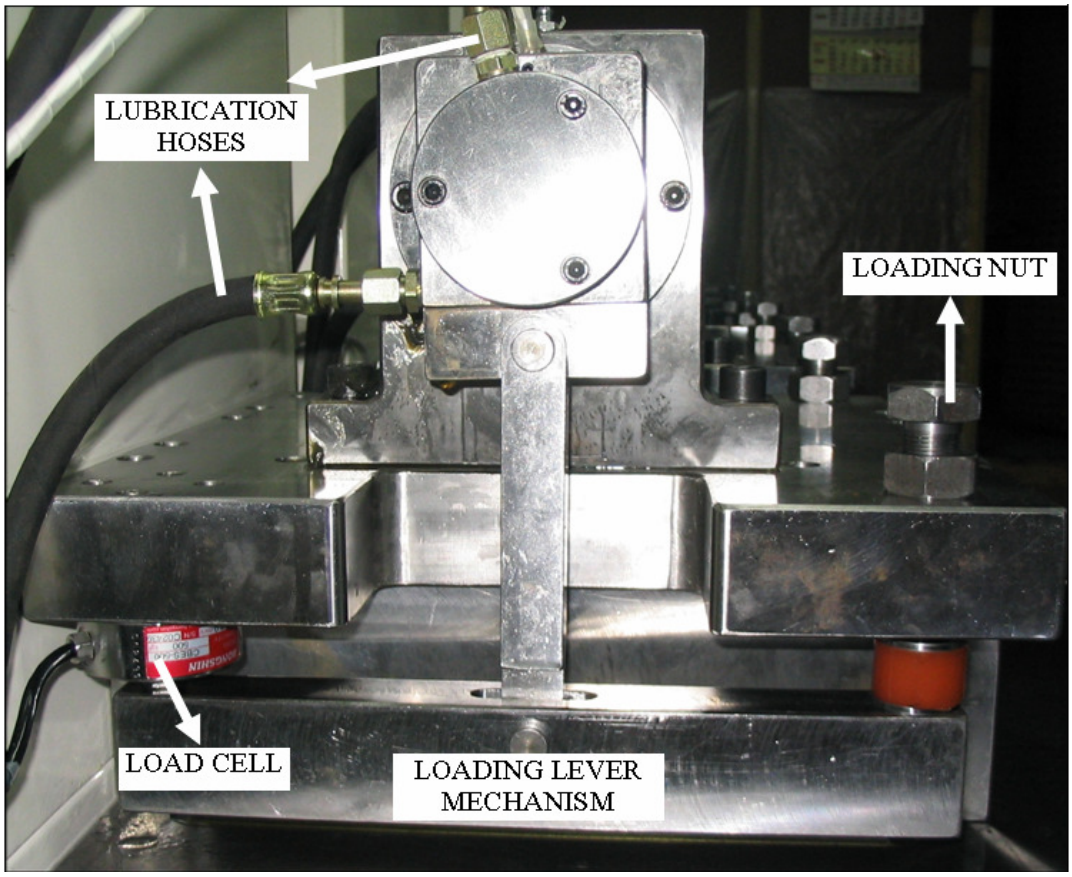

Figure 4.4 Life Test Equipment Loading Mechanism (Güley, 2004).

Test groups are employed in fatigue tests and the life in hours are recorded and given as Weibull statistical distribution as multiples of L_{10} life. L_{10} life means 90% of the bearings will not fail during the test and only 10% failed, so it is meaning is 90% reliability about not to fail. L_{10} life, as a general technical receiving, is calculated according to the following formula:

$$L_{10,h} = (C/P)^3 10^6/60n \qquad (4.3)$$

$L_{10,h}$: 90% reliable life time rating, in hours.
C : Dynamic load rating, in Newton.
P : Dynamic load applied, in Newton.
n : Rotation speed, in rpm.

In this work the applied load and rotation speed are 13730 N, 4000 rpm respectively. The dynamic load rating, C, value is 25670 N for 6207 type and so the life rating is;

$$L_{10,\,h} = (25670/13730)^3 10^6/4000.60 = 27 \text{ hours.}$$

Totally 75 bearings were tested and 54 among them are taken into consideration for evaluation of the effects of residual stresses on fatigue life. Bearings having life smaller than 27 hours and failed due to ball or outer ring are not included. Because experiments are conducted on inner rings and life period lower than 27 hours is out of reliability range (90%), only bearings in 90% reliability range and failed from inner ring fatigue are considered. Out of the groups given in *Table 6.1* one group including 8 bearings produced with standard production process but inner ring super-finished with 2.6 bar stone pressure (group SF) is tested for evaluation of effect of increasing super-finishing stone pressure on fatigue life.

Since the applied load is high, nearly the static load limit, compared to normal working loads of this type ball bearing in order to finish the tests faster due to time and equipment limitations, life tests do not resemble exact normal working conditions. Also, 54 bearings can be said enough to see the general trend but sample quantity must be increased for stronger observations.

CHAPTER 5

RESULTS OF THE EXPERIMENTS-I
RESIDUAL STRESS MEASUREMENTS

This chapter covers manufacturing process experiments about bearing inner ring production. Parameter studies on shot peening and super-finishing operations and their effect on residual stress and retained austenite are discussed.

5.1 Effect of Shot Peening Parameters on Residual Stress

Residual stress development on bearing rings start after heat treatment as mentioned before. Rings manufactured for this work are from AISI E52100 through hardening bearing steel with composition and inspection test results given in Chapter 1. Before coming to the heat treatment workshop they followed the production route given in *Figure 1.5*. The inner rings and outer rings are both hardened after austenitization by quenching in double oil tank so transformed into martensite by following double quench tank cooling curve (blue) on CCT diagram given in *Figure 1.6*.

Following hardening, rings are tempered for achieving ductility and toughness for hard and brittle martensite. Hardening and tempering parameters are given in *Table 5.1*. Also a representative heat treatment cycle (time vs. temperature diagram) is given in *Figure 5.1*. After tempering, residual stress on both circumferential and axial directions and retained austenite from inner ring raceways and hardness are measured. Values obtained are as tabulated in *Table 5.2*. Stress measurement directions are shown on *Figure 5.2*.

Table 5.1 Applied Heat Treatment Process Parameters

PARAMETERS	Inner Rings	Outer Rings
Furnace Temperature	865 ^{O}C	870 ^{O}C
Furnace Time	35 minutes	30 minutes
1st Oil Temperature	165 ^{O}C	165 ^{O}C
2nd Oil Temperature	50 ^{O}C	50 ^{O}C
Quench Times	90 sec, 70 sec	90 sec, 70 sec
Water Temperature	15 – 20 ^{O}C	15 – 20 ^{O}C
Hardness Before Tempering	65 – 65.5 HRC	65 – 65.5 HRC
Tempering Temperature	180 ^{O}C	200 ^{O}C
Tempering Time	90 minutes	90 minutes
Hardness After Tempering	62.5 – 63 HRC	61.5 – 62 HRC

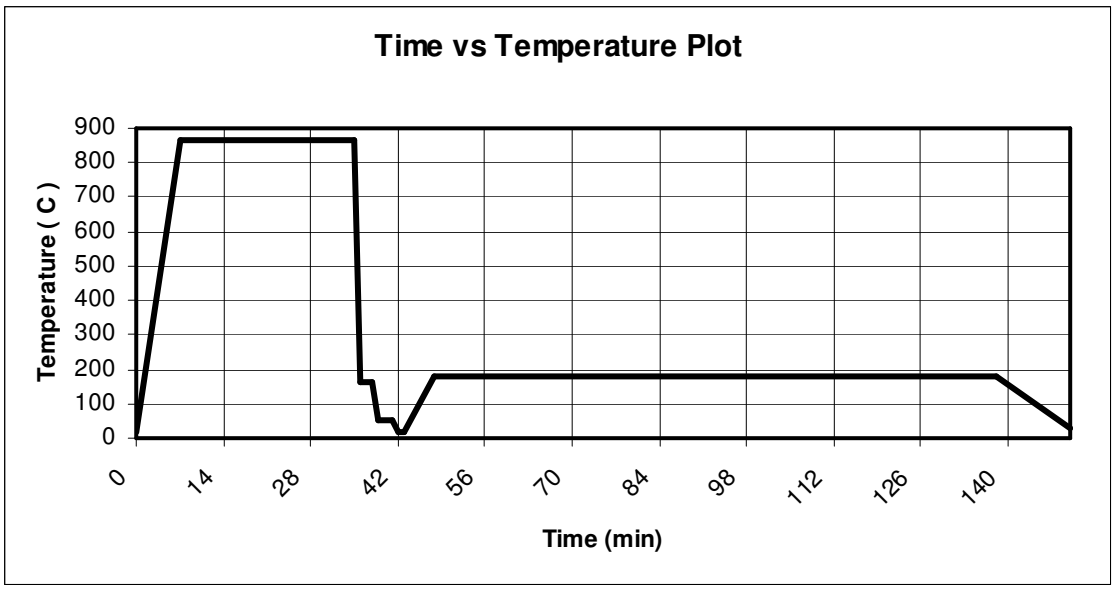

Figure 5.1 Heat Treatment Process Cycle.

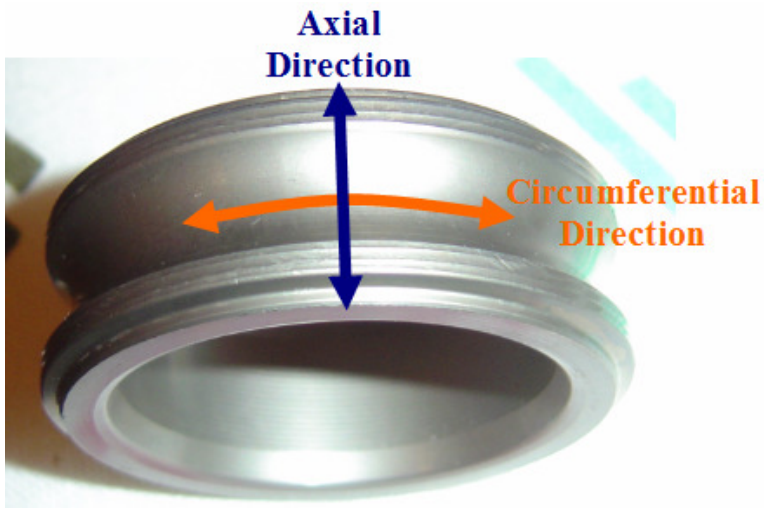

Figure 5.2 Residual Stress Measurement Directions.

Table 5.2 Residual Stress and Retained Austenite Measurements After Tempering.

Ring	Circum. (MPa)	Axial (MPa)	Ret. Austenite (%)	Hardness (HRC)
1	70	140	16	63.0
2	90	150	16	62.5
3	100	140	18	62.5
4	70	110	16	62.5
5	60	150	17	63.0
6	30	100	16	63.0
7	130	210	16	62.5
8	120	180	18	63.0
9	110	160	17	63.0
10	90	190	18	62.5
11	20	150	16	62.5
12	120	160	17	62.5
13	130	160	16	63.0
14	30	160	20	63.0
15	80	130	19	62.5
16	100	160	19	63.0

Hardness measurements in Rockwell C scale (HRC) are performed with 150 kg load applied via diamond cone having 120^{O} angle. Some hardness measurements throughout this study are conducted by microhardness device in Vickers scale (HV) with 500 grams load applied via diamond pyramid having 136^{O} angle. For all hardness data 3 measurements are conducted and average is taken as result according to EN ISO 6508-1 Standard.

Residual stresses on raceway surfaces of bearing rings are known to become 0 MPa after 5 – 10 µm beneath the surface as also given before in *Figure 1.8*. Due to this fact subsurface measurements are not considered as necessary to be done.

All measurement device calibrations, including XRD, hardness measurement, micrometers and comparators, roughness and surface profile measurement, roundness, calibration masters, furnace thermocouples and oil quality analysis are done according to related standards with periods ranging between 3 months to 1 year. Also they are traceable from calibration certificates and records kept in conformance to ISO EN 16949 and 9001 standards requirements. Tolerance for all temperatures given is ± 5 ^{O}C, all hardness measurements is ± 0.5 HRC, for all stress measurements is ± 20 MPa, for all retained austenite measurements is ± 1%.

Within this work 16 test groups, differentiated due to shot peening parameters and super-finishing stone pressure, are studied. 16 inner rings after tempering are measured for stress, retained austenite and hardness and numbered in order to be distributed to these 16 product batches. All following measurements discussed in later sections are also done on these rings. The type of bearing studied is 6207, so experiments about process parameters are applied on 6207 IR (inner ring). 6207 OR (outer ring) is manufactured with standard production route. Schematic representative of 6207 IR is shown in *Figure 5.3*.

Variables in parameter studies are allowed to change as far as it obeys the final product specifications. Since, a ball bearing is a commercial product which has very

strict quality aspects, dimensional and structural limitations have to be standardized. For 6207 IR allowed minimum hardness after tempering was 59 HRC and maximum austenite was 20%.

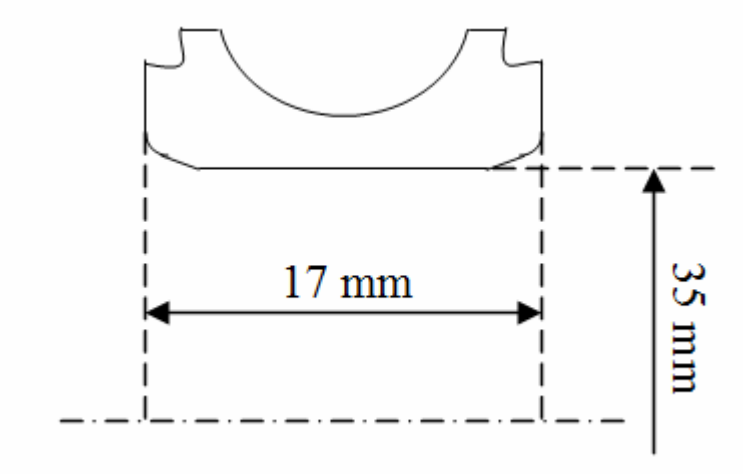

Figure 5.3 6207 IR Representative Drawing.

Hardened and tempered 6207 type inner rings were sent to grinding shop for face, bore and raceway grinding. After face and bore grinding to final dimensions raceways were ground to + 30 µm from nominal raceway diameter with a - 12µm to 0 µm tolerance range.

Next step in manufacturing test batches was shot peening operation applied on raceways of inner rings. Rings were lined up on a vertical shaft which is connected to a rotating disk called satellite, and during rotation they were bombarded by a nozzle guided steel shot stream while the nozzle is moving also in vertical direction. Schematic representation of the process is shown in *Figure 5.4*.

Shot peening of 6207 inner rings were performed by keeping shot class, shot hardness, satellite rotation speed and direction, nozzle speed and nozzle angle as constant, these values are tabulated in *Table 5.3*. Parameters studied in shot peening are:

- Air pressure
- Flow rate
- Coverage

A combination of studied parameters is given in *Table 5.4*.

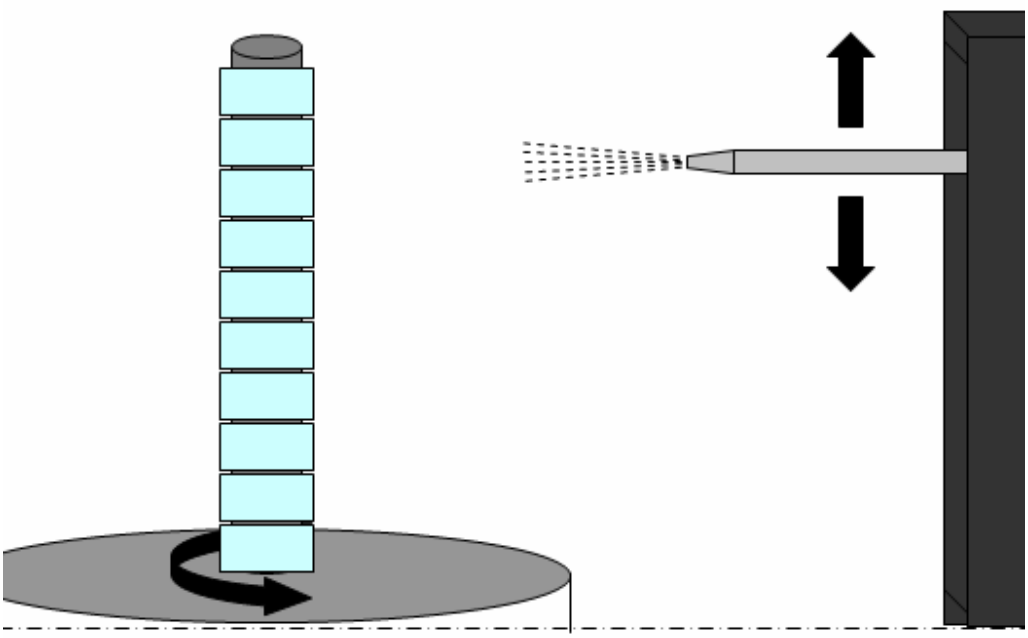

Figure 5.4 Schematic Illustration of Shot Peening Process.

Table 5.3 Constant Shot Peening Parameters.

Parameter	**Value**
Shot Class (No)	S 230 (0.50-0.85 mm)
Shot Hardness	58 – 62 HRC
Shot Microstructure	Tempered Martensite
Satellite Speed	20 rpm
Rotation Direction	Counter-clockwise
Nozzle Speed	150 mm/min (vertical)
Nozzle Angle	80^{O} (with vertical)
Nozzle to Ring Distance	150 mm
Standard	MIL-S-13165C

About the values given in *Table 5.3*, shot hardness is measured from three sample balls, by mounting the balls into bakelite, grinding, polishing and measuring hardness with Vickers microhardness device. Microstructure is observed under optical microscope by etching the polished balls.

Table 5.4 Shot Peening Parameter Studies.

Group	Air Pressure (Bar)	Shot Flow Rate (kg/min)	Coverage (%)	Almen A Intensity (mm)
1	2	2	100	0.37
2	2	2	200	0.41
3	2	3	100	0.36
4	2	3	200	0.39
5	3	2	100	0.45
6	3	2	200	0.49
7	3	3	100	0.44
8	3	3	200	0.48

For the group having coverage parameter 100% in each two groups having the same parameters other than coverage in *Table 5.4*, coverage is attained by testing a sample ring covered completely with a fluorescent dye and inspection after peening. By use of determined time for 100% coverage doubled time peening is applied for 200% coverage groups. Almen A class strips, dimensions can be seen from *Figure 1.14*, are used for intensity determination.

The 16 rings, measured after heat treatment, were distributed to the eight shot peening groups as follows:

Ring 1,2 to group 1, ring 3,4 to group 2, ring 5,6 to group 3, ring 7,8 to group 4, ring 9,10 to group 5, ring 11,12 to group 6, ring 13,14 to group 7 and ring 15,16 to group 8.

Residual stresses and retained austenite from 16 rings, also by cutting and mounting one ring from each group out of these 16, micro-hardness just below peened raceway surface (30 – 50 µm below the surface) were measured. Investigated results are as given in *Table 5.5*.

Table 5.5 Residual Stress and Retained Austenite Measurements After Rough Grinding and Shot Peening.

Group	Ring	Circum. (MPa)	Axial (MPa)	Ret. Austenite (%)	Hardness (HRC)
1	**1**	-900	-980	14	62.5 - 63.0
	2	-890	-980	15	
2	**3**	-880	-980	14	63.0 - 63.5
	4	-830	-960	15	
3	**5**	-850	-940	13	63.0 - 63.5
	6	-810	-960	15	
4	**7**	-890	-950	13	63.5 - 64.0
	8	-850	-970	15	
5	**9**	-830	-910	13	64.0 - 64.5
	10	-780	-840	13	
6	**11**	-740	-830	11	64.0 - 64.5
	12	-800	-880	14	
7	**13**	-800	-920	15	63.5 - 64.0
	14	-840	-940	15	
8	**15**	-840	-900	13	65.0
	16	-810	-980	13	

When compared to measurements after heat treatment, retained austenite transformation and increase in residual compression and hardness can obviously be seen from *Table 5.5*.

For observation of air pressure effect on residual stress, rings processed in the same way but only peened with different air pressures have to be compared. So, comparison of group 1 with group 5, group 2 with group 6, group 3 with group 7,

group 4 with group8 will resemble the air pressure effect. Necessary data for comparison purpose is given in *Table 5.6*. These groups are compared according to the following parameters:

- Circumferential residual stress change compared to after heat treatment.
- Axial residual stress change compared to after heat treatment.
- Retained austenite transformation compared to after heat treatment.
- Hardness increase by comparison of core and raceway Vickers micro-hardness measurements of cut and mounted rings.

Table 5.6 Effect of Air Pressure on
Surface Stress, Hardness, Almen Intensity, Retained Austenite.

Group	Circum. (ΔMPa)	Axial (ΔMPa)	Ret. Austenite (Δ%)	Hardness (ΔHRC)	Almen A Intensity (mm)
1	-975	-1125	-1.5	0	0.37
5	-905	-1050	-4.5	1.5	0.45
2	-940	-1095	-2.5	0.75	0.41
6	-840	-1010	-4	1.75	0.49
3	-875	-1075	-2.5	0.25	0.36
7	-900	-1090	-3	0.75	0.44
4	-995	-1155	-3	1	0.39
8	-915	-1085	-6	2.25	0.48

Looking at tabulated values in *Table 5.6* following results can be seen, arising from air pressure increase from 2 bar to 3 bar:

- Average stress change in circumferential direction is +56.25 MPa.
- Average stress change in axial direction is +53.75 MPa.
- Average retained austenite transformation difference is -2%.
- Average hardness increase is 1.06 HRC.
- Average Almen intensity increase is 0.08 mm Almen A.

By evaluating the above observations, as air pressure increases:

- ✓ Surface residual stress increases, so becomes less compressive.
- ✓ Retained austenite decreases, so transforms more into martensite.
- ✓ Hardness increases.
- ✓ Peening intensity increases.

Evaluation of flow rate change on residual stress can be done by comparing rings with same process parameters only with flow rate difference. Within this respect, group 1 and group 3, group 2 and group 4, group 5 and group 7, group 6 and group 8 are compared. Comparison table can be seen as *Table 5.7*. Comparison is done, based on the measurements after heat treatment, according to the following parameters:

- Circumferential residual stress change.
- Axial residual stress change.
- Retained austenite transformation.
- Hardness increase by comparison of core and raceway Vickers micro-hardness measurements of cut and mounted rings.

From the data tabulated in *Table 5.7*; for an increase in flow rate from 2 kg/min to 3 kg/min. the following results can be obtained:

- Average stress change in circumferential direction is -6.25 MPa.
- Average stress change in axial direction is -31.25 MPa.
- Average retained austenite transformation difference is -0.5%.
- Average hardness increase is 0.06 HRC.
- Average Almen intensity decrease is 0.01 mm Almen A.

Table 5.7 Effect of Shot Flow Rate on
Surface Stress, Hardness, Almen Intensity, Retained Austenite.

Group	Circum. (ΔMPa)	Axial (ΔMPa)	Ret. Austenite (Δ%)	Hardness (ΔHRC)	Almen A Intensity (mm)
1	-975	-1125	-1.5	0	0.37
3	-875	-1075	-2.5	0.25	0.36
2	-940	-1095	-2.5	0.75	0.41
4	-995	-1155	-3	1	0.39
5	-905	-1050	-4.5	1.5	0.45
7	-900	-1090	-3	0.75	0.44
6	-840	-1010	-4	1.75	0.49
8	-915	-1085	-6	2.25	0.48

By evaluating the above observations, as shot flow rate increases:

- ✓ Surface residual stress decreases slightly, so becomes a little more compressive.
- ✓ Retained austenite decreases very slightly, so transforms very little more into martensite.
- ✓ Hardness can not be said increases.
- ✓ Peening intensity can not be said changed.

To sum up, shot flow rate from 2 -3 kg/min does not make any significant change, so effect is too small. It only decreases the time to achieve 100% coverage.

Observing the coverage effect on stress development is possible by comparing rings with different coverage percentages but all other parameters are same with each other. In order to achieve this group 1 with group 2, group 3 with group 4, group 5 with group 6 and finally group 7 and group 8 are compared in *Table 5.8*. As in air pressure and flow rate effect evaluation cases, comparison is done again on heat treatment measurements basis and according to the following parameters:

- Circumferential residual stress change.
- Axial residual stress change.

- Retained austenite transformation.
- Hardness increase by comparison of core and raceway Vickers micro-hardness measurements of cut and mounted rings.

Table 5.8 Effect of Coverage on
Surface Stress, Hardness, Almen Intensity, Retained Austenite.

Group	Circum. (ΔMPa)	Axial (ΔMPa)	Ret. Austenite (Δ%)	Hardness (ΔHRC)	Almen A Intensity (mm)
1	-975	-1125	-1.5	0	0.37
2	-940	-1095	-2.5	0.75	0.41
3	-875	-1075	-2.5	0.25	0.36
4	-995	-1155	-3	1	0.39
5	-905	-1050	-4.5	1.5	0.45
6	-840	-1010	-4	1.75	0.49
7	-900	-1090	-3	0.75	0.44
8	-915	-1085	-6	2.25	0.48

By use of above given data results listed below can be issued:

- Average stress change in circumferential direction is -8.75 MPa.
- Average stress change in axial direction is -1.25 MPa.
- Average retained austenite transformation difference is -1%.
- Average hardness increase is 0.81 HRC.
- Average Almen intensity increase is 0.04 mm Almen A.

Thus, as coverage increases:

- ✓ Surface residual stress decreases very slightly, so becomes very little more compressive.
- ✓ Retained austenite decreases slightly, so transforms a little more into martensite.
- ✓ Hardness increases.
- ✓ Peening intensity increases.

As a summary, surface stress does not change, but retained austenite, hardness and intensity changes significantly.

The effect of shot peening parameters on surface residual stresses has been studied. Also, effects of parameters on subsurface residual stress are studied in the following section. The hardness, retained austenite and Almen intensity measurements have been done on test specimens. The most effective parameter is the air pressure when retained austenite, hardness and Almen Intensity are considered. The effect of shot flow rate and coverage on surface residual stress is nearly identical. Surprisingly air pressure increase made the surface stress become less compressive. But effect of parameters on residual stress should be evaluated with especially the subsurface stress distribution and depth of compressive stress. So, surface stress level comparison which does not possess too much difference is not considered as important.

The effect of shot peening parameters on residual stresses, retained austenite, hardness and peening intensity is summarized in *Table 5.9*. In this table values in parenthesis are with respect to the highest one taken as 100%. Green highlighted values are the highest ones in the expected direction. Every effect from parameters are well matching with the theory, except increase in surface residual stress in tensile direction as air pressure increases, but in next section subsurface stress evaluation is performed so it is more important and considerable than surface residual stresses.

Table 5.9 Effects of Shot Peening Parameters on
Surface Residual Stress, Retained Austenite, Hardness, Intensity.

Parameter	Circum. (ΔMPa)	Axial (ΔMPa)	Ret. Aust. (Δ%)	Hardness (ΔHRC)	Almen A Int. (Δmm)
Air Pressure 2 → 3 bar	56.25 (100)	53.75 (100)	**-2.0 (-100)**	**1.06 (100)**	**0.08 (100)**
Flow Rate 2 → 3 kg/min	-6.25 (-11)	**-31.25 (-58)**	-0.5 (-25)	0.06 (6)	0.01 (13)
Coverage 100% → 200%	**-8.75 (-16)**	-1.25 (-2)	-1.0 (-50)	0.81 (76)	0.04 (50)

After evaluation of results, effects in verbal manner are tabulated in *Table 5.10.*

Table 5.10 Summary of Effects of Shot Peening Parameters on
Surface Residual Stress, Retained Austenite, Hardness, Intensity.

	Effect on	Surf. Res. Stress	Ret. Aust. Transform.	Hardness Increase	Int. Increase
Parameters	**Air Pressure 2 → 3 bar**	Small Opposite	Important	Important	Important
	Flow Rate 2 → 3 kg/min	Small	Small	Poor	Poor
	Coverage 100% → 200%	Poor	Considerable	Considerable	Considerable

5.2 Effect of Super-finishing Stone Pressure on Residual Stress

As next step after shot peening, inner ring raceways which were ground to +30 µm from nominal diameter were final ground and super-finished to -10 µm from nominal raceway diameter. By the way, fillets on raceways due to peening were eliminated by material removal from the raceway. Material removal from raceways after shot peening was between 28 – 40 µm in diameter so from one side this means 14 – 20 µm.

Parameter, which is the one that effect on residual stress was tried to be observed during the final process step, super-finishing, was stone pressure which was 1.8 bar and 2.6 bar during the studies. All other parameters namely oscillation speed, ring rotation speed, process time were kept constant. As ring rotation over stone oscillation ratio; 18 rpm/oscillation was used, this was determined as the best in thesis study submitted by Güley (2004). Process time was 8 seconds. After super-finishing, raceway dimensional and geometrical measurements were done in the laboratory and the obtained results with tolerances are given in *Table 5.11*.

Table 5.11 Dimensional Control Results After Super-finishing.

Parameter	**Diameter**	**Form**	**Ra**	**Roundness**	**Radius**	**Run out**
Tolerance	-8 to-20 µm	1.8 µm	0.04 µm	1.5 µm	±30 µm	3 µm
Group	Measurements					
1	-10	1.0	0.02	0.77	18	0.95
2	-11	1.1	0.02	0.24	20	0.98
3	-10	1.1	0.02	0.17	18	1.05
4	-10	1.1	0.02	0.60	19	1.02
5	-11	1.0	0.03	0.65	20	1.15
6	-10	0.9	0.03	0.34	19	0.99
7	-11	1.0	0.02	0.29	19	1.12
8	-10	1.0	0.03	0.51	20	1.09

In *Table 5.11*, run out value is the radial run out of raceway with respect to face and Ra value is the average roughness of raceway surface. The 8 samples for *Table 5.11* are randomly selected from the shot peening groups without caring super-finish stone pressure; because several trials had shown before, changing the pressure from 1.8 bar to 2.6 bar negligibly effect the above measured values. Thus, in these 8 samples some are super-finished with 2.6 bar and some are with 1.8 bar pressure. The parameters of shot peening and super-finishing stone pressure trials with 1.8 bar and 2.6 bar resulted in 16 different groups which are listed with all parameters in *Table 5.12*.

Table 5.12 Groups After Super-finishing.

		Group	Air Pressure (Bar)	Flow Rate (kg/min)	Coverage (%)	Stone Pressure (Bar)
Shot Peening Group	**SP 1**	1	2	2	100	1.8
		2	2	2	100	2.6
	SP 2	3	2	2	200	1.8
		4	2	2	200	2.6
	SP 3	5	2	3	100	1.8
		6	2	3	100	2.6
	SP 4	7	2	3	200	1.8
		8	2	3	200	2.6
	SP 5	9	3	2	100	1.8
		10	3	2	100	2.6
	SP 6	11	3	2	200	1.8
		12	3	2	200	2.6
	SP 7	13	3	3	100	1.8
		14	3	3	100	2.6
	SP 8	15	3	3	200	1.8
		16	3	3	200	2.6

Finishing the rings manufacturing, surface residual stress and retained austenite from the 16 samples (samples measured after heat treatment) and hardness just below the raceway surfaces, after subsurface residual stress measurement, by cutting, mounting and polishing followed by Vickers micro-hardness measurements are performed and results are tabulated as *Table 5.13*. Residual stress profiles beneath the surface observed via subsurface measurements are plotted also for each group.

Table 5.13 Surface Residual Stress and Retained Austenite Measurements After Super-finishing.

Group	Circum. (MPa)	Axial (MPa)	Ret. Austenite (%)	Hardness (HRC)
1	-1230	-1410	12	63.0
2	-1240	-1340	13	63.5
3	-1220	-1390	11	64.0
4	-1210	-1350	13	64.0
5	-1190	-1390	11	64.0
6	-1200	-1280	15	64.0
7	-1210	-1410	13	64.5
8	-1320	-1420	14	64.5
9	-1170	-1380	13	64.5
10	-1190	-1320	13	64.0
11	-1220	-1380	10	64.0
12	-1340	-1420	11	64.5
13	-1210	-1350	12	64.0
14	-1210	-1340	13	64.0
15	-1220	-1420	13	65.0
16	-1290	-1390	10	65.0

Comparison of results given in *Table 5.13* is done according to the following parameters and given in *Table 5.14*:

- Circumferential residual stress change with respect to measure after shot peening.
- Axial residual stress change with respect to measure after shot peening.
- Retained austenite transformation compared to measure after shot peening.

- Hardness increase by comparison of core and raceway Vickers micro-hardness measurements of cut and mounted rings.

Table 5.14 Effect of Final Grinding and Super-finishing on Surface Stress, Hardness, Retained Austenite.

Group	Circum. (ΔMPa)	Axial (ΔMPa)	Ret. Austenite (Δ%)	Hardness (ΔHRC)
1	-330	-430	-2	1.0
2	-350	-360	-2	1.0
3	-340	-410	-3	1.5
4	-380	-390	-2	1.5
5	-340	-450	-2	1.0
6	-390	-320	0	1.0
7	-320	-460	0	2.0
8	-470	-450	-1	1.5
9	-340	-470	0	1.5
10	-410	-480	0	1.5
11	-480	-550	-1	1.5
12	-540	-540	-3	2.0
13	-410	-430	-3	1.0
14	-370	-400	-2	1.0
15	-380	-520	0	2.0
16	-480	-410	-3	2.0

By looking to *Table 5.14* it is obviously seen that final grinding and super-finishing increases residual surface stress in compression direction. Some retained austenite also transforms into martensite during these processes. Since, hardness increase is with respect to core hardness of the cut and mounted rings; increase after tempering can be seen. This increase is due to total effect of shot peening, grinding and super-finishing operations. When compared to average hardness increase detected after shot peening, that is 1.03 HRC; final grinding and super-finishing can said to be very slightly affecting hardness. Main hardness increase can be attributed to shot peening.

In order for determining effect of super-finishing stone pressure on surface residual stress, groups with same manufacturing parameters except stone pressure are compared by use of data in *Table 5.14* and results listed below are issued for stone pressure increase from 1.8 bar to 2.6 bar:

- Average stress change in circumferential direction is -56.25 MPa.
- Average stress change in axial direction is 46.25 MPa.
- Average retained austenite transformation difference is -0.25%.
- Average hardness increase could not be determined due to the fact that hardness increase only from super-finishing is not known. For this to be determined, hardness measurement from the same ring raceway has to be done after shot peening and after super-finishing. But impossible to do because for raceway hardness measurement, one slice from the ring is cut and mounted into bakelite, a cut ring can not be ground and super-finished. Thus different samples for hardness measurement are used after super-finishing and shot peening.

As a summary, as stone pressure increases:

- ✓ Surface residual stress very slightly decreases in circumferential, increases in axial direction. But no significant effect is detected.
- ✓ Retained austenite decreases slightly.

For observation of shot peening parameters effect on subsurface stress profile the following plots and *Table 5.15* are inspected:

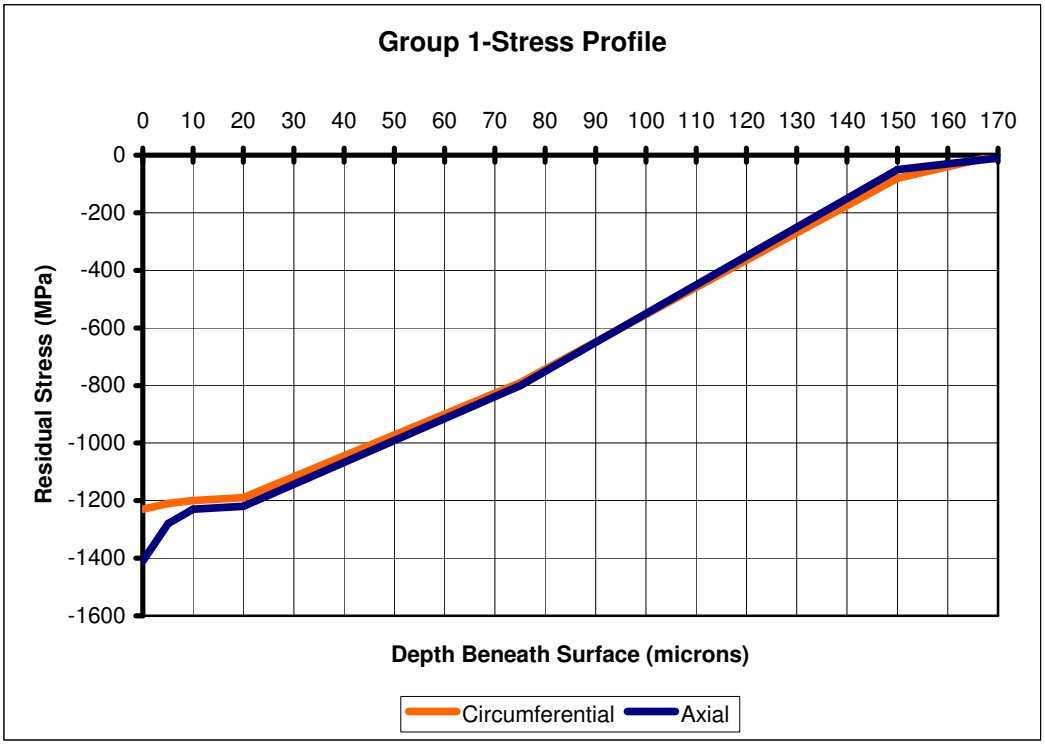

Figure 5.5 Group 1 Residual Stress Profile.

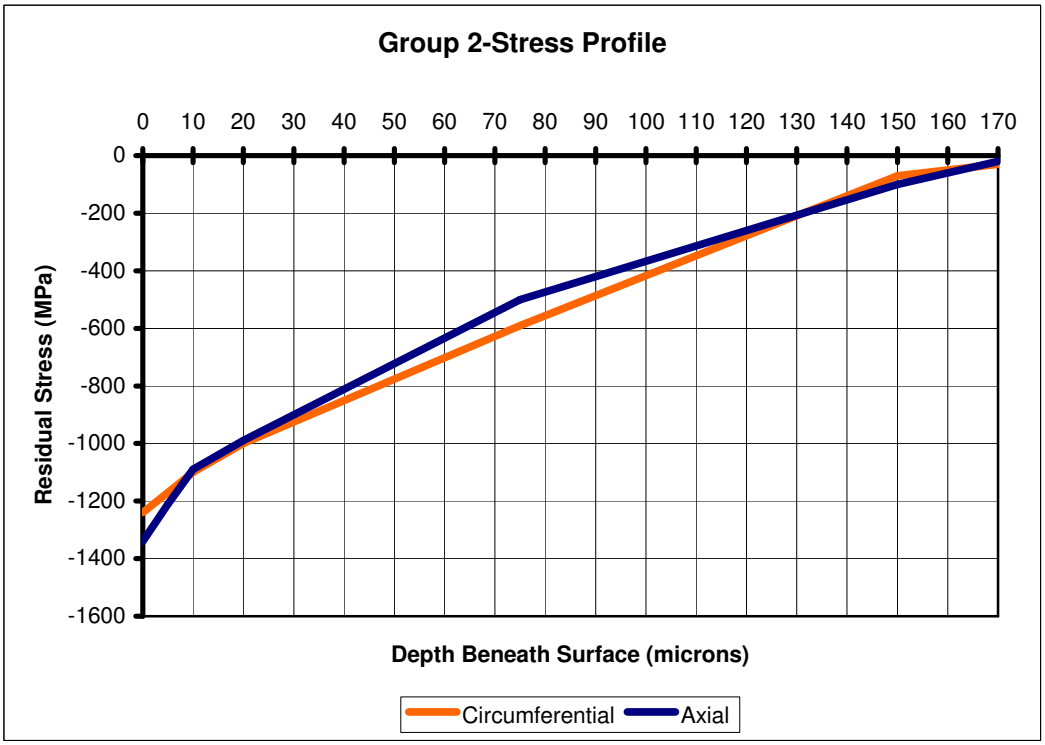

Figure 5.6 Group 2 Residual Stress Profile.

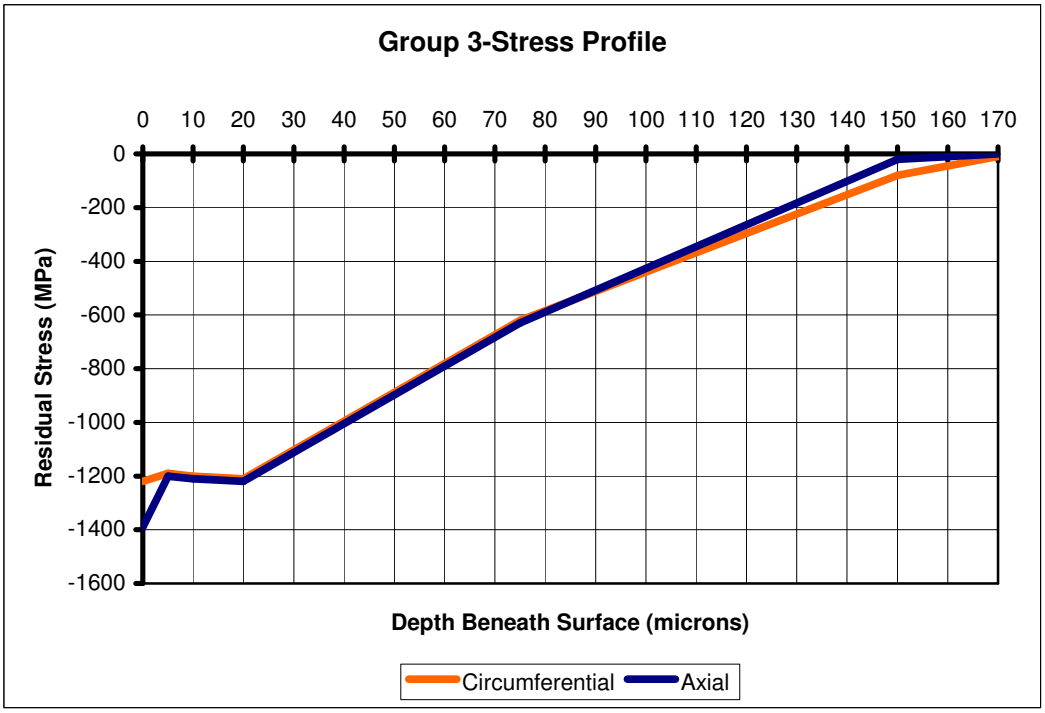

Figure 5.7 Group 3 Residual Stress Profile.

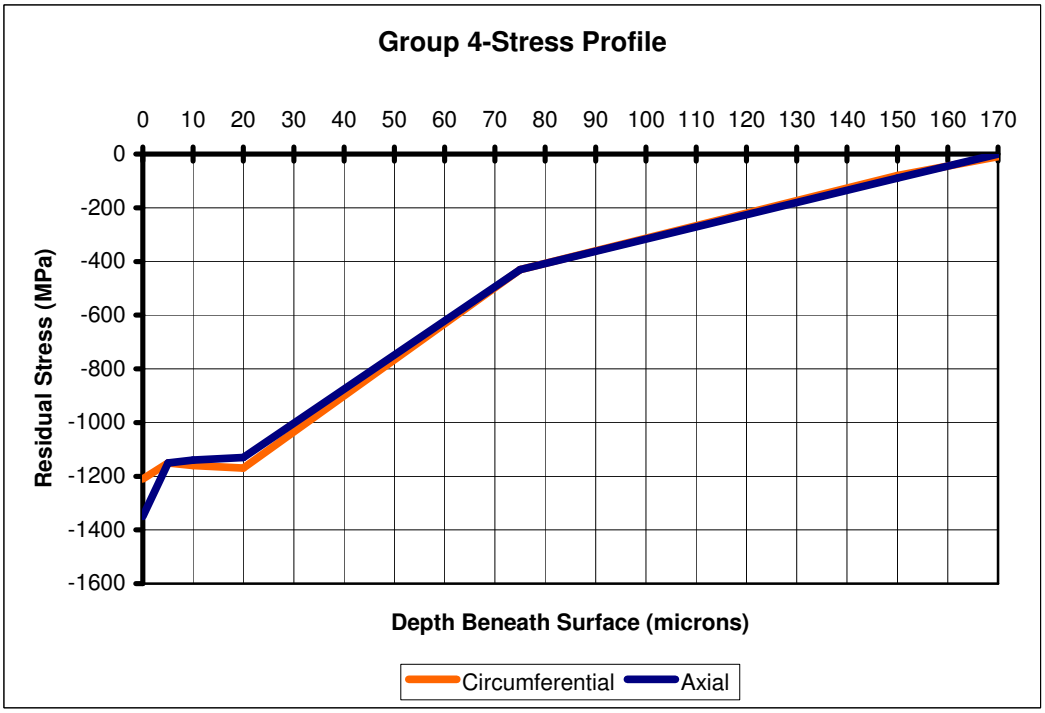

Figure 5.8 Group 4 Residual Stress Profile.

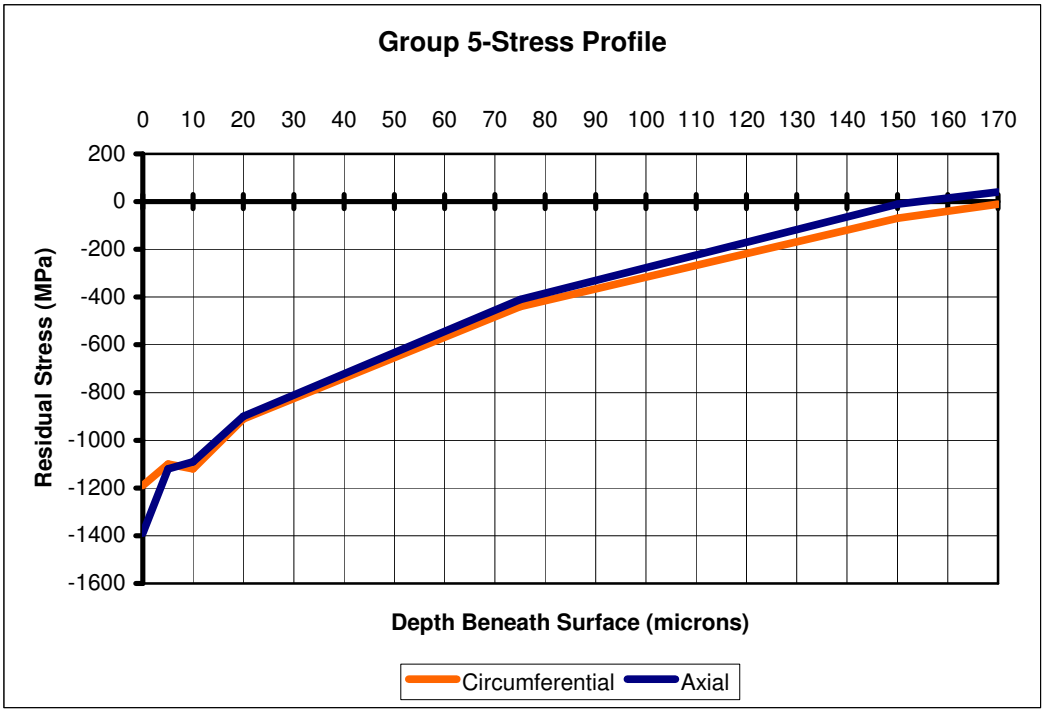

Figure 5.9 Group 5 Residual Stress Profile.

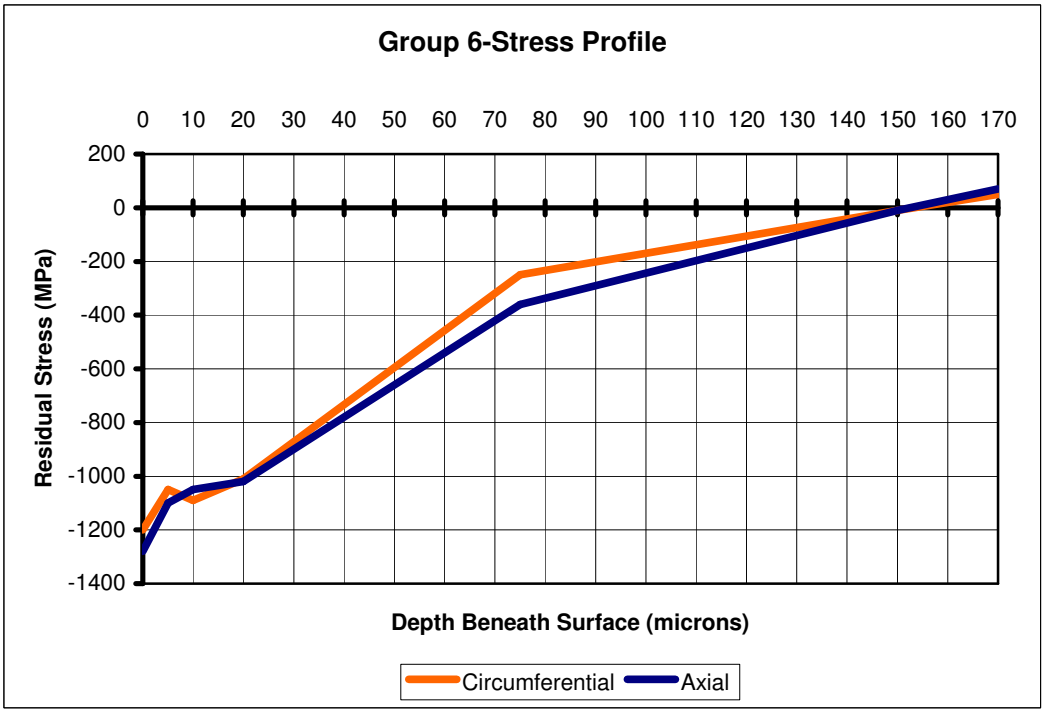

Figure 5.10 Group 6 Residual Stress Profile.

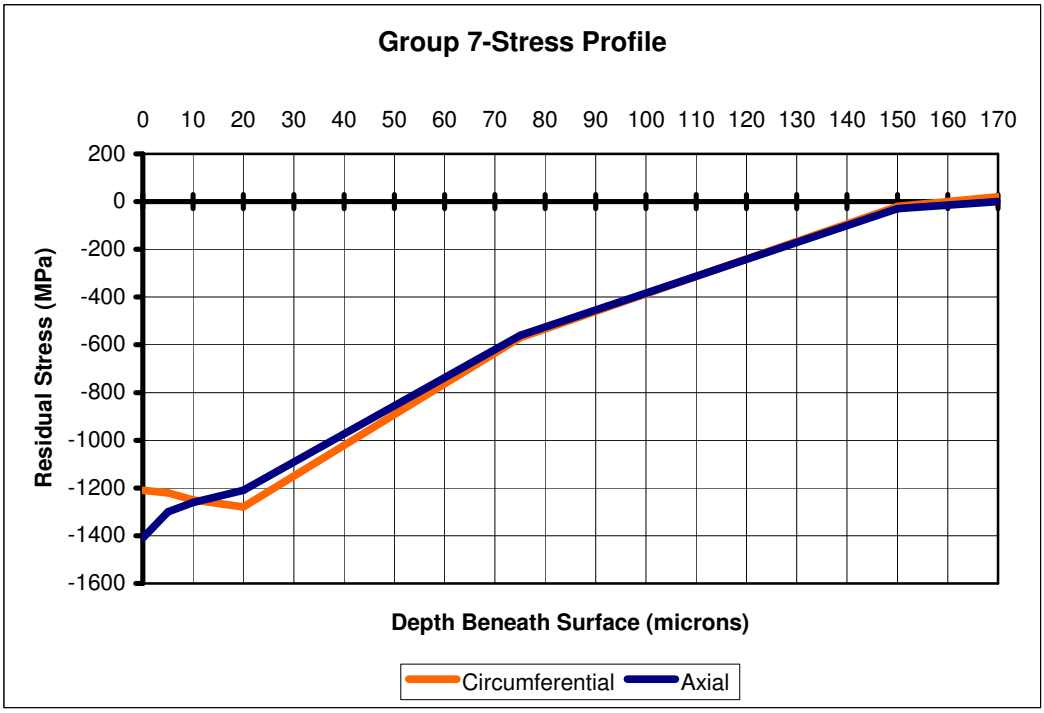

Figure 5.11 Group 7 Residual Stress Profile.

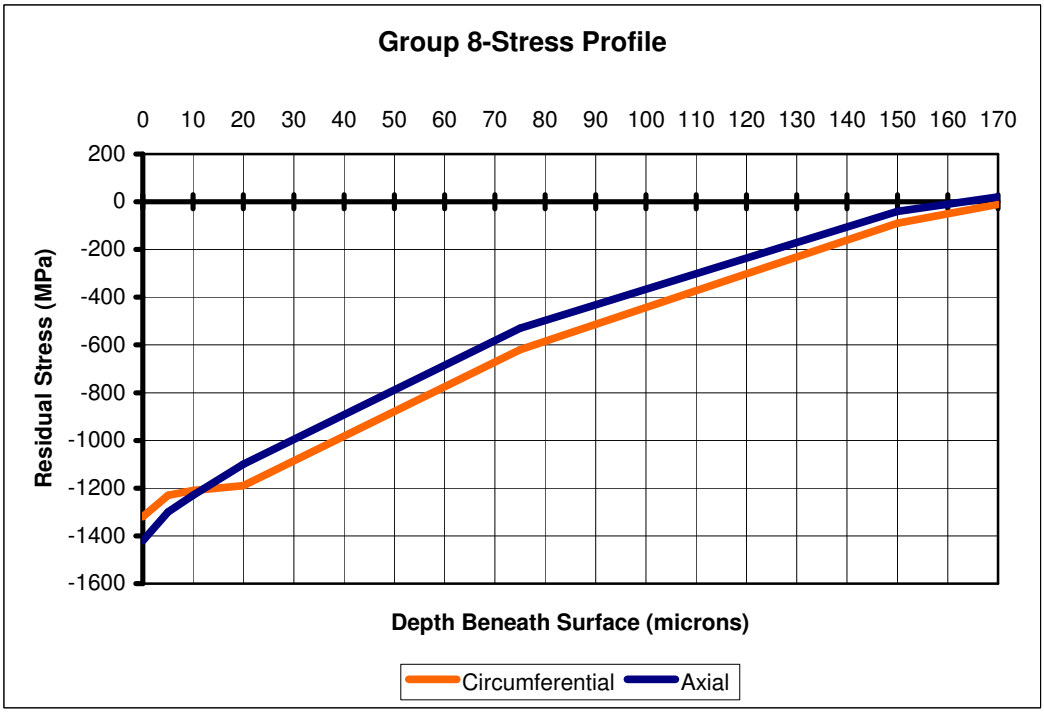

Figure 5.12 Group 8 Residual Stress Profile.

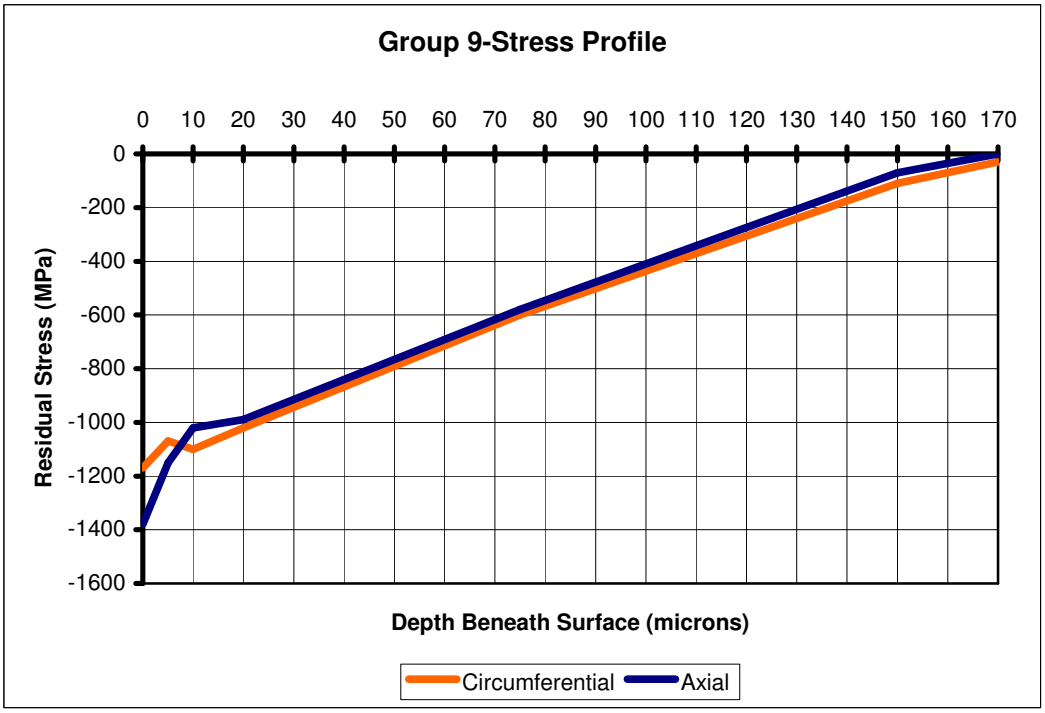

Figure 5.13 Group 9 Residual Stress Profile.

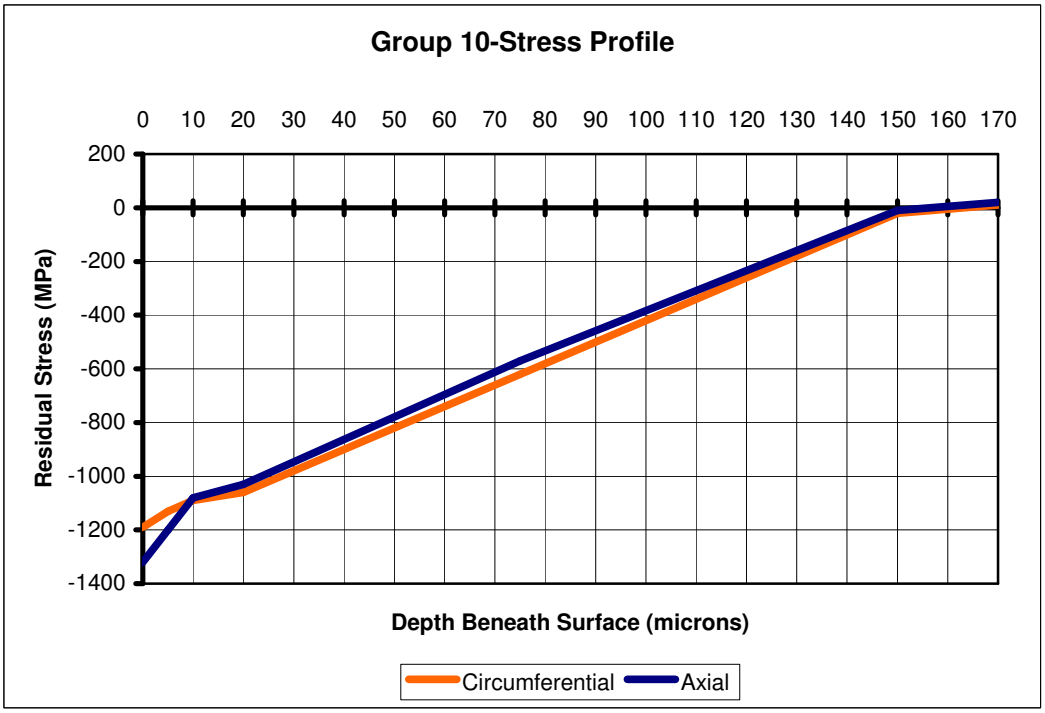

Figure 5.14 Group 10 Residual Stress Profile.

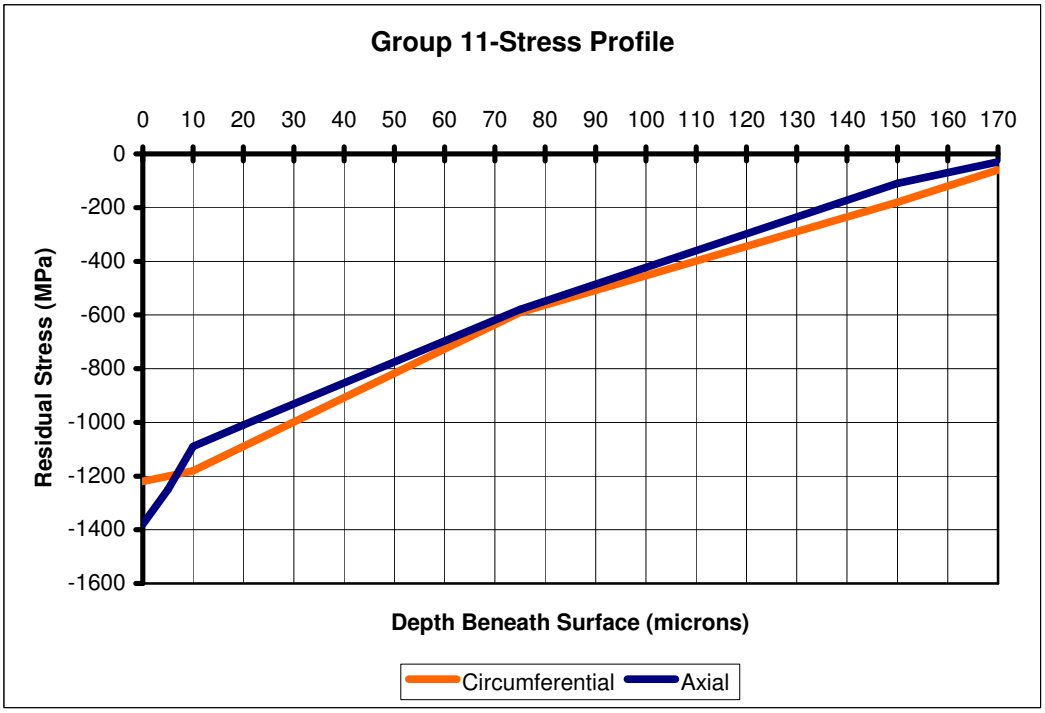

Figure 5.15 Group 11 Residual Stress Profile.

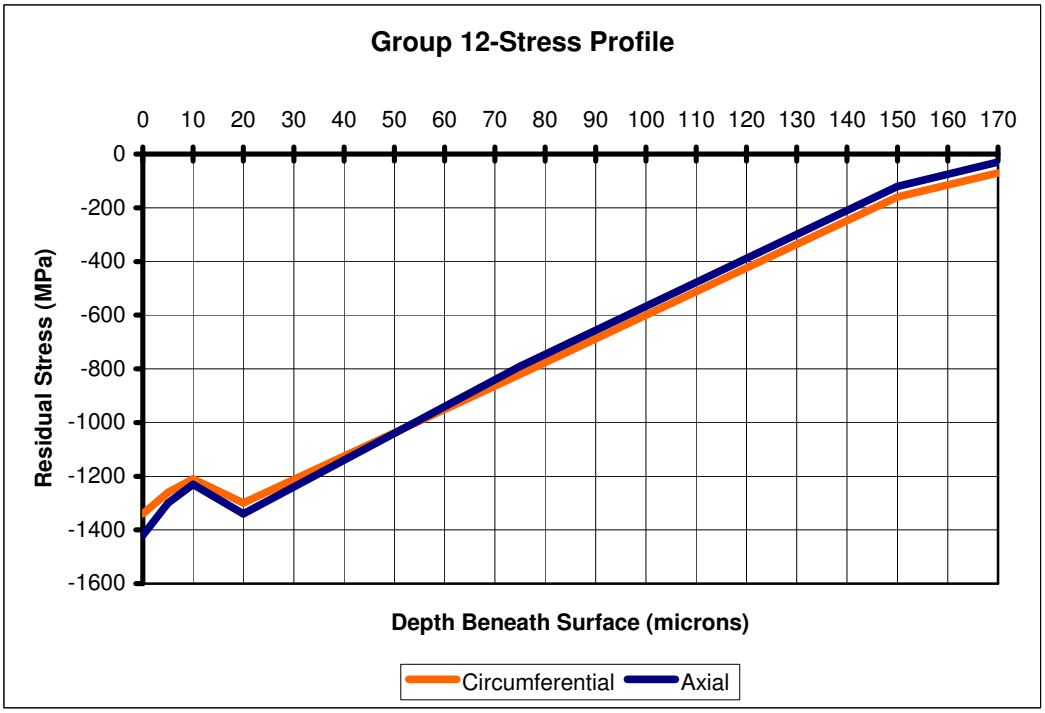

Figure 5.16 Group 12 Residual Stress Profile.

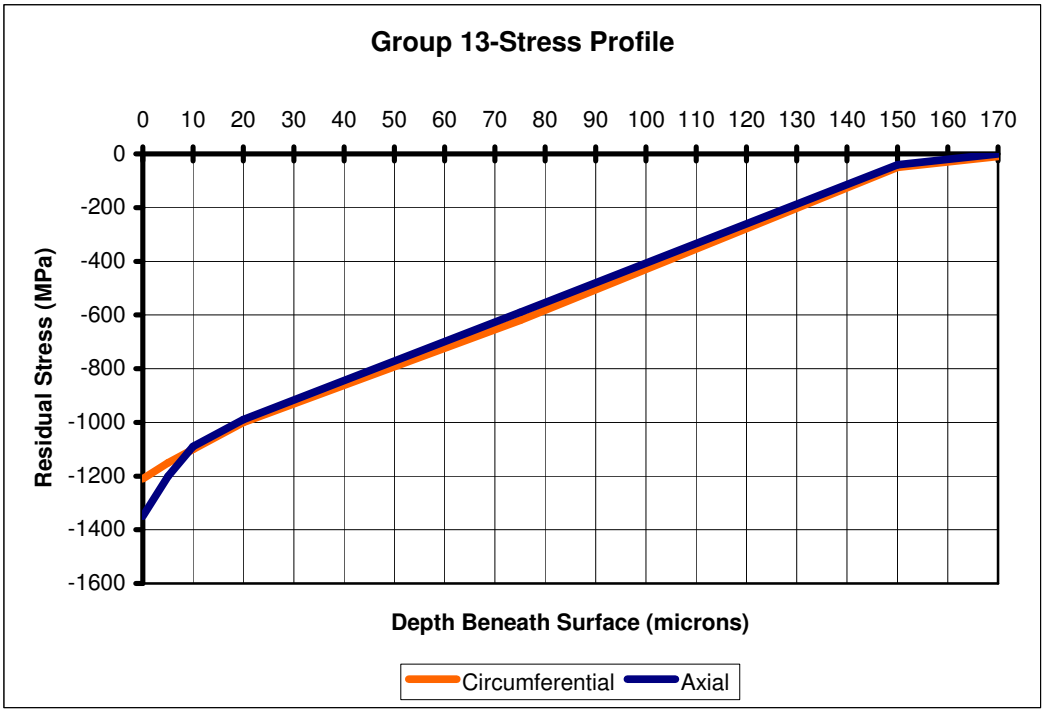

Figure 5.17 Group 13 Residual Stress Profile.

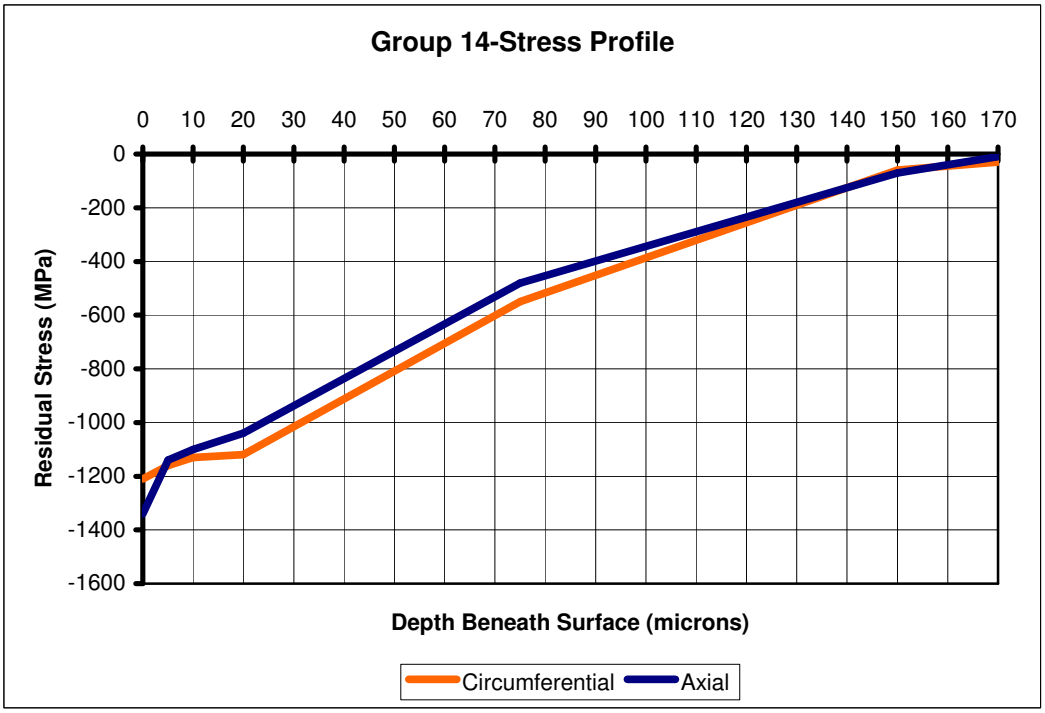

Figure 5.18 Group 14 Residual Stress Profile.

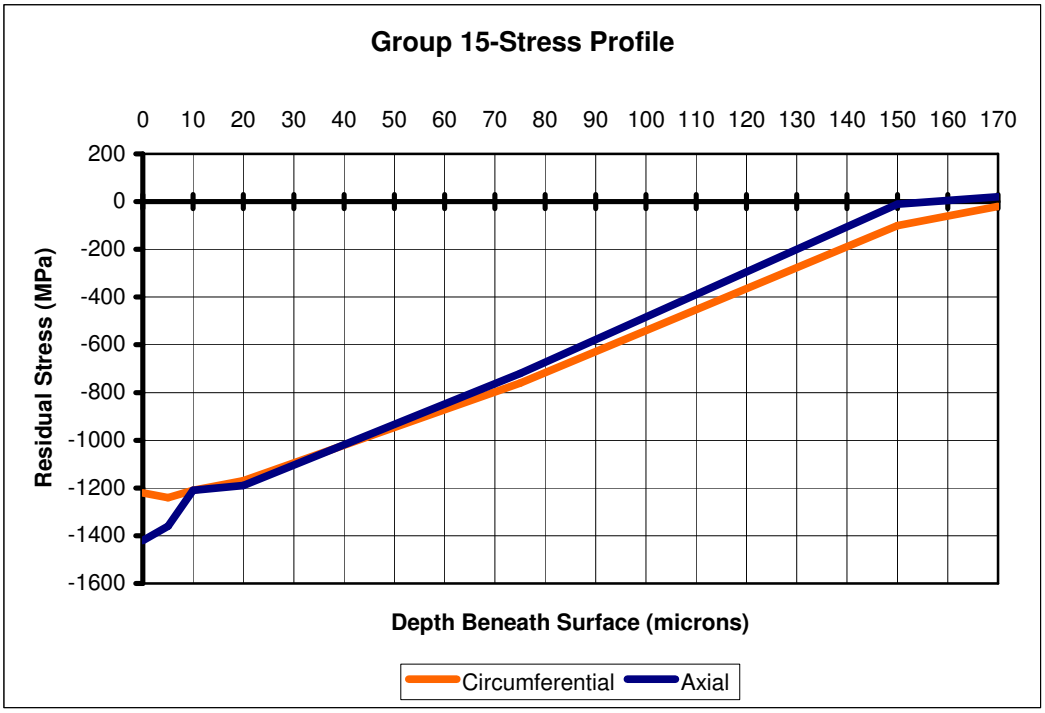

Figure 5.19 Group 15 Residual Stress Profile.

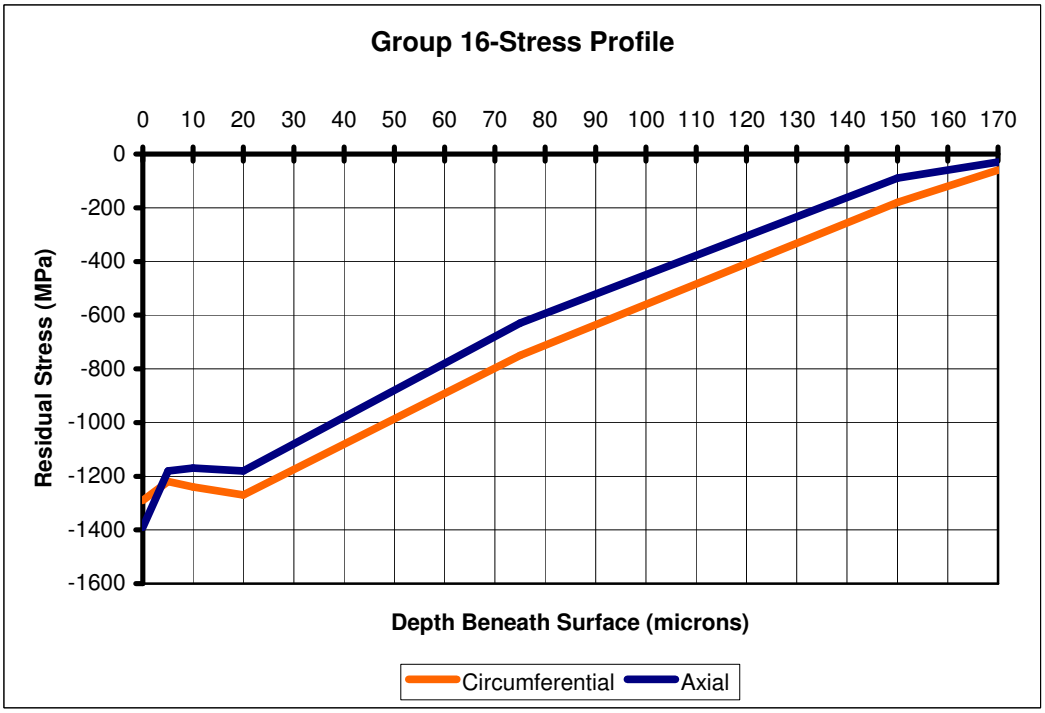

Figure 5.20 Group 16 Residual Stress Profile.

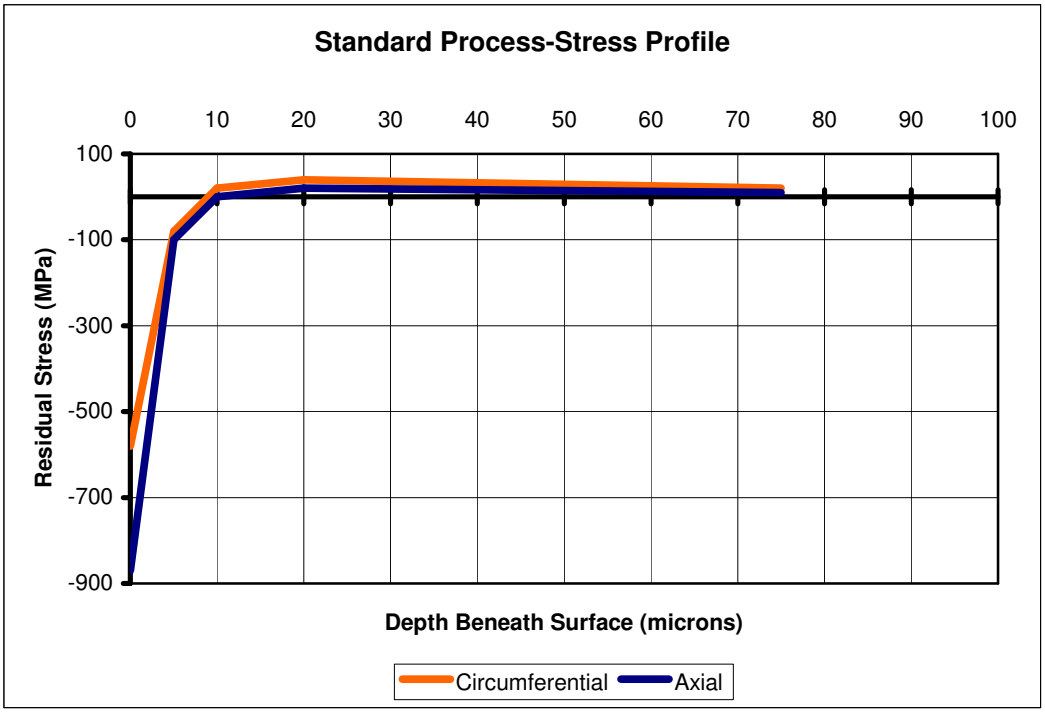

Figure 5.21 Standard Production Residual Stress Profile.

Application of shot peening during production of 6207 IR on raceways gave high compressive residual stresses with reasonable depth from surface, this was the condition theoretically expected to be achieved. These high compressive residual stresses are introduced in different levels and depths as can be seen from figures in between *Figure 5.5* to *Figure 5.20*, by sixteen different parameter sets, hoping to improve rolling contact fatigue life of bearing rings.

Compared to standard 6207 type bearings, stress profile is given in *Figure 5.21;* residual stress on the raceway surfaces is doubled in magnitude in compressive direction by application of shot peening, and in terms of depth beneath surface, shot peened rings possessed compressive stress patterns up to 16 times the depth of compressive region in standard product. Retained austenite measured after super-finishing on raceway surface of standard 6207 inner ring was 17% and it was 19% after tempering. While, retained austenite transformed with shot peening was around 5%, on the other hand with standard production 2% was transformed.

Table 5.15 Subsurface Residual Stress Measurements.

Group	Direction	Depth (microns) and Stress (MPa)							Compressive Area (Mpa.mm)
		0	5	10	20	75	150	170	
1	circ.	-1230	-1210	-1200	-1190	-790	-80	0	-138,4
	axial	-1410	-1280	-1230	-1220	-800	-50	-10	-145,7
2	circ.	-1240	-1170	-1100	-1000	-590	-70	-30	-126,3
	axial	-1340	-1210	-1090	-990	-500	-100	-20	-127,5
3	circ.	-1220	-1190	-1200	-1210	-620	-80	-10	-134,3
	axial	-1390	-1200	-1210	-1220	-630	-20	0	-137,7
4	circ.	-1210	-1150	-1160	-1170	-430	-80	-10	-126,5
	axial	-1350	-1150	-1140	-1130	-430	-90	0	-128,5
5	circ.	-1190	-1100	-1120	-910	-440	-70	-10	-117,5
	axial	-1390	-1120	-1090	-900	-410	-10	40	-123,0
6	circ.	-1200	-1050	-1090	-1010	-250	-10	50	-115,3
	axial	-1280	-1100	-1050	-1020	-360	-10	70	-120,5
7	circ.	-1210	-1220	-1250	-1280	-570	-20	20	-138,8
	axial	-1410	-1300	-1260	-1210	-560	-30	0	-140,1
8	circ.	-1320	-1230	-1210	-1190	-620	-90	-10	-137,7
	axial	-1420	-1300	-1230	-1100	-530	-40	20	-140,5
9	circ.	-1170	-1070	-1100	-1020	-600	-110	-30	-123,9
	axial	-1380	-1150	-1020	-990	-580	-70	0	-126,0
10	circ.	-1190	-1130	-1090	-1060	-620	-20	10	-127,8
	axial	-1320	-1200	-1080	-1030	-570	-10	20	-130,3
11	circ.	-1220	-1200	-1180	-1090	-590	-180	-60	-134,1
	axial	-1380	-1250	-1090	-1010	-580	-110	-30	-132,4
12	circ.	-1340	-1260	-1210	-1300	-820	-160	-70	-149,6
	axial	-1420	-1300	-1230	-1340	-790	-120	-30	-151,3
13	circ.	-1210	-1150	-1100	-1000	-620	-50	-10	-124,8
	axial	-1350	-1200	-1090	-990	-590	-40	0	-127,7
14	circ.	-1210	-1160	-1130	-1120	-550	-60	-30	-127,7
	axial	-1340	-1140	-1100	-1040	-480	-70	-10	-125,8
15	circ.	-1220	-1240	-1210	-1170	-760	-100	-20	-138,9
	axial	-1420	-1360	-1210	-1190	-720	-10	20	-147,8
16	circ.	-1290	-1220	-1240	-1270	-750	-180	-60	-146,0
	axial	-1390	-1180	-1170	-1180	-630	-90	-30	-137,7
Standard Product.	circ.	-580	-80	20	40	20	*	*	-2,1
	axial	-870	-100	0	20	10	*	*	-3,2

For purpose of determining the shot peening parameters on stress profile, subsurface distribution of residual stress, comparison on the area under the curve, compressive area basis is the best way. Groups are compared in the same manner in shot peening parameter effect determination subheadings. Comparison tables are given below.

Table 5.16 Effect of Air Pressure on Subsurface Residual Stress.

Group	Circum. Comp. Area (MPa.mm)	Axial Comp. Area (MPa.mm)	Max. Circum. $\sigma_{surf.}$ (MPa)	Max. Axial $\sigma_{surf.}$ (MPa)
1	-132,4	-136,6	-1240	-1410
5	-125,8	-128,1	-1190	-1380
2	-130,4	-133,1	-1220	-1390
6	-141,8	-141,8	-1340	-1420
3	-116,4	-121,8	-1200	-1390
7	-126,3	-126,8	-1210	-1350
4	-138,2	-140,3	-1320	-1420
8	-142,4	-142,7	-1290	-1420

By examining above tabulated results the following can be said on subject of air pressure increase from 2 bar to 3 bar:

- Average area change in circumferential direction is -4.7 MPa.mm.
- Average area change in axial direction is -1.9 MPa.mm.

Thus, the general trend is; as compressed air pressure increases subsurface stresses becomes more compressive.

Shot flow rate increase effect is investigated by the given data in *Table 5.17* given below, and the following results are understood:

- Average area change in circumferential direction is 3.6 MPa.mm.
- Average area change in axial direction is 2.0 MPa.mm.

Table 5.17 Effect of Shot Flow Rate on Subsurface Residual Stress.

Group	Circum. Comp. Area (MPa.mm)	Axial Comp. Area (MPa.mm)	Max. Circum. $\sigma_{surf.}$ (MPa)	Max. Axial $\sigma_{surf.}$ (MPa)
1	-132,4	-136,6	-1240	-1410
3	-116,4	-121,8	-1200	-1390
2	-130,4	-133,1	-1220	-1390
4	-138,2	-140,3	-1320	-1420
5	-125,8	-128,1	-1190	-1380
7	-126,3	-126,8	-1210	-1350
6	-141,8	-141,8	-1340	-1420
8	-142,4	-142,7	-1290	-1420

The general trend is; as shot flow rate increases subsurface stresses becomes a little more compressive, averages are positive because of group number one it is an unusual case. Totally can be said flow rate has no significant effect on subsurface.

Table 5.18 Effect of Coverage on Subsurface Residual Stress.

Group	Circum. Comp. Area (MPa.mm)	Axial Comp. Area (MPa.mm)	Max. Circum. $\sigma_{surf.}$ (MPa)	Max. Axial $\sigma_{surf.}$ (MPa)
1	-132,4	-136,6	-1240	-1410
2	-130,4	-133,1	-1220	-1390
3	-116,4	-121,8	-1200	-1390
4	-138,2	-140,3	-1320	-1420
5	-125,8	-128,1	-1190	-1380
6	-141,8	-141,8	-1340	-1420
7	-126,3	-126,8	-1210	-1350
8	-142,4	-142,7	-1290	-1420

From *Table 5.18* effect of difference in coverage percentage, 100% to 200% can be summarized as the following items:

- Average area change in circumferential direction is -13.0 MPa.mm.
- Average area change in axial direction is -11.2 MPa.mm.

As coverage increases from 100% to 200% subsurface compression is increasing and the most significant effect on development of subsurface compression is by coverage.

CHAPTER 6

RESULTS OF THE EXPERIMENTS-II
FATIGUE LIFE TESTS

This chapter covers results of the fatigue life tests for sample ball bearings with different residual stress states in terms of surface and subsurface values. At the end correlation between residual stress and fatigue life is discussed. Investigation is done by using Weibull statistics. Including residual stress profile of standard production the minimum and maximum distributions obtained are plotted in circumferential (*Figure 6.1*) and in axial (*Figure 6.2*) directions.

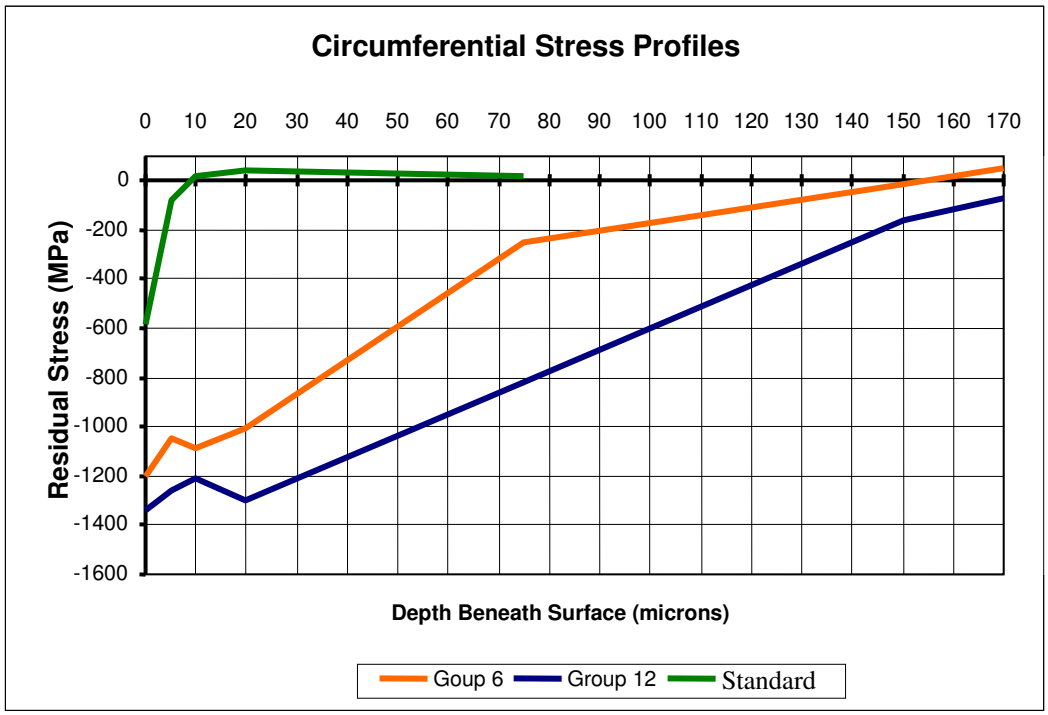

Figure 6.1 Circumferential Residual Stress Profiles.

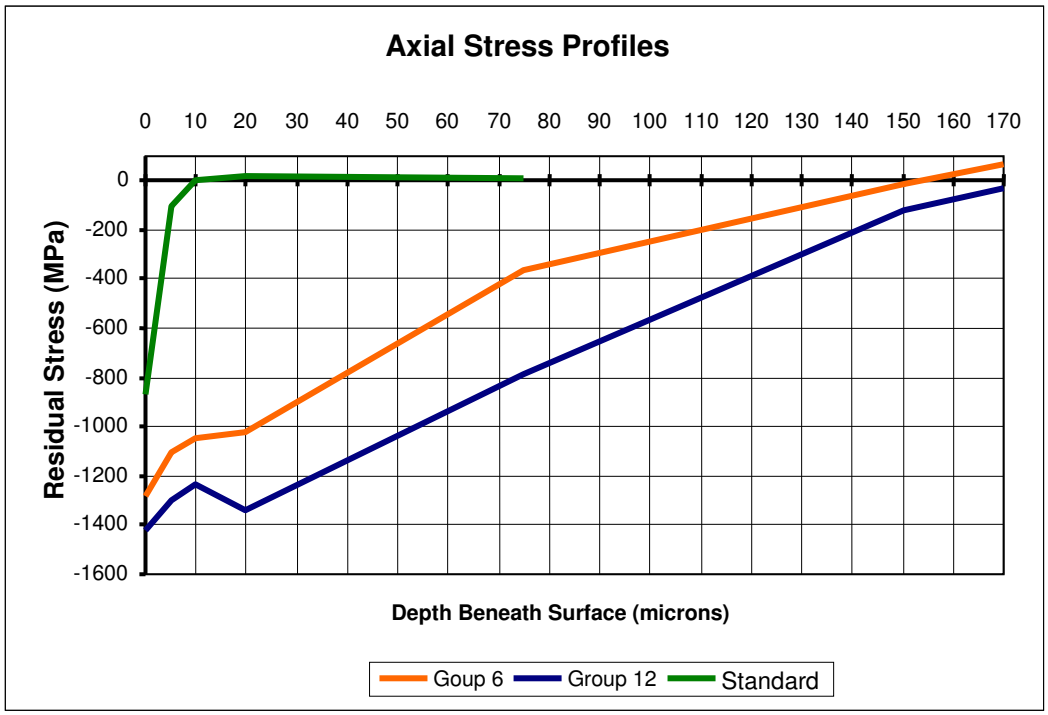

Figure 6.2 Axial Residual Stress Profiles.

Inspection of residual stress profiles of group number 6 and 12 makes it possible to observe that they posses similar behavior in both circumferential and axial directions. Maximum surface residual stress is also detected in group 12 and minimum in group 6 when circumferential and axial stresses are averaged. Also, compressive stress becomes zero before 150 µm for group 6 while this depth is above 170 µm for group 12. With respect to standard production surface stress is doubled and compressive region depth is 15 times deeper.

Hence, manufacturing parameters in terms of shot peening and super-finishing are different, results obtained showed similar, very near stress distributions and test batches are grouped into six in between group 6 and group 12 according to residual compressive field size in circumferential direction. Life test groups are as given in *Table 6.1*.

Table 6.1 Fatigue Test Groups.

Life Test Group	Parameter Group	Circum. Comp. Area (MPa.mm)	Circum. Surface Stress (MPa)
1	12	-149,6	-1340
	16	-146,0	-1290
2	1	-138,4	-1230
	7	-138,8	-1210
	15	-138,9	-1220
	8	-137,7	-1320
3	3	-134,3	-1220
	11	-134,1	-1220
4	4	-126,5	-1210
	10	-127,8	-1190
	14	-127,7	-1210
	2	-126,3	-1240
5	9	-123,9	-1170
	13	-124,8	-1210
6	5	-117,5	-1190
	6	-115,3	-1200

Weibull distributions of life cycles as multiples of rated $L_{10,\,h}$ life are given for the test groups in *Figure 6.3*.

In *Figure 6.3* bearings having life cycles longer than 10 times the rated $L_{10,\,h}$ life are shown as one group designated as 10+. For information, data obtained during life cycle tests are also given in *Table 6.2*. This table also includes the stress field under the surface, surface stress value and average life of each group. *Figure 6.3* is plotted by use of these data. In *Figure 6.4* distributions of life cycles in again Weibull statistical approach for shot peened and standard production can be seen. Finally in *Figure 6.5* distribution for standard production and bearings super-finished with 2.6 bar stone pressure (SF) are given.

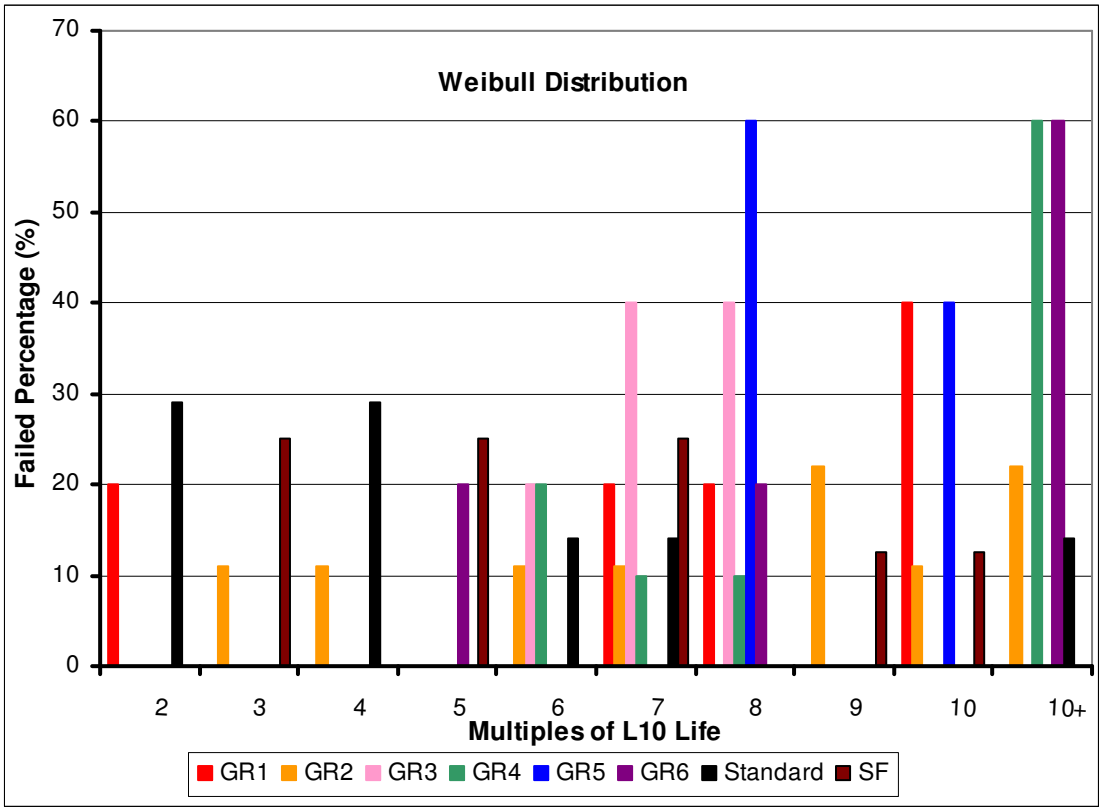

Figure 6.3 Weibull Distribution of Fatigue Life of Test Groups.

Table 6.2 Bearing Life Cycles.

Test Group	Life As Multiple of $L_{10,h}$											Circumferential	
	Av.	Value For Each Tested Bearing										$A_{comp.}$	$\sigma_{Surf.}$
GR1	7	7	10	10	8	2						-148	-1315
GR2	9	7	23	4	11	3	10	6	9	9		-139	-1245
GR3	7	8	8	7	6	7						-134	-1220
GR4	15	13	8	31	11	6	17	23	31	6	7	-127	-1213
GR5	9	10	10	8	8	8						-124	-1190
GR6	11	8	13	11	19	5						-116	-1195
SP Av.	10											-132	-1229
Stand.	5	2	2	4	6	11	4	7				-2	-580
SF	6	7	3	5	5	7	3	9	10			*	*

SP Av.	: Shot peened rings average.
SF	: 2.6 bar stone pressure super-finish trial.
Stand.	: Standard production.
Av.	: Average of life value for each tested bearing.
$A_{comp.}$	: Compressive stress area under raceway surface.
$\sigma_{Surf.}$	: Raceway surface residual stress.

From *Table 6.2*, as a general trend, it can be said that as the compressive field under surface increases, surface residual stress in compression direction also does. Average life of shot peened rings is 10 times the life rating while standard production average is 5 times the $L_{10, h}$.

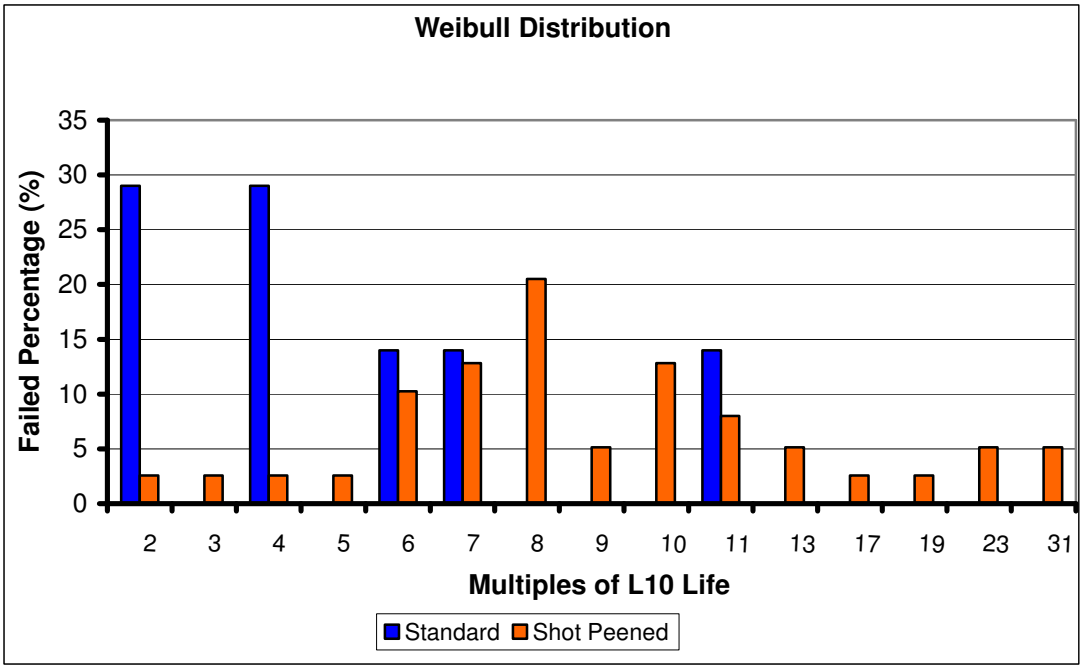

Figure 6.4 Weibull Distributions of Life Cycles of Shot Peened and Standard Bearings.

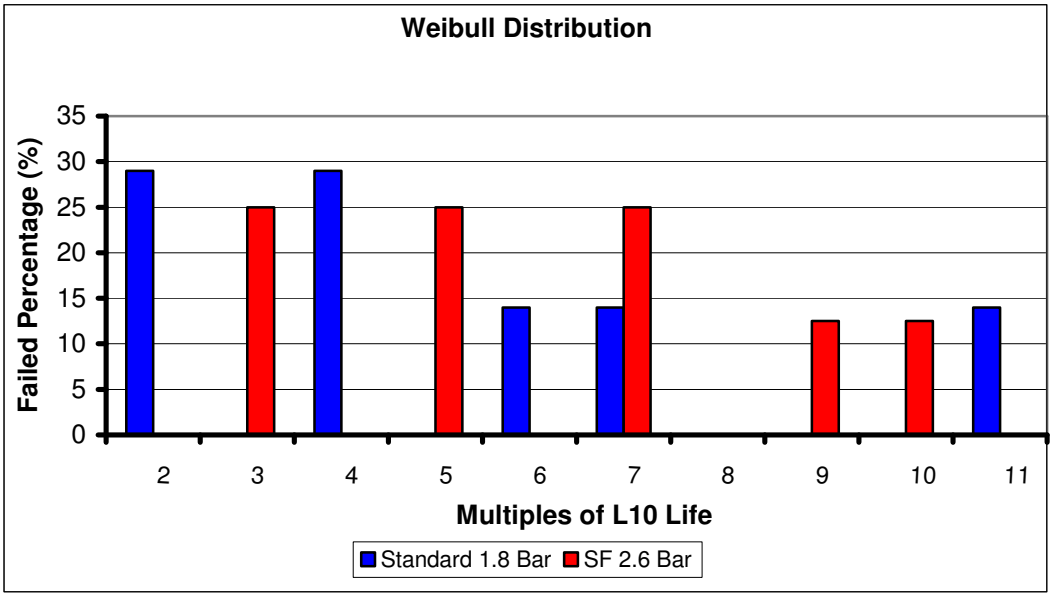

Figure 6.5 Weibull Distributions of Life Cycles of
2.6 Bar and 1.8 Bar Super-finished Bearings.

Looking at the above given table and statistical distributions the following results can be explained:

- From *Figure 6.3* and *Table 6.2* groups in terms of fatigue life can be arranged in the following order from the highest to the lowest:

  GR4 > GR6 > GR5 > GR2 > GR3 > GR1 > SF > Standard Production

  Average life of GR5 and GR2 are equal but GR2 has a spread out distribution while GR5 has a better distribution values all near average value so it is preferred better. Same condition appears for GR1 and GR3, again due to better distribution around the average GR3 is taken as better.
- Shot peening as can obviously be seen from *Figure 6.4* and *Table 6.2* increases the fatigue life.
- Super-finishing stone pressure seems to improve fatigue life from *Figure 6.5* and *Table 6.2* but the effect is not as significant as in shot peening case.

- Improvement in residual compressive stress depth and value on surface contributes positively to fatigue life but it can not be said that as compression increases life increases. Maximum compressive stress on surface and/or maximum compressive subsurface area does not mean maximum life. It is true that compressive stress improves the fatigue life under rolling contact ball bearing fatigue but they do not have a direct proportionality.

As mentioned before, data in this thesis are not sufficient; for reliable test data further tests have to be conducted. Data in hand only gives a general view. Thus, for better understanding and observing the effects sample number must be increased, test batch for each group have to be enlarged and tests must be conducted under load and rotation speeds similar to normal working environment.

Tested rings that are not considered due to having life lower than 27 hours rated life and failed due to outer ring or balls are given in *Table 6.3* for information.

Table 6.3 Life Cycles of Tested Bearings Out of Consideration.

Test Group	**Life As Multiple of $L_{10,h}$**					**Failure Reason**	
	Av.	**Value For Each Tested Bearing**				**Outer Ring or Ball**	**Inner Ring**
GR1	0.75	0.6	0.9			1	1
GR2	6.03	0.7	0.4	17		2	1
GR3	0.6	0.9	0.3			0	2
GR4	10.53	0.6	12	19		2	1
GR5	0.65	0.5	0.8			1	1
GR6	3.1	0.4	0.9	8		2	1
SP Av.	4.2					8	7
Stand.	0.6	0.3	0.6	0.5	1	1	3
SF	0.65	0.8	0.5			1	1

CHAPTER 7

DISCUSSION AND CONCLUSION

The state of stress produced by rolling contact is concentrated in a volume of material and produces intense plastic strain. Strain produced accumulates as the same volume is stressed with each rolling cycle until a crack initiated and finally by propagation forms a spall. Analysis of subsurface stress state yields that a maximum shear stress exists at a given depth below surface. The maximum shear stress is shown increasing with depth below surface as discussed by Kloss et al. (1981). In bearings manufactured from AISI E52100 steel, accumulation of strain under raceway surface forms dark etching areas and further strain causes martensite decay and butterflies. Lubrication, micro-cleanliness and carbide structure so steel making practice, surface condition of raceway and contact surface area are all effective in ball bearing life time. Beside these, compressive residual stresses are known to retard crack initiation and propagation under rolling contact fatigue and this is the subject of this thesis.

Through out this work, residual compressive stresses are inserted on bearing raceway surfaces by different shot peening parameters and their effect on stress development are investigated. Also super-finishing pressure effect on residual stress on raceways is analyzed. Finally by fatigue life tests correlation between residual stress state and fatigue life tried to be established.

In previous sections, all through out Chapter 5, effect of shot peening process parameters and super-finishing stone pressure on residual surface and subsurface stresses, retained austenite transformation, hardness change and peening intensity are investigated. The observations in hand are summarized in *Table 7.1*. Residual

stresses in the direction of rolling, namely circumferential direction are known to be important in terms of fatigue crack nucleation retardation and slowed down propagation. Also, observations prove that circumferential and axial stresses behave in the same manner with changing shot peening parameters and super-finishing stone pressure increase. Thus, only circumferential stress deviations due to parameter alterations are given in the table.

Green colored values in *Table 7.1* are the highest changes in the expected direction. Numbers in parenthesis are percentages with respect to the highest one which is 100%. By evaluation of results following can be judged:

- In terms of surface stress change, super-finishing stone pressure is the most effective in increasing surface compression. Stone pressure can not be increased more within the current conditions and all other super-finishing parameters are kept constant, because the raceway surface form goes out of tolerance. Among the shot peening parameters the most effective is the shot flow rate also the coverage but the effect is small.

- For subsurface compressive field increase coverage has a significant effect and it is the most effective. Air pressure tends to increase compression but flow rate has nearly no effect on field magnitude.

- Retained austenite transformation increases by air pressure increase in first order and secondly by coverage. Super-finishing stone pressure has very little, almost no effect for transformation.

- Hardness is increased by again air pressure first and secondly by coverage.

- The largest Almen intensity increase was observed by air pressure increase and after with coverage percentage increase.

- The maximum surface stress in circumferential and axial directions was obtained by group 12 parameters set.

- The maximum compressive subsurface area was obtained via again group 12 parameters.

- The highest surface retained austenite transformation was observed in group 16. Average transformation in shot peened rings is 5% but with standard process 2% in martensite plus austenite phase mixture. This means nearly 30% of initial retained austenite is transformed during shot peening while 10% is transforming in standard production.

- Compared to standard process, surface compressive stress is doubled by shot peening application and compression depth under surface is around 15 times widened.

Table 7.1 Summary of Process Parameter Effectiveness on Residual Stress, Retained Austenite, Hardness and Peening Intensity.

Parameter	**$\sigma_{Surf.}$ Change (ΔMPa)**	**$A_{Comp.}$ Change (ΔMPa.mm)**	**$\gamma_{Ret.}$ Trans. (Δ%)**	**Hardness Change (ΔHRC)**	**Intensity Change (Δmm)**
Air Pres. 2 → 3 bar	56.25 (100)	-4.7 (-36)	**-2.0 (-100)**	**1.06 (100)**	**0.08 (100)**
Flow Rate 2 → 3 kg/min	-6.25 (-11)	3.6 (28)	-0.5 (-25)	0.06 (6)	0.01 (13)
Coverage (%) 100 → 200	-8.75 (-16)	**-13.0 (-100)**	-1.0 (-50)	0.81 (76)	0.04 (50)
Stone Pres. 1.8 → 2.6 bar	**-56.25 (-100)**	N.A.	-0.25 (13)	N.A.	N.A.

N.A. : Not Applicable.

$\sigma_{Surf.}$: Surface Residual Stress.

$A_{Comp.}$: Subsurface Compressive Area.

$\gamma_{Ret.}$: Retained Austenite.

Intensity : Almen A Strip Arc Height.

Effects of air pressure, flow rate and coverage on residual stress development are studied. Among these, flow rate has a little more sensible effect on surface residual stress but any parameter can not be said effecting more the stress developed they all have nearly the same effect. For subsurface compressive field increase coverage has a significant effect and it is the most effective. Air pressure tends to increase compression but flow rate has nearly no effect on field magnitude.

Shot peening parameters also affected the retained austenite transformation under strain and hardness near the surface region. Air pressure is observed to have the largest effect on retained austenite transformation and hardness increase, secondly the coverage. As Almen intensity increased by air pressure transformed austenite and hardness increased but effect on residual stress in terms of stress field under surface and surface stress can not be observed clearly.

Beside the above parameters, effect of stone pressure during super-finishing is investigated. In terms of surface stress change, super-finishing stone pressure is more effective than shot peening parameters in increasing surface compression, but it has nearly no effect on subsurface stress field. It has very little, almost no effect for austenite transformation and hardness. So, mostly the hardness increase is related with deformation but residual stress development is contributed by retained austenite transformation and deformation.

Observed overall effect of shot peening application on raceways are doubling of surface compressive residual stress and 15 times increase in subsurface compressive

field width. Beside this, average retained austenite transformation in shot peened rings was nearly 30% of initial retained austenite while 10% is transformed in standard production.

Fatigue life tests are applied for correlating the residual stress pattern and fatigue life. Bearings with different levels of surface and subsurface stress values are employed in the tests. As a result what can be said is; maximum compressive stress on surface and/or maximum compressive subsurface area does not mean maximum life. It is true that compressive stress improves the fatigue life under rolling contact ball bearing fatigue but they do not have a direct proportionality. A certain amount of surface compression and subsurface to a depth seems to be enough for crack retardation so improvement of life. This is understood from the observed fact that all shot peened bearings life increased to an extent.

In terms of fracture mechanical approach, combined mode I (tearing under tension) and II (sliding under shear) fatigue loading, as exist during the spalling macro-crack propagation phase, has been reviewed by Qian et al. (1996). These reviews indicate that the possibility to propagate a crack in another direction than mode I is dependent on material, load magnitude and loading sequence. Thus, in hard bearing steel subjected to mode I and mode II load, other directions of crack propagation other than mode I is unlikely. Gao et al. (1985) performed mixed mode (mode I and II) fatigue propagation experiments on steel and stated that; the effect of a mode II field is twofold: Firstly, the crack will turn towards the pure mode I direction and secondly, the mode II field reduces the mode I fracture toughness threshold, and therefore promote crack propagation. Due to this mixed mode present during rolling contact fatigue depending on superposition of applied and residual stresses, compressive residual stresses retard crack propagation under mode I but for the other modes, namely II and III, does not have a retarding effect. So, depending on the fracture mode, level of improvement in fatigue life by compressive stress magnitude differs.

As a summary; shot peening increases the fatigue life. But it must be optimized in terms of depth of compressive stress field required due to the fact that as depth increases surface fillets and deformation so martensite decay increases. Thus shot peening should not be applied at higher intensities than needed for elimination of negative effects on formation of deep surface fillets and over deformation of martensitic structure which causes decay into first dark etching than white etching (ferrite) areas which in turn has a negative effect on fatigue life. Super-finishing stone pressure increase seems to improve fatigue life but the effect is not as significant as in shot peening case.

CHAPTER 8

RECOMMENDATIONS AND FURTHER STUDIES

Effect of experimented parameters and processes including residual stress can only be achieved by application of representative fatigue tests. Fatigue life tests must represent the real working conditions including environment, lubrication, loading and turning speed in ball bearing case. So, life cycle test must include a real rolling motion under load. Any other cyclic loading like rotating bending or five point rolling contact fatigue test etc… can create meaningless results because of not representing the real working conditions and exact geometry so load distribution exerted on bearings. Moreover, the reliability of the tests depends to a large extent on how the inputs are controlled and outputs are evaluated, beside these how many times they are repeated. By concerning the scatter of fatigue lives of bearings, tests batch size have to be large and tests must be repeated until satisfactory number of data points is obtained also failure analysis of tested bearings must be carefully employed.

From the beginning, from scrap before steel production, the bearing rings under investigation must be from the same lot, cast number and bearing manufacturing lot, and the probable variations must be kept at minimum. All rings should be manufactured with the same machine and same tools with same dimensional and structural tolerances for each process. Heat treated together by the same furnace. Balls and lubricant from the same manufacturer with same lot number should be used during assembly. Test machine and environmental conditions must be the same; they should not be tested with different machines at different temperatures, with different lubrication conditions. Shortly, all parameters other than investigated that have an

effect on fatigue life are obligated to be kept same for test samples to have healthy judgments.

In subject of determining the effects of shot peening on bearing fatigue life tests must be conducted with exact working conditions that the type of bearing will put into service. Batch of test samples for each parameter study must be as large as possible, such that a minimum of 20 bearings per parameter study, and this necessitates the availability of time and fatigue test equipment. For optimum peening parameters determination and correlation with fatigue life, test samples manufactured with several peening intensities should be employed between 0.15 to 0.50 mm Almen A. These samples after shot peening as being 100% sure that the fillets are removed completely, should be ground with different stock removal quantity in order to obtain different subsurface compressive field depth. The best surface stress level and subsurface depth combination must be determined by this way and the study should be spread over other bearing types.

Finally, fatigue life of ball bearings can be improved by further studies on certain topics having effect on. Lubrication, surface contact geometry, microstructure and phases present after heat treatment, cleanliness level of bearing steel. Behavior of different grade steels for a certain application, surface coatings are some of them. For all of these studies, including residual stress investigating the mechanism of crack initiation and propagation for all failed test samples can provide an answer to the effect of studied parameter on the fatigue lives of ball bearings.

REFERENCES

Agha, S. R.; Liu, C. R.: Experimental Study on the Performance of Super-finish Hard Turned Surfaces in Rolling Contact. Journal of Wear, Elsevier, 2000.

Alfredsson, B.: A Study on Contact Fatigue Mechanisms, Doctoral Thesis, Department of Solid Mechanics Royal Institute of Technology, Stockholm, 2000.

Almen, J. O.; Black P. H.: Residual stresses and fatigue in metals. United States, McGraw-Hill Book Company, 1963.

ASM Handbook, Volume 5.: Surface Engineering, ASM International Handbook Committee, Materials Park, OH, USA.

ASM Handbook, Volume 10.: Materials Characterization, ASM International Handbook Committee, Materials Park, OH, USA.

ASTM E915.: Standard Method for Verifying the Alignment of X-ray Diffraction Instrumentation for Residual Stress Measurement, ASTM Standards, ASTM, Philadelphia, 1984.

Barzoukas, H.; Jauffret, J.: Peening with Ceramic Shot. SEPR-92096 Paris La Defense, France.

Brändlein, J.; Eschmann, P.; Hasbargen, L.; Weigand, K.: Ball and Roller Bearings: Theory, Design and Application. 3rd Edition, New York, John Wiley & Sons, 1999.

Cullity, B. D.: Elements of X-Ray Diffraction. 3rd Edition, Addison-Wesley Publishing, 1967.

Dieter, G. E.: Mechanical Metallurgy. SI Metric Edition, McGraw-Hill Book Company, Singapore, 1988.

Dommarco, R. C.; Kozaczek, K. J.; Bastias, P. C.; Hahn, G. T.; Rubin, C. A.: Residual stresses and retained austenite evolution in SAE 52100 steel under non-ideal rolling contact loading. Wear, Elsevier, 2004.

Gao, H.; Alagok, N.; Brown, M. W.; Miller, K. J.: Growth of Fatigue Cracks Under Combined Mode I and Mode II Load. Multiaxial Fatigue, ASTM STP 853, American Society for Testing and Materials, Philadelphia, 1985.

Güley, V.: Experimental investigation of residual stresses and their effect on fatigue life of ball bearings, Master of Science Thesis, Middle East Technical University, 2004.

Hashimoto, M.; Shiratori, M.; Nagashima, S.: The Effects of Shot Peening on Residual Stresses and Fatigue Strength of Carburized Gear Steels. Sumitomo Heavy Industries Ltd., Japan.

Heat Treater's Guide - Practices and Procedures for Iron and Steel. ASM International, 2nd Edition, USA, 1995.

Hongbin, X.; Quing, C.; Eryu, S.; Dengzhen, W.; Zhaohong, C.; Zhengle, W.: The Effects of Shot Peening on Rolling Contact Fatigue Behavior and its Crack Initiation and Propagation in Carburized Steels. Luoyang Institute of Technology, Henan, China.

Huo, C. Y.; Gao, H. L.: Strain-induced martensitic transformation in fatigue crack tip zone for a high strength steel. Materials Characterization, Elsevier, 2005.

James, M.; Lu, J.; Roy, G.: Handbook of Measurement of Residual Stres / Society for Experimental Mechanics. United States, The Fairmont Press, 1996.

Kalpakjian, S.: Manufacturing Processes for Engineering Materials. 3rd Edition, California, Addison Wesley Longman, 1991.

Kloos K. H.; Schmidt F.: Metallurgical Aspects of Wear. Journal of Surface Fatigue and Wear, 1981.

Kobayashi, M.; Matsui, T.; Murakami, Y.: Mechanism of Creation of Compressive Residual Stress by Shot Peening. International Journal of Fatigue, Great Britain, Elsevier, 1998.

Kumar, R.: Physical Metallurgy of Iron and Steel. Asia Publishing House, New York.

Leslie, W. C.: The Physical Metallurgy of Steels. Tech Books, India, 1991.

Lorösch, H. K.: Influence of Load on the Magnitude of the Life Exponent for Rolling Bearings. Rolling Contact Fatigue Testing of Bearing Steels, ASTM STP 771, American Society for Testing and Materials, Philadelphia, 1982.

McCool, J. I.: Load Ratings and Fatigue Life Prediction for Ball and Roller Bearings. Transactions of the ASME, 1970.

Naito, K.; Ochi, T.; Takahashi, T.; Suzuki, N.: Effect of Shot Peening on the Fatigue Strength of Carburized Steels. Nippon Steel Corporation, Japan.

Ortadoğu Rulman Sanayi ve Ticaret A.Ş.: Interactive Catalogue, 2005.

Porter, D. A.; Easterling, K. E.: Phase Transformations in Metals and Alloys. 2nd Edition, Chapman & Hall, Great Britain, 1992.

Prevéy, P. S.: X-ray Diffraction Characterization of Residual Stresses Produced by Shot Peening. Shot Peening Theory and Application, IITT-International, France, 1990.

Qian, J.; Fatemi, A.: Mixed Mode Fatigue Crack Growth: A Literature Survey. Engineering Fracture Mechanics, Volume 55, 1996.

Rangaswamy, P.; Scherer, C. P.; Bourke, M. A. M.: Experimental measurements and numerical simulation of stress and microstructure in carburized 5120 steel disks. Materials Science and Engineering, Elsevier, 2001.

Residual Stress Measurement by X-Ray Diffraction, SAE International, USA, 2003.

Rivero, I. V.; Ruud, C. O.: Deviation of residual stress patterns in 52100 bearing steel due to inherent microstructural transformations after rolling contact. Materials Characterization, Elsevier, 2004.

Seno, T.; Horiuchi, H.; Naito, T.: Effect of Various Peening Parameters on Compressive Residual Stress for Carburized Steel. Tokyo Heat Treating Co. Ltd., Yokohama, Japan.

Shot Peening Applications, Metal Improvement Company, 9th Edition, USA, 2005.

Shot Peening of Metal Parts, Aerospace Material Specification, AMS-S-13165, SAE International, USA, 1997.

Tallian, T. E.: Failure Atlas for Hertz Contact Machine Elements. ASME Press, 1992.

Tool and Manufacturing Engineer's Handbook. Society of Manufacturing Engineers, 3rd Edition, USA, 1976.

Torres, M. A. S.; Voorwald, H. J. C.: An evaluation of shot peening, residual stress and stress relaxation on the fatigue life of AISI 4340 steel. International Journal of Fatigue, Elsevier, 2002.

User Manual, Seifert 3003 PTS.

Verhoeven, J. D.: Fundamentals of Physical Metallurgy. John Wiley & Sons, USA, 1975.

Voskamp, A. P.: Material Response to Rolling Contact Loading, Journal of Tribology, Volume 107, 1985.

Voskamp, A. P.: Microstructural Changes During Rolling Contact Fatigue, Metal Fatigue in the Subsurface Region of Deep Groove Ball Bearing Inner Rings, 1997.

Wang, J. Y.; Tan, Y. X.; Zhu, R. H.: Transmission Electron Microscopy Analysis of Shot Peened Layer for Some Industrial Alloys. Xi'an Instutute of Technology, Xi'an, China.

Webster, G. A.; Ezelio, A. N.: Residual stress distributions and their influence on fatigue lifetimes. International Journal of Fatigue, Elsevier, 2001.

Widmark, M.; Melander, A.: Effect of material, heat treatment, grinding and shot peening on contact fatigue life of carburised steels. International Journal of Fatigue, Elsevier, 1999.

Zhuang, W. Z.; Halford, G. R.: Investigation of residual stress relaxation under cyclic load. International Journal of Fatigue, Elsevier, 2001.